

University of Strathclyde

Department of Physics

Design Study into a Very High Temporal
Resolution (<10 ps), 2D Imaging, Modular UV
and X-ray Diagnostic: The Orion Time Dilation
Imager (TIDI)

By

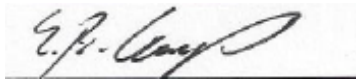
Samuel Giltrap

A thesis presented in fulfillment of the
requirements for the degree of Master of
Philosophy

2013

This thesis is the result of the author's original research. It has been composed by the author and has not been previously submitted for examination which has led to the award of a degree.

The copyright of this thesis belongs to the author under the terms of the United Kingdom Copyright Acts as qualified by the University of Strathclyde regulation 3.50. Due acknowledgment must always be made of the use of any material contained in, or derived from, this thesis.

Signed: 

Date: 15th October 2013

Abstract:

This Thesis details a design study into a new diagnostic of X-ray emission of intense laser-plasma interaction, the Orion Time Dilation Imager (TIDI). The principles behind the novel technique of pulse-dilation (the acceleration of a photoelectron, based on time-dilating a pulse by a time-varying potential, which results in velocity dispersion of the pulse traversing a drift region and causes image temporal magnification), are reported and analysed to inform the design decisions. Research is also performed into the initial use of pulse-dilation on the Dilation X-ray Imager (DIXI) instrument, which has been fielded and characterized on NIF, and the design considerations for developing a device capable of very high temporal resolution (<10 ps), 2D imaging of laser-plasma experiments.

The scope for utilising TIDI in previously unobtainable regimes in HED physics experiments is assessed. Experimental applications are identified and described, and their compatibility with a proposed design for TIDI is explored. Three key experimental applications are: Time resolved broadband x-ray diffraction, time resolved point-projection spectroscopy, and UV colour temperature measurements. The design constraints are explained and justified, including; the necessity of a modular design for UV and x-ray sensitivity, ensuring compatibility of the device with a Ten-Inch Manipulator (TIM) as used on the Orion target chamber at AWE, and the benefits and trade-offs of critical design parameters.

Experimental work to characterise an optical arrangement similar to one which would be used for the UV colour temperature measurements is reported. The optical pyrometry set up was characterised for the Orion target chamber and found to perform as expected. The system provided very high optical resolution ($\sim 1\mu\text{m}$), a wide unvignetted field of view of $\sim 0.5\text{mm}$ at a magnification of 12.5x. The colour correction of the system showed no significant aberrations. Other sources of image degradation were tested and found to be not significant.

Acknowledgments

The author would like to thank the following for large amount of time and effort given over during the completion of this project.

Firstly thanks must go to Anthony Meadowcroft (AWE) for preparing and organising the project, also for highlighting to the author the key physic required for understanding a time dilation imager. His diagnostics background was valuable and contributed to the assessment of the potential Orion TIDI designs.

Thanks also to Prof. Paul McKenna (The University of Strathclyde) for supervising me from Strathclyde and making this project possible, and assisting me in attending the ICOPS2012 conference in order to present the potential of the Orion TIDI to the international physics community.

Also, thanks are extended to Ed Gumbrell (AWE) who spent time outlining the key optical concepts and methods required for fully characterising an optical system, specifically the optical pyrometry, and for providing a wealth of optical components to assist with testing. Thanks to Jim Fyrth (AWE) for not only operating the laser, but also for bringing his experience to hand when attempting to trouble-shoot the Innolas Monojoule laser. And thanks to Sid Patankar (AWE/Imperial College London) for providing hands on help in the lab and explaining the many subtleties that come with characterising optical systems.

A large contribution to this project came from many meetings with Jonathon Hares, Tony Dymoke-Bradshaw (Kentech), Kevin Oads (AWE), and Anthony Meadowcroft. In these meetings the requirements of an Orion TIDI were outlined and designs that potentially meet these requirements were presented and explained by J.Hares and T.Dymoke-Bradshaw, their experience in designing diagnostic systems was invaluable when assessing the limitations of a time dilating device.

I am indebted to the Plasma Physics group at AWE for providing information on the potential applications of an Orion TIDI and the requirements of the front end optics for particular experimental set ups, particularly Andy Comely, Paul Kemshaw, and Ed Gumbrell.

I would also like to extend thanks to the scientists at LLNL who took time out of their hectic schedules in order to provide illuminating conversations about time dilation imagers (specifically the DIXI) and diagnostics in general. Sabrina Nagel provided very useful information on how she was characterising the DIXI which helped form an idea of the potential of the Orion TIDI.

Finally I am grateful to Chris Bentley (AWE) and his team for providing me support throughout this project.

Contents:

Chapter 1: Introduction	13
1.1. Introduction to HED physics and x-ray imaging	14
1.2. X-ray Imaging of High speed phenomena & Project Objectives	18
Chapter 2: Pulse Dilation	24
2.1. Overview of technique	25
2.2. Prototype pulse dilation imager	27
2.3. 1st Generation PDI- The DIXI	28
2.4. 2nd Generation PDI- The SLOS imager	30
Chapter 3: Application Requirements on Orion	33
3.1. Justification for an Orion Time Dilation Imager (the TIDI)	34
3.2. Time resolved Broadband X-ray Diffraction (BBXRD)	36
3.3. Time resolved Point Projection Spectroscopy (PPS)	42
3.4. UV colour temperature Pyrometry	45
3.5. Summary of Application Requirements	46
Chapter 4: Design Limitations of the Instrument	47
4.1. Design limits to temporal resolution	49
4.2. Design limits to spatial resolution	46
4.3. Design limits to framing capability	52
Chapter 5: Design of the Instrument	56
5.1. Basic component description and analysis	57
5.1.1. The Photocathode	57
5.1.2. The MCP-Phosphor as an image intensifier	65
5.1.3. The CCD/CMOS sensor	68
5.1.4. The Drift region manipulator	69
5.1.5. Shielding	70
5.2. Development of the Orion TIDI	71
5.2.1. TIDI 1: SLOS design with oblique transmissive photocathodes	73

5.2.2.	TIDI 2: SLSO single shot	76
5.2.3.	TIDI 3: Multiple lines of sight, segmented PC, no MCP design	78
5.2.4.	Summary	83
Chapter 6: Testing to inform design and predict performance		85
6.1.	Introduction and justification for practical work	86
6.2.	Theory	88
6.2.1.	GOI	88
6.2.2.	Pyrometry system	89
6.3.	Method	90
6.4.	Predicted performance	96
6.4.1.	Vignetting	96
6.4.2.	Chromatic performance	99
6.4.3.	Magnification, resolution, and fluence	101
6.5.	Results	103
6.5.1.	Initial vignetting	103
6.5.2.	Resolution of pyrometry system	104
6.5.3.	Magnification, FOV and vignetting test over Orion OPD	108
6.5.4.	Resolution of GOI	110
6.6.	Discussion	111
Chapter 7: Conclusion and further work		113
References		117
Appendix		121

Figures:

Figure 1.1 Graphical depiction of the HED regime [2]

Figure 1.2 Products of laser-target interactions [5]

Figure 1.3 X-ray framing camera example

Figure 1.4 Gated strip-line MCP

Figure 2.1 Principle of Pulse Dilation technique used in DIXI and proposed for SLOS

Figure 2.2 Hilsabeck, proof of concept prototype

Figure 2.3 DIXI schematic [20]

Figure 2.4 SLOS schematic

Figure 3.1 Temporal Capabilities of Orion Diagnostic Suit

Figure 3.2 Spatial Capabilities of the Orion Diagnostic Suit

Figure 3.3 Spectral Capabilities of the Orion Diagnostic Suit

Figure 3.4 Current BBXRD arrangement

Figure 3.5 altering the unit cell aspect ratio

Figure 3.6 BBXRD scale drawings (accounted for source size in solid angle calculation and not assumed point source)

Figure 3.7 Nickel Photocathode Response Curve

Figure 3.8 Fuji BAS Image plate Response Curve

Figure 3.9 PPS with a flat dispersion crystal [27]

Figure 3.10 PPS with curved dispersion crystal causing a focus in the spectral output [28]

Figure 3.11 Potential PPS set up for TIDI with aperture

Figure 4.1 The Potential's influence a photoelectron's time of flight

Figure 4.2 drift time as a function of voltage for a series of drift lengths

Figure 4.3 Resolution of the total system as a function of the Magnetic field

Figure 4.4 Resolution at the Photocathode as a function of the Magnetic field at the PC

Figure 4.5, The temporal magnification provided by a -10V/s potential ramp over a 50cm drift space

Figure 4.6 Prediction of the voltages needed for frame spacing for a given drift length

Figure 4.7 Example of several potential pulse profiles that achieve ~50 ns separation between frames at the phosphor

Figure 4.8 Minimum lengths required for number of frames due to the constraints of drift length, sweep gradient and minimum drifting voltage

Figure 5.1 Schematic layout of a Time Dilation Imager

Figure 5.2 Photoemission schematic, Φ is work function [36]

Figure 5.4 Example of QE for a selection of PC materials [12]

Figure 5.3 Potential enhancement of QE of PC by structuring in order to have an increased photon interaction length and minimised electron escape depth [38]

Figure 5.5 Variable-Design dependence

Figure 5.6 TIDI 1 design

Figure 5.7 ‘Short leg’ refers to the shorter of the two slanted drift regions, and ‘long leg’ the longer.

Figure 5.8 Schematic of component layout within the Innolas Monojoule laser enclosure for functional testing of single GOI heads. Routing for electronic cabling and front panel access to the power supplies is shown.

Figure 5.9 TIDI 2 design schematic for TIM compatibility

Figure 5.10 Temporal magnification for TIDI 2

Figure 5.11 40 cm drift length is around the limit of a two frame device

Figure 5.12 Gating using the threshold of the Phosphor and a short accelerating region

Figure 5.13 Example of segmented PC

Figure 5.14 Benefit of a concentric circle PC for BBXRD demonstrates the flexibility of this design

Figure 5.15 to scale schematic for pointing off centre and avoiding straight through

Figure 5.16 Protecting the CCD against straight through

Figure 6.1 Table Layout for Pyrometry measurements [30]

Figure 6.2 GOI head schematic

Figure 6.3 Vignetting example

Figure 6.4 Depiction of a Lambertian Source

Figure 6.5 (a) set up for measurement of vignetting by eye, (b) same set up for measurement with a CCD

Figure 6.6 Schematic layouts for passive optics testing

Figure 6.7 Schematic representation of delays

Figure 6.8 Laser cavity setup

Figure 6.9 Optical table arrangement

Figure 6.10 infinity corrected microscope and tube lens

Figure 6.11 Full aperture layout for Orion optical pyrometry system

Figure 6.12 Chromatic blur due to window

Figure 6.13 Chromatic defocusing through sapphire entrance window

Figure 6.14 Image diameter as a function of microscope and tube lens separation

Figure 6.15 Passive testing with full aperture arrangement

Figure 6.16 Intensity line out for group 7 on USAF grid

Figure 6.17 Contrast function for the Optical Pyrometry

Figure 6.18 Magnification check at intermediate image plane

Figure 6.19 Magnification check after full pass of the system

Figure 6.20 FOV of entire system for 10x and 5x magnifications

Figure 6.21 Relative intensity of GOI heads

Figure 6.22 example of reduced intensity as gate time is shorter than the laser pulse

Definitions

MCP – Microchannel Plate, similar in principal to a photomultiplier tube, an MCP will intensify detected photons through the process of secondary electron emission. The MCP differs from a PM tube in that it has an array of different channels which mean it can provide spatial resolution.

Pulse Dilation – Stretching a pulse in the axis of the accelerating field direction to improve temporal resolution

CCD – Charged coupled device

Gated – Gating in imaging is the time for which the detection surface is active (e.g. having the shutter open)

Frame – There can be multiple frames in a gate

Photocathode – A material which can take a photon signal and store it until it is released as a photoelectron signal by an applied voltage, essentially utilising the photoelectric effect.

Phosphor – A detector which responds to an electron incident on its surface by releasing a photon.

FWHM – Full width half maximum

ICF – Inertial confinement fusion, fusion performed by using the fuels own inertia as the method of confinement, in this report it will always refer to ‘indirect drive’ fusion using lasers unless otherwise stated.

Hohlraum – The radiation enclosure used in ICF

Motional Blur – Image aberrations caused an insufficient gate time which is less than the speed of the object trying to be imaged.

Bremsstrahlung – The x-ray radiation emitted by accelerating electrons

SLOS – A proposed Single Line Of Sight x-ray imaging device utilising the technique of Pulse Dilation

DIXI – The Dilation X-ray Imager designed for NIF, being characterised at time of writing

NIF- National Ignition facility

Chapter 1

Introduction

In this chapter the reader is introduced to the concept of high energy density physics (HED) and the theory behind high-speed x-ray imaging. The limitations of the current generation of x-ray imaging devices are presented, alongside the experimental requirements of the Orion laser facility, in order to explain the drive towards a higher temporal resolution x-ray diagnostic.

1.1. Introduction to High Energy Density (HED) physics and x-ray imaging

Large laser systems are used to access the HED physics regime due to the high irradiances they can achieve on target. Laser light is produced within the kJ energy range in ns time scale pulses. Focusing this power onto areas of a few hundred microns results in irradiances of 10^{14} - 10^{15} W/cm²[1].

High energy density physics is the study of energy and matter and energies exceeding 10^{11} J/m³. This area of physics spans across a wide range of topic, from the exploration of astrophysical environments within a laboratory setting, to understanding the fundamental processes governing Inertial Confinement Fusion (ICF).

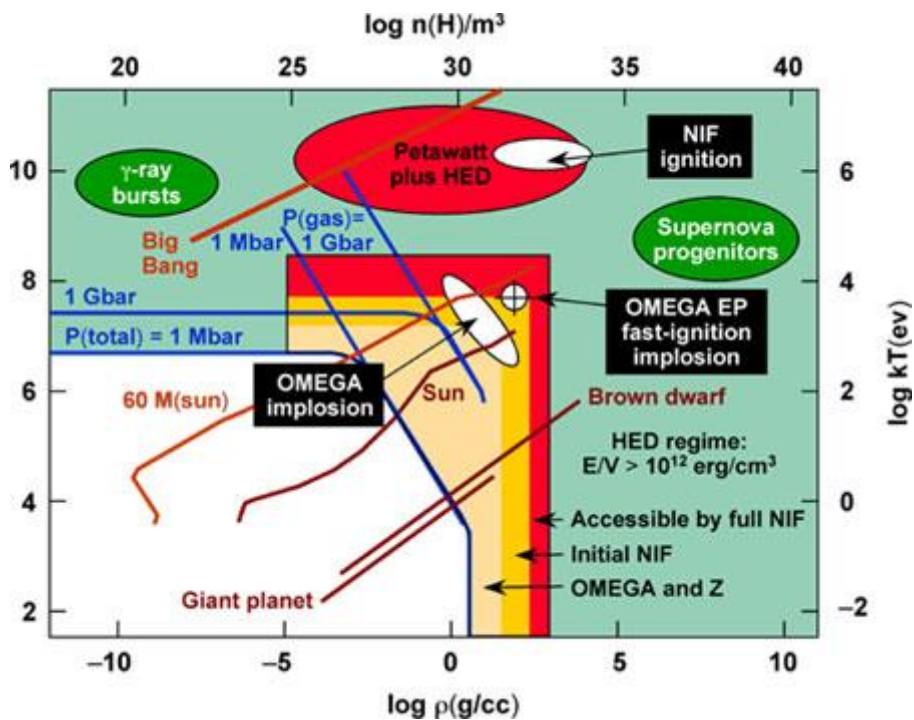


Figure 1.1 Graphical depiction of the HED regime [2]

Laser plasma interactions are of interest as they provide a way access high energy and density regimes in physics. Experiments in laser-plasma interactions take place in various facilities world-wide. Laser-plasma interactions depend not only on the

composition of the plasma but also on the properties of the laser (wavelength, intensity, pulse length, etc), Laser capabilities vary from one facility to another, allowing a wide range of experiments to take place. For example, the National Ignition Facility's (NIF's) Jupiter laser suite at Lawrence Livermore National Laboratory has a range of lasers which permit highly detailed measurements to be performed in areas such as plasma instabilities, filamentation, and coupling in HED physics.[3]

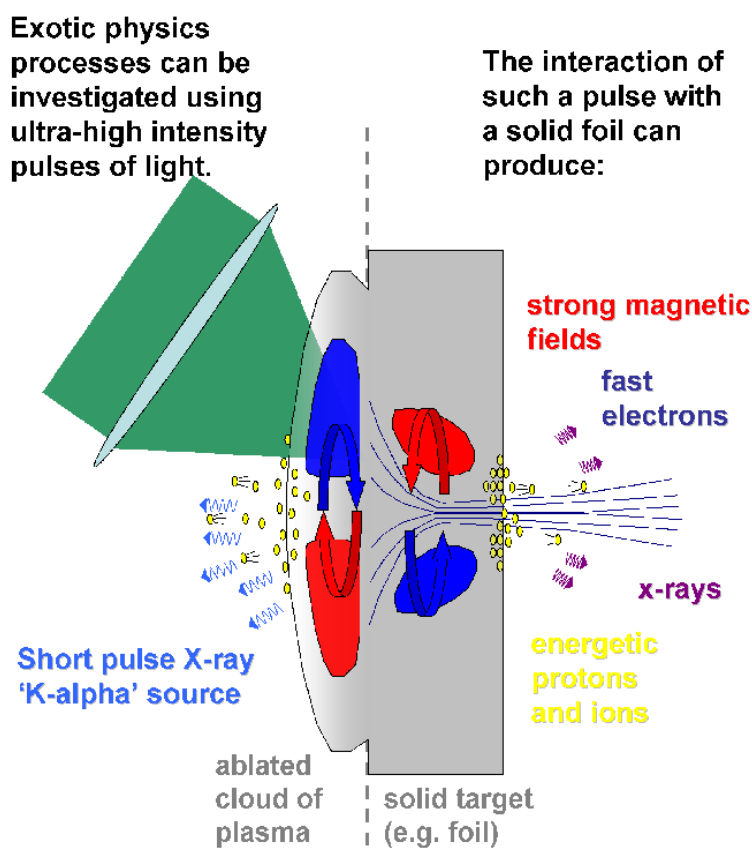
At AWE, plasma physics plays a crucial role in enabling research into the high energy density environments which would be produced by an exploding nuclear weapon, without contravening the Comprehensive Test Ban Treaty (CTBT) which prevents the carrying out of underground nuclear testing. Research using the recently commissioned Orion laser facility, provides insight into a wide range of topics such as shock compression for equation of state calculations, and hohlraum research into radiation conversion efficiency studies.

High-powered lasers are used at AWE to provide experimental data on the properties of matter under extreme temperatures and pressures. The purpose of these experiments is to allow modelling of the processes which are present in the operation of a nuclear warhead. The Orion laser facility houses the most powerful lasers at AWE; it has ten 'long pulse' beams for the compression of a target and two 'short pulse' beams (one for heating a target and the other acting as a diagnostic beam). The long pulse beams "deliver up to 500 J of 3rd harmonic, ultra-violet light in a pulse of 1 nanosecond duration", the short pulse beams each deliver "500 J of infra-red light in a pulse of 500 femtosecond duration", this means that the short pulse beams can produce an intensity up to 10^{21} W/cm². The diagnostic equipment needs to be able to resolve events which occur under these conditions, this requires high temporal and spatial resolutions.[4]

Short-pulse lasers have the ability to produce astounding irradiances; at AWE experiments have used irradiances in the range of 10^{18} to 10^{21} W/cm². At these intensities the laser light can apply huge pressure on a surface which can lead to

many interesting physical phenomena that are worth studying, for example exploring rapid changes in density and pressure caused by electron collisions; expansion is prevented via having a layer of test material buried within a second material which will not expand as quickly. Measurements are then made using x-ray emission and absorption spectroscopy and proton radiography.

During laser-plasma interactions there are several products that can be utilised for diagnostic purposes, among these are: K-alpha x-rays, an x-ray spectrum, high magnetic fields, fast and slow electrons and energetic protons and ions.



State of the art technology enables a laser pulse to deliver: 500 J of energy in a pulse lasting less than 0.5 ps creating a petawatt ($10^{15}W$) pulse.

Figure 1.2 Products of laser-target interactions [5]

Characteristic radiation is produced when an electron is excited from its state and the rest of the electrons respond to this hole by rearranging into a lower energy state, in

doing so, any 'falling' electron must release an x-ray photon of energy equal to the transition between states. These transition produced photons are specific to each kind of element (although the resolution of the diagnostic needs to be good enough to separate out the lines if we get several elements within a sample which have very close peaks), the intensity of these transitions stands out from the Bremsstrahlung radiation (a result of decelerating electrons interacting with the target).

The x-rays can be measured by spectra or can be imaged depending on the type of information desired.

There are two principal ways of looking at the x-ray spectrum; fluorescent x-ray spectroscopy and diffraction x-ray spectroscopy. In fluorescent (energy dispersive) spectroscopy a source of x-rays (typically an x-ray tube but electron beams can also be used) will be filtered to cut off the lower energy x-rays. The hard x-rays (5-10 keV) interact with a target and three kinds of secondary radiation are emitted: Scattered incident x-rays, excited electrons liberated from their nucleus, and characteristic x-radiation. [6]

Temperature and density information can be obtained through the measurement and analysis of these emission lines. The line radiation received will not be purely monochromatic, it will be broadened in frequency space; this broadening can be caused by the thermal motion of the atoms or the pressure from collisions or even the electric fields from surrounding ions and electrons. The line height gives us the intensity of the radiation recovered.

Since the properties of the emission lines are so dependent on temperature and density we are able to use them to diagnose those aspects of the plasma. The temperature could be found from a measurement of the absolute intensity of the optically thick transitions (as they approach a black body). However as it isn't quite close enough to a black body it is easier to measure a ratio of the optically thick lines from neighbouring ionisation states. The ratio of ionisation states is very sensitive to temperature and the ratio of the population of two energy levels will be governed by

the Boltzmann equation, therefore we can use the ratio of intensities from two lines to get a good diagnostic of the temperature.

The density could be found from the absolute intensity of spatially resolved optically thin resolution but this method leads to large margins of error, instead we use the Stark effect. The Stark effect is when energy levels, of hydrogenic ions, shift in the presence of an electric field. This shift causes a broadening in the emission lines, the electric field is some function of the electron density and is therefore also a function of the overall plasma density, and thus we can use the line widths as a suitable density diagnostic. [7]

X-ray imaging is simply the position and intensity sensitive recording of x-ray photons and can be applied over a wide range of topics, from medical (x-ray radiographs) to ICF (the implosion of capsules). X-ray photons interact with matter in three principal ways which contain useful information for diagnostics these are; Compton scattering, Rayleigh Scattering and photo-absorption/attenuation. The way x-ray photons interact with matter can reveal useful information about the composition of a sample, for example medical radiography. [8]

Images or spectra can be collected in a time integrated or time resolved way. A time resolved image is when the data is collected at a series of time intervals after/during an event whereas a time integrated image is related to the exposure time (the integration being the interval during which the camera will capture signal), so a time integrated image will give you the temporal evolution over a fixed window but only a time resolved image allow for the selection a moment in time to be specifically observed.

1.2. X-ray imaging of High speed phenomena and Project Objectives

The Orion experimental facility recently began its first experimental campaign. In order to meet future requirements of the experimental programme new technology is being sought to advance the capabilities of the Orion diagnostic suit for exploring

high speed phenomena. One example of an experiment being developed is point projection absorption spectroscopy. PPSA will be used to study the properties of hot dense matter with spatial, temporal and spectral resolution. The key aim is to find the opacity of a sample target foil under an evolving temperature/pressure. The heating x-ray source is generated by a laser beam incident on a converter foil target. X-rays are radiated symmetrically; forward propagating x-rays go on to heat the sample foil. A point x-ray source is provided by the backlighter pin when irradiated by a pulsed laser. The point source x-rays provide a 2D radiograph of the sample on the film. A Bragg crystal gives spectral resolution in one direction. By comparing the spectrum of the radiation transmitted through the sample to the spectrum of the un-attenuated beam the opacity of the sample can be measured. [9]

The x-ray pulses in proposed experiments are of a very short time scale (on the order of 10-100ps) [10]. X-ray pulse duration is typically comparable to the heating laser pulse duration, that is to say the rise time of the x-ray emission pulse is defined by the time required to heat the plasma and the fall time is set by the time scale of the plasma cooling (which is determined largely by rate of radiation emission and rate of expansion). The duration of the x-ray pulse can be useful in several applications including the rapid expansion of plasma and the propagation of shock waves in solids. [11]

Thin low mass targets are good for laser-plasma experiments as they rapidly absorb the laser energy and drop their density. This increases the mean free path of the x-radiation, allowing x-rays to escape with minimal absorption and reemission. However, low mass targets also cool more efficiently. The net result is a very short x-ray pulse for low mass targets irradiated by a picosecond-scale laser pulse (as in Orion). Diagnosis of such laser-plasma experiments therefore requires very high temporal resolution diagnostics. [11]

An x-ray framing camera is based around the principle of pulsing a photocathode, which produces an electron bunch via the photoelectric effect (see section 5.2) which is then collected by a Microchannel Plate (MCP) and the signal output is recorded by

a CCD, see below schematic (fig 1.3). While the x-ray signal is incident on Photocathode (e.g. CsI), the 500v reverse bias prevents the electrons from leaving the photocathode until a pulse is sent to release them (this is the act of framing the image). To record an image frame a high voltage gate pulse is sent across the photocathode. In the below case the pulse is created using a photoconductive switch. The rise time of the gate pulse corresponds to the temporal width of the trigger light pulse. [14]

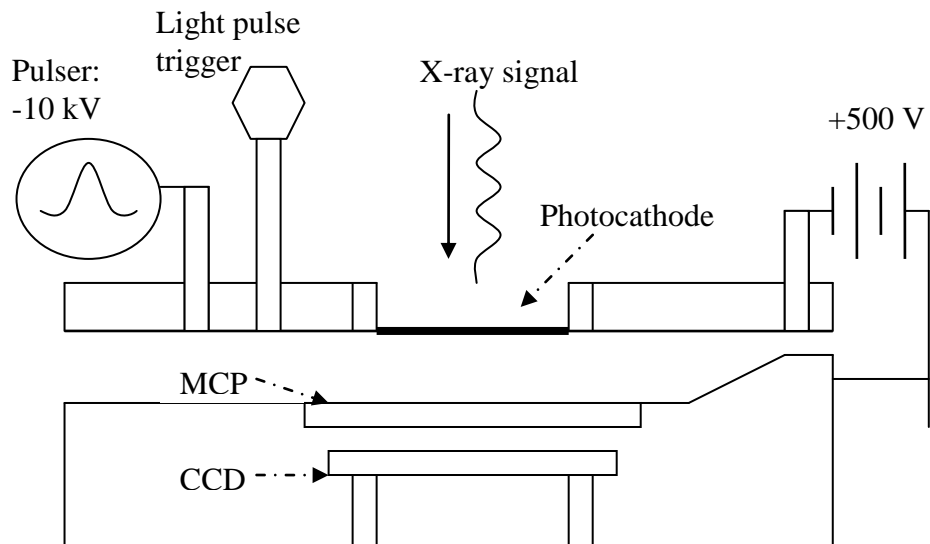


Figure 1.3 X-ray framing camera example [15]

Another way framing can be created is by using a gated MCP.[15], x-rays generated by a laser-target interaction are incident on an MCP. A pinhole array is used to focus these x-rays onto four horizontal electrically conductive strips. Electrical pulses can be sent down each strip independently of the other strips. However, the signal will only travel down the MCP once the strip has been activated. Utilising this method creates an arbitrary delay gating the image (see below image). [15]

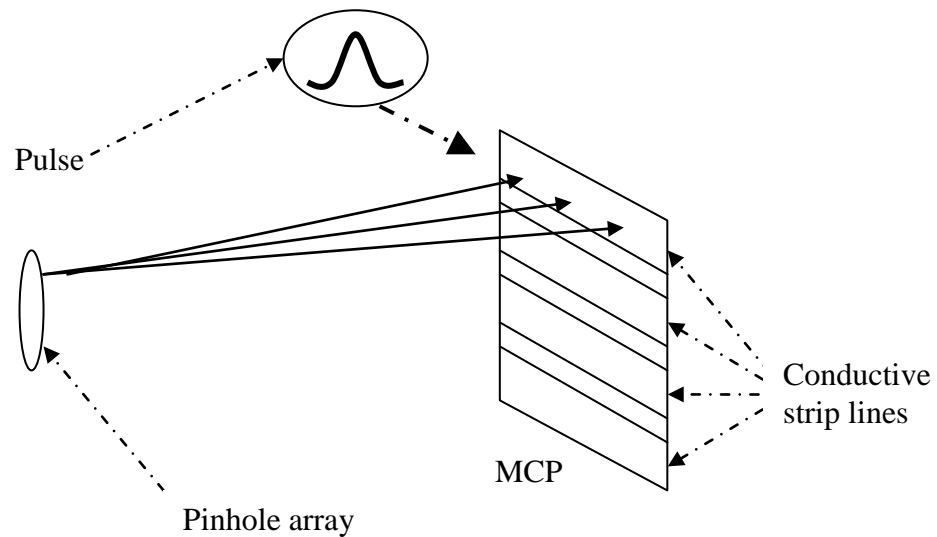


Figure 1.4 Gated strip-line MCP

The MCP is gated, rather than the subsequent detector (e.g. a CCD) as it prevents us from assuming uniformity on the MCP; if we were to gate a CCD which is immediately after an MCP we would be relying on the transit time being consistent all along the MCP, considering the small times we are already dealing with this could be a crucial factor. There are other practicalities to consider also, such as the fact that a CCD is run off the mains (as opposed to a high voltage source) so it can be more difficult to control and trigger.

X-ray framing cameras and gating imagers are effective as they are able to resolve extremely quick events. X-ray framing cameras have been shown to be able to get down to temporal resolutions of 30-40 ps, this was done by adjusting the length to diameter ratio of the pores on an MCP. It has been show that the resolution of an imager is dependent on the electron transit time and the electron transit time is defined as:

$$T_e = \sqrt{\frac{m}{eV}} \cdot L \cdot \sqrt{\frac{L}{D}}$$

Equation 1.1

where T_e is the transit time, m is the mass of an electron, e is the fundamental charge, V is the applied voltage, L is the length of a pore and D is the diameter. [13]

X-ray framing cameras can be made to be flexible enough to cover an extremely high range of requirements. The FXI (flexible x-ray imager) was created to cover incredibly fast events (e.g. capsule implosion) and not so fast events by implementing a variable gate time (100 ps – 2 ns) which could prevent motional blur and provide high temporal resolution for a number of situations. This was achieved by making the FXI modular and adaptable to the type of data you wish to record. Its two main constructions were; soft x-ray framing camera (SXRFC) and gated x-ray imager (GXI). The Magnification is adjusted by target-to-pinhole distance and the spatial resolutions are around 10 μ m (GXI) and 12 μ m (SXRFC). [16]

The main objective of this project is to assess the feasibility of overcoming the limit of current generation x-ray framing cameras. Unless there is a drastic discovery in the field of MCP research a new technique is required to get 2D imaging with a temporal resolution below 40 ps.

MCPs have been used for years but now a higher temporal resolution is needed. There are a number of drivers for improving the temporal resolution of diagnostics beyond that which can be achieved with a framing camera. For instance, shock experiments. We currently use proton radiography to observe the time evolution of a low density plasma inside of a hohlraum, the temporal resolution is such that we are only able to speculate about that causes the prominent features within the shocked plasma, however with a higher temporal resolution we would be able to further confirm computer modelling of this system. [17]

In “indirect drive” fusion a hohlraum holds at its centre a spherical capsule of D-T fuel. The laser geometry is set up so that the beams enter the hohlraum through LEHs (laser entrance holes) which allow the lasers to deposit energy into the inner side of the hohlraum. The hohlraum acts as a radiation enclosure, converting the optical laser light into soft X-rays. The x-ray radiation compresses the spherical fuel fusion

capsule (which contains a layer of frozen D-T fuel and a low density D-T gas) through the process of x-ray ablation; the x-rays heat and compress the outer shell quickly turning it to ablated plasma which implodes the fuel within to extreme densities, the D-T gas heats up to ignition temperature and fusion can then occur within a window of 10 – 100 picoseconds i.e. very fast indeed. [18]

Symmetry is important for ICF as the critically high density at the centre of the fuel pellet is caused by shockwaves travelling from the outside in and meeting perfectly in the centre will give us the high density required. The current generation of framing cameras are unable to reach the temporal resolution required to accurately assess this symmetry.

Chapter 2

Introduction to Pulse Dilation Imaging (PDI)

Pulse dilation imaging is a relatively novel method in the field of x-ray imaging therefore a whole introductory chapter follows in order to fully familiarise the reader with the theory behind the technique. This chapter also includes an overview of how PDI has so far been put into practice and the results of these experiments.

2.1. Overview of technique

Pulse Dilation is a method in which a bunch of electrons emitted from a photocathode is manipulated such that the incident photon signal is temporally magnified. The inherent temporal resolution limitation of an MCP (up to 30- 40ps) may be overcome by removing the direct dependence of the photoelectron production from a photocathode and their time of arrival on the MCP as follows. Prior to detection on the MCP, the photoelectrons leave the photocathode and enter a region of time varying potential. The time-varying electric field is due to a voltage sweep and causes earlier emitted electrons to drift at a higher velocity than the electrons emitted at a later time, thus dilating the temporal shape of the signal; another way of looking at it is that it has been temporally magnified. The electron cloud (now with a range of accelerations) leaves the area of potential and is sent to drift down a vacuum towards the MCP when the signal can be gated with an apparent temporal resolution of <10ps (dependent on the pulse architecture and drift length used) [19]

Electron signal manipulation is a technique used in several already existing diagnostic devices, for example a streak camera. Similar to pulse dilation, a streak camera uses a high voltage field to manipulate a bunch of photoelectrons. The photoelectron signal is sent through a pulsed voltage (which has to be triggered for periodic events) perpendicular to the camera axis so the position of the signal incident on the phosphor is a function of the time of passing through the high voltage potential.

In a similar way to pulse dilation, a streak camera entails generation of an electron pulse at the photocathode and makes use of a voltage sweep. However unlike pulse dilation, the temporal signal is spread perpendicular to the axis of motion such that temporal variation is imaged in a 1D spatial domain. [19]

The pulse-dilation mechanism has been described in physical terms from a model by Hilsabeck et. al. [19]. A schematic of the pulse-dilation technique is shown in Figure 2.1. In the model the time that an electron exits the drift space is given by

$$t'_i = \left(L \cdot \sqrt{\frac{m}{2e\phi_t}} \right) + t_i$$

Equation 2.1

where, t'_i = Time that electron leaves the drift region, L =drift length, m =mass of electron, e =fundamental charge, ϕ_t =Potential at a time t which accelerates the electron, and t_i =time electron enters the drift region.

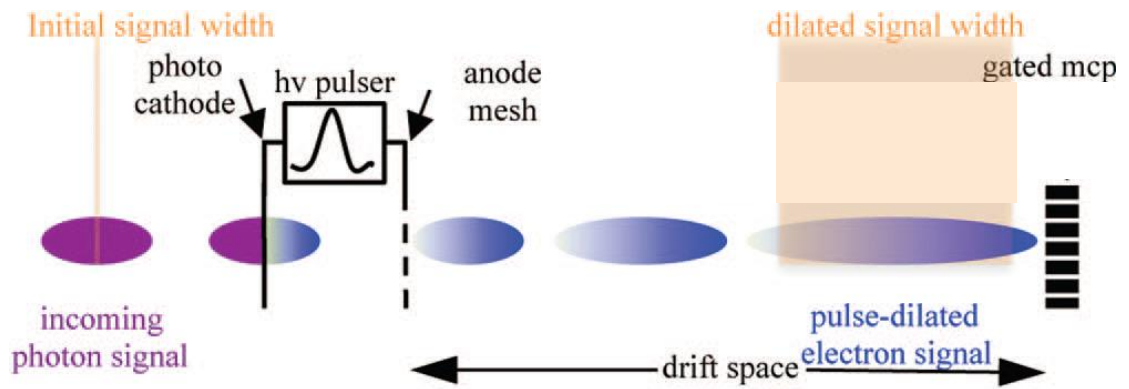
Earlier emitted electrons enter the drift zone at t_0 and the back of the signal at t_1 the time that each arrives at the MCP is dependent on the potential difference between the anode and cathode which provides the kinetic energy to the electrons, where t' = time electron exits drift space, L = drift length (const), m = mass of electron, e = fundamental charge, ϕ_t = Time dependent acceleration voltage, and t = time electron enters the drift region.

The temporal magnification of the pulse-dilated signal relative to the incident photon signal along the direction of propagation is given by

$$m_{(t_1, t_0)} = \frac{(t'_1 - t'_0)}{(t_1 - t_0)} \approx 1 + \frac{L}{2v_d} \frac{|\dot{\phi}|}{\phi}$$

Equation 2.2

where $m_{(t_1, t_0)}$ = the magnification of the signal and v_d = the average velocity for electrons within the signal pulse.



Photoelectrons → accelerated by a time varying electric field → energy dispersion → signal stretches as it traverses the drift region → sampled by gated mcp.

Figure 2.1 Principle of Pulse Dilation technique used in DIXI and proposed for SLOS [22]

This model assumes that the photoelectrons are born with zero energy. However in reality they are born with a range of energies and these can begin to affect the process (i.e. if the back electron is born with more energy than the front electron, it can catch up with it which ruins the temporal causality of the process). A model finds that the temporal causality starts to be affected when the electrons are normally distributed with a temperature of 1eV. [19]

Space charge propulsion is another limitation of the temporal resolution. If the photocurrent density (number of electrons per second) is high enough the electric fields produced by the electrons will modify the particle trajectories. This is counter acted in the transverse axis by a large magnetic field.

2.2. Prototype pulse dilation imager

A proof-of-concept experiment was devised by Hilsabeck et al [19], in which a prototype pulse-dilation imager was developed to demonstrate 5ps-gated framing using UV light from a short-pulse laser. The prototype design used a 2inch photocathode of a fused silica window coated with 100 nm Au.. An accelerating gap of 1.6 mm was utilised to pulse the electron signal with a -10V/ps gradient before entering a vacuum ($<10^{-5}$ Torr) region extending 50cm from anode to detector. A large magnetic field (400 G) was used to prevent defocusing of the electron signal as

it is drifted. The pulse dilated signal was gated using an X-ray framing camera (the FXI) which has a gating capability of 80ps [19]

The experimental procedure was as follows; a short-pulse laser (100 fs, 1mJ at 800nm) with a rep rate of 500 Hz. The pulse was sent through an 80 ns optical delay in order to allow time for the photocathode to trigger. After the optical delay the pulse was sent through a Mach-Zehnder interferometer. This allowed the continual adjustment of delay between two short pulses (i.e. simulating a very fast event). Each arm of the interferometer has a different arrow shaped aperture (A1 and A2 in fig 2.2).

To measure the temporal resolution the path difference was adjusted in small steps until the variable leg aperture appeared and disappeared from the image. This gave a temporal resolution for the instrument of around 5ps.

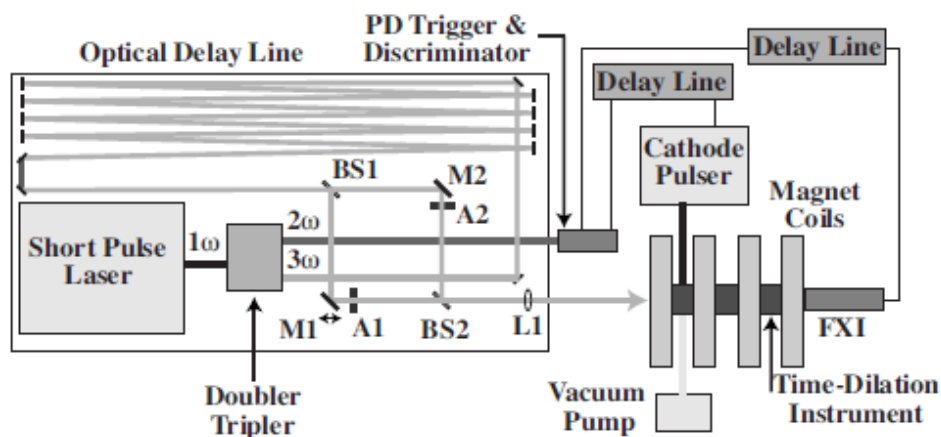


Figure 2.2 Hilasabeck, proof of concept prototype [19]

2.3. 1st Generation Pulse Dilation Imager (PDI)- The DIXI

Following first successful demonstration of pulse-dilation in this experiment [19], a diagnostic utilising the technique was built for NIF. Designed to image the fast ICF events mentioned earlier (in particular the symmetry of implosions), the Dilation X-

ray Imager (DIXI) has been tested on the Comet laser and proved to show up to 6 ps temporal resolution, 2D imaging. DIXI is now being commissioned for use on NIF

DIXI is the first Dilation X-ray Imager to be put to use at NIF. It utilises the pulse dilation in order to achieve temporal gate times of <10 ps.

In DIXI x-ray radiation is incident on an Al or CsI transmission photocathode, this produces an electron signal with a defined temporal length. The electron signal is sent through a pulsed potential electric field and out through an anode mesh in a drift space which is under a high vacuum. During the electron bunch's time in drift space, due to the uneven acceleration given by the pulsed PC, the signal dilates as the disparity between the front (high accelerated) electrons and the back (low accelerated) electrons becomes more pronounced. The drift space is subjected to a magnetic field which keeps the electron signal focused by limiting transverse spreading. The dilated signal hits a gated MCP detector, which is then followed by a phosphor, fiber block and CCD or film. The MCP is pulsed in time with the PC to gate the signal effectively.

The temporal resolution is dependent mostly on the drift length of the device and gradient of the voltage ramp used to accelerate the electron bunch. The spatial resolution a convolution of resolutions of the individual components, primarily in DIXI it is dominated by the MCP [21] however it's worth noting that the resolution contribution from the photocathode material choice (due to the much larger energy spread produced by a gold photocathode it has a far poorer resolution than the CsI photocathode) is significant [20]. The fundamental spatial resolution is set by the magnetic field which constrains the electron bunch as it traverses the drift region, In a solenoid the transverse excursion of the photoelectrons is limited to 4 times their cyclotron radius

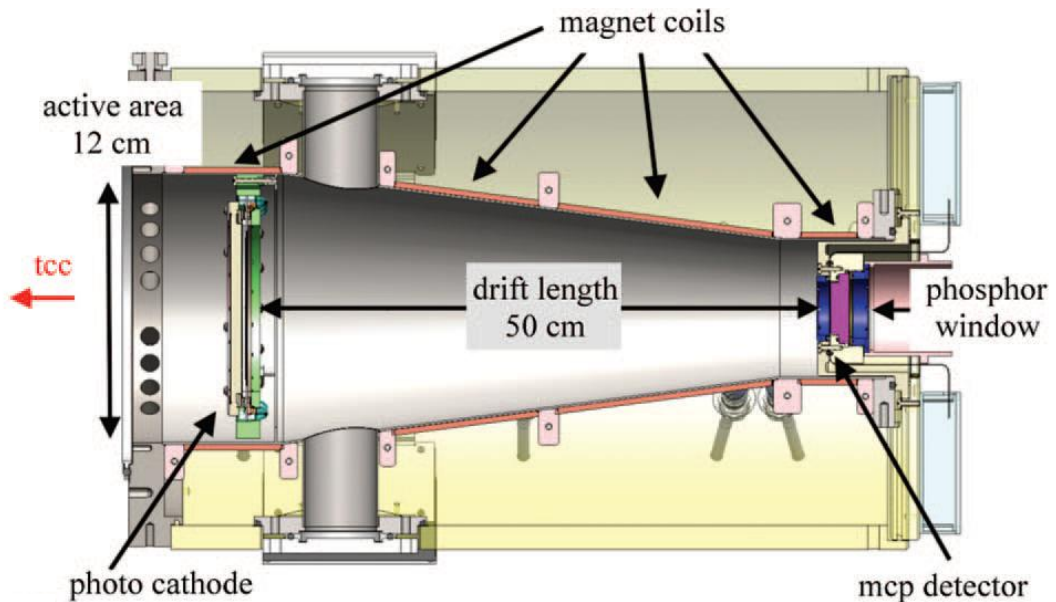


Figure 2.3 DIXI schematic, mounting at the chamber wall of NIF made it a requirement to have such a large area photocathode in order to gain enough signal [20]

The DIXI is located on the equatorial plane of the NIF target chamber so that gravitational effects are minimised, to protect the CCD the device is tilted at a 20° angle. An imaging pinhole array mounted within the target chamber gives the DIXI an magnification of 65x, a field of view (FOV) of 150 µm giving an image of ~9.8 mm. The MCP has 4 individually delayed strips which each have a time window of around 250ps

DIXI was tested by imaging a flat foil target irradiated by a high intensity laser. The detector was run in pulsed mode and the strips were close to co-timed. The FWHM of the shortest signals measured came out as around 6.5 ps. The spatial resolution could also be determined from this test and was found to be around 360µm for a 370 Gauss field. The jitter was found to be < 1 which is sufficient for the interleaved image method required for a 10 ps gate time.[21]

2.4. 2nd Generation PDI- The SLOS imager

The Single Line Of Sight (SLOS) x-ray framing camera is a new diagnostic being developed for NIF, following on from the DIXI. Similarly to DIXI, it uses pulse

dilation. However the SLOS instrument will have a repetitively pulsed photocathode (as opposed to the singular pulse used in DIXI) to acquire four successive frames, albeit at lower temporal resolution. The spatial resolution is improved over that of the DIXI with the aid of a higher magnetic field. One of the critical steps in the SLOS is to arrange the axial streak so the frames are separated by an interval which is greater than the decay time of the phosphor. [22]

In SLOS x-ray radiation is incident on a PC. The photocathode pulses 4 times at 4 different acceleration voltages for 100ps “on” time and a 100ps “off” time. The different voltage ramps are necessary to allow enough temporal spread between photoelectrons in adjacent frames to capture and store one frame signal before the next. The signals enter a drift space (which is 2m to accommodate the 4 frames required - substantially longer than the 50cm used for DIXI) and due to the different voltage ramps, the photoelectron bunches travel at different velocities, allowing the signals to individually dilate and for the interval between the signals to increase. The interval for arrival at the MCP is about 50 ns, sufficient for the MCP pulse to gate each frame. The drift space is subjected to a high magnetic field to overcome the MCP resolution limit. The signal is then sent through the fast phosphor, an imaging lens, a gated image intensifier and then to a CCD.

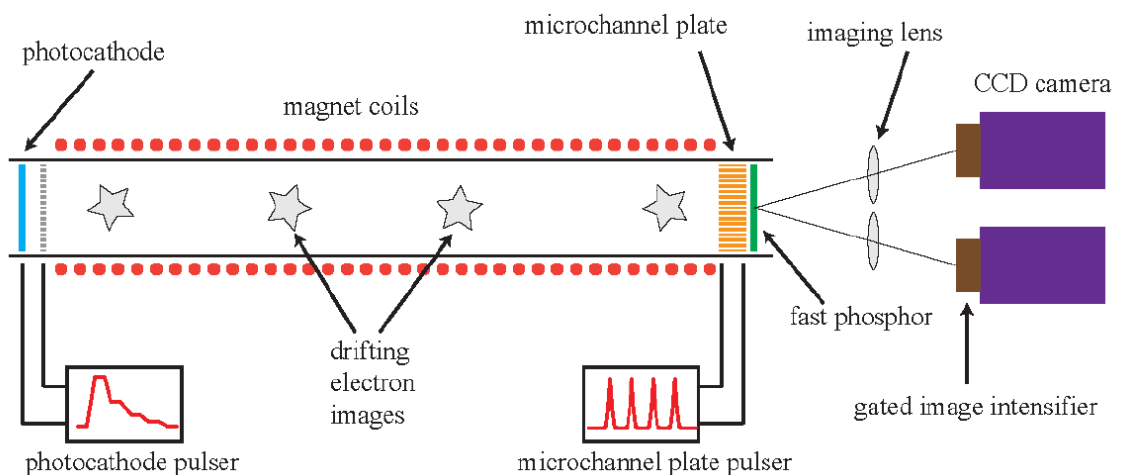


Figure 2.4 SLOS schematic

A fundamental limit on the frame rate comes from the maximum pulser potential ramp of 60 V/ps. The drift voltage of the first frame is proposed to be 2500 V and the drift voltage of the second frame will be defined by the drift length so as to comply with the 50 ns frame separation required at the fast phosphor.

For SLOS the 4 'frames' should be incident on the MCP around 50 ns in separation (each 'frame' is pulsed 100 ps apart at potentials that should lead to this condition), this allows time for the fast phosphor to decay. The limit of fast phosphor decay is the limit on frame rate.

Chapter 3

Application Requirements on Orion

Chapter 2 outlined the potential to have a very high temporal resolution x-ray framing camera, in Chapter 3 the justification for building such a diagnostic for the Orion laser facility is explained. The current suite of x-ray diagnostics at Orion is out-lined and their limitations are highlighted. Three key experimental aims, which are currently unachievable without PDI, are explained and the motivation behind achieving these aims is explored. Design specifications placed on an Orion pulse dilation imager are explained in the context of the three key experimental applications.

3.1. Justification for an Orion Time Dilation Imager (TIDI)

The Orion laser system at AWE includes a suite of target diagnostics to diagnose the plasmas produced by laser-target interactions. The target diagnostics are designed to record x-ray, optical and charged particle emission from laser-produced plasmas. A key subset of the x-ray target diagnostics covering temporal, spatial and spectroscopic domains is as follows:

- DANTE – Time resolved measurement of low-energy x-ray emission, for measuring target temperature in laser target interactions.
- HEX-ID – High resolving power spectroscopy of x-ray backlighter materials for measuring plasma opacity.
- FFLEX – diagnostic for measuring in the hard x-ray and bremsstrahlung spectrum, giving information of electron temperatures.
- HXRS – diagnostic for measuring in the hard x-ray and bremsstrahlung spectrum, giving information of electron temperatures.
- TLD ARRAY – an array of thermo luminescent dosimeters for measuring bremsstrahlung radiation dose level.
- GXD – A gated x-ray detector

This suite of target diagnostics allows measurements underpinning many detailed aspects of high density and energy physics such as equation of state measurements and opacity research, in the below table we can see the parameters of the current diagnostics (table 1). New technology is being sought to advance the capabilities of the Orion target diagnostic suite for capturing high speed phenomena. Plotting the temporal (fig 3.1), spectral (fig 3.3) and spatial (fig 3.2) resolutions of associated diagnostics in the current diagnostic suite enables determination of these capability gaps.

Experiments such as thermal emissions from microwire targets or the implosion of spherical targets have events that occur on a scale of 10s of ps (see table 2), these are difficult to image even with our highest temporally resolving camera (GXD). A pulse dilation (DIXI like) device is therefore proposed to cover that temporal range. The DIXI like device (TIDI: Time dilation imager), has the added challenge of needing to fit into a Ten Inch Manipulator (TIM), this is partly due to lack of space on Orion, but will also have the added benefits of portability and adaptability.

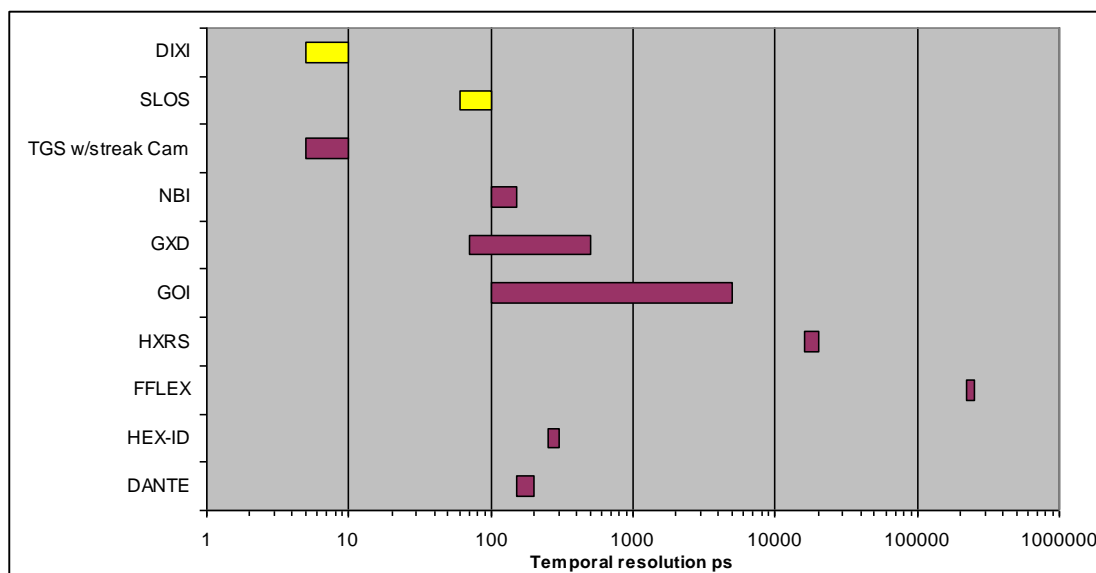


Figure 3.1 Temporal Capabilities of Orion Diagnostic Suite

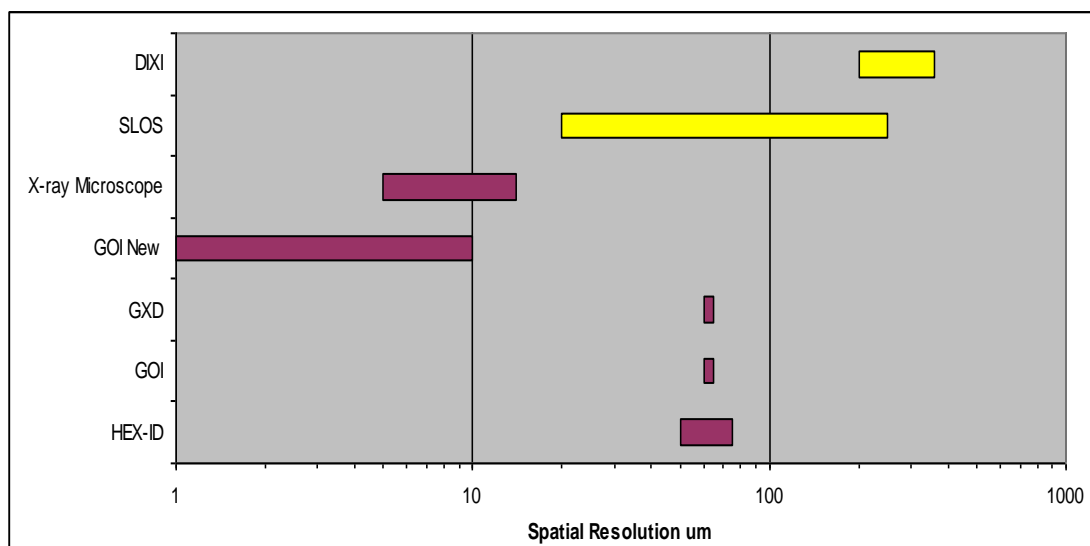


Figure 3.2 Spatial Capabilities of the Orion Diagnostic Suite

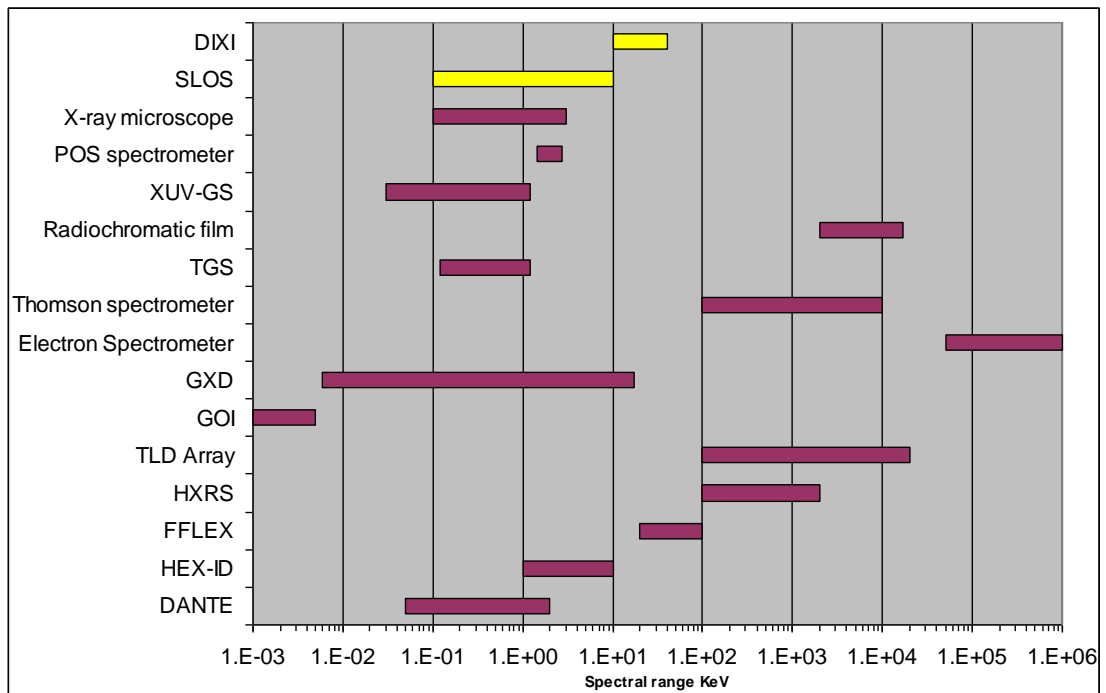


Figure 3.3 Spectral Capabilities of the Orion Diagnostic Suite

Figures 3.1-3.3 have SLOS and DIXI shown to hypothetically highlight the potential coverage of a time dilation image

Table 2 details the various experimental applications which benefit from high temporal resolution 2D imaging. Of the potential applications detailed in table 2, there are three principal experiments which will most define the design of an Orion TIDI. These applications will be explain in further detail here, they are as follows:

- Time resolved broadband x-ray diffraction
- Point projection spectroscopy
- UV colour temperature measurements

3.2. Time resolved Broadband X-ray Diffraction

Time resolved broad band x-ray diffraction has been used in an attempt to characterise the response of materials to dynamic compression loading. If a material is subjected to shear stress during compression along one axis, where the shear stress

is beyond the elastic limit, then relaxation processes will attempt to reduce the stress up until the “material strength” limit is reached. The material strength is a function of material parameters and the load parameters and is important when studying wave propagation, compression and hydrodynamic instabilities in metals. [10]

X-ray diffraction can be used to characterise the state of the shock compressed material. X-ray diffraction with the Orion BBXRD (BroadBand X-Ray Diffraction) is typically done with ~1-20keV x-rays and in time-integrated manner, the material is compressed and multiple planes in the crystal meet the requirements for Bragg diffraction which gives rise to a diffraction spot per plane. The location of the spot is dependent on the strain state of the material

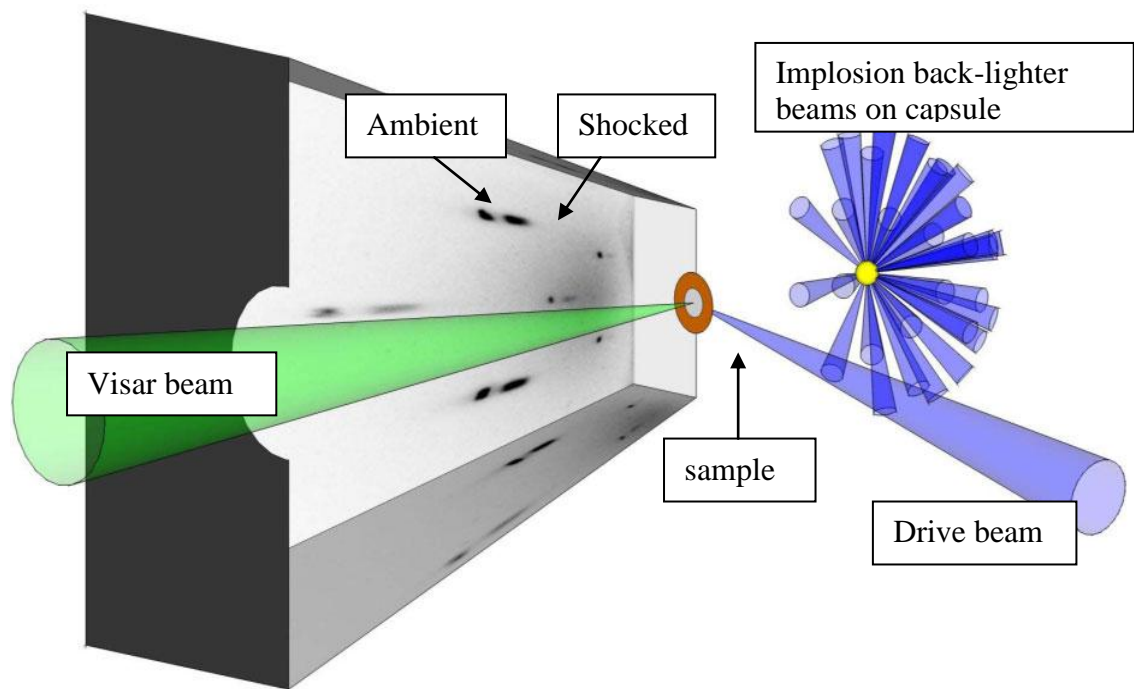


Figure 3.4 Current BBXRD arrangement

In a previous experiment the set up was a diffracted x-ray pattern recorded on image plate detectors set into a pyramid shaped enclosure (see figure 3.4) as the crystal is shocked the movement of the diffraction spots on the image plate is recorded [10]. The shift in spot position is a function of the aspect ratio of a unit cell in the crystal which has been compressed by the laser driven shock:

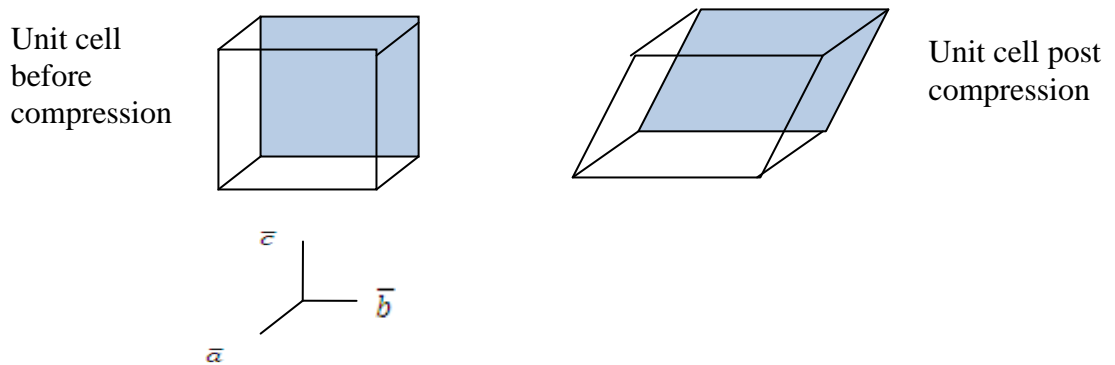


Figure 3.5 altering the unit cell aspect ratio

The aspect ratio is defined as:

$$\alpha = \frac{|\bar{a}|}{|\bar{b}|} = \frac{|\bar{a}|}{|\bar{c}|} = \frac{1 - \varepsilon_s}{1 - \varepsilon_T}$$

Equation 3.1

where $|\bar{a}|$, $|\bar{b}|$ and $|\bar{c}|$ are the unit vectors of the cell and ε_T and ε_s are the strains in the transverse direction and shock direction. In order to determine α Braggs law is used to fit the expected, uncompressed, diffraction pattern and establish the precise orientation of the sample and labelling each spot with their miller indices, with this known the compressed diffraction pattern can be fit using α as the fit parameter.

In the previous experiment no observable difference in strain as a function of time was found with 1 ns temporal resolution, also no evidence of a partial relaxed region was observed.

It was concluded that the time scale for the relaxation processes was much shorter than 1 ns (simulations suggest <5ps) which is why a very highly temporally resolved 2D x-ray camera would be a useful diagnostic for exploring this topic further.

BBXRD is currently recorded by an Image plate, this is a simple set-up that offers a high sensitivity and a wide detection area (giving a broad spectral range). Employing the TIDI in place of the image plate allows for time-resolved, as opposed to time-integrated, recording of complex x-ray diffraction patterns. Due to the smaller solid angle received by the photocathode (a result of geometric constraints and a limit to the physical diameter of the PC) when compared to the IP it is necessary to judge the relative sensitivities of the two methods

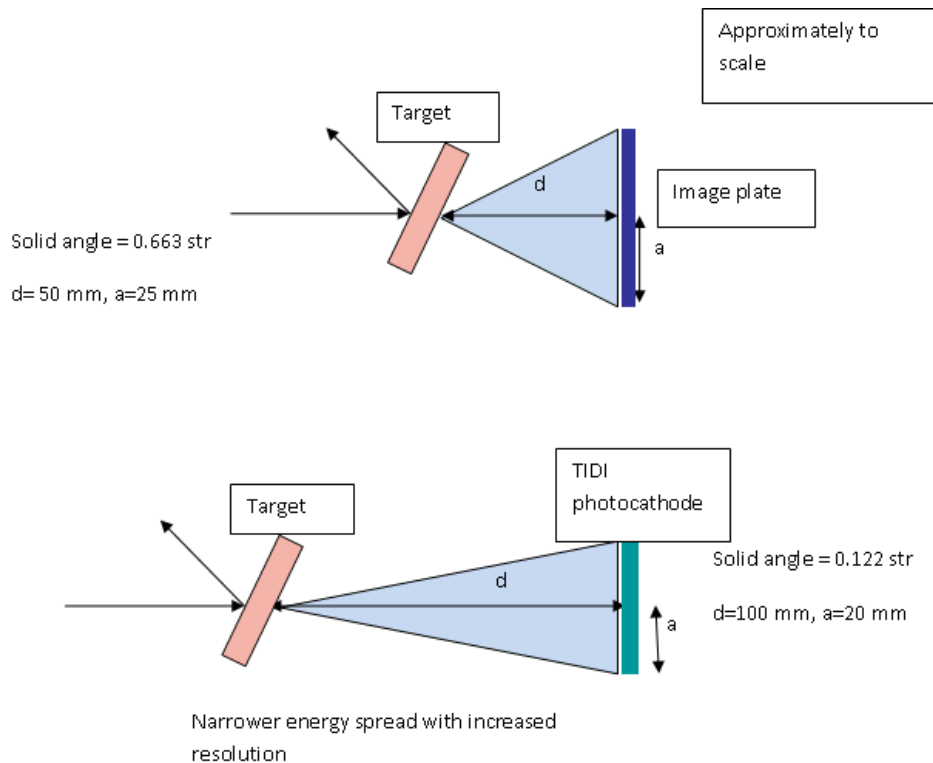


Figure 3.6 BBXRD scale drawings (accounted for source size in solid angle calculation and not assumed point source [24])

In order to make this comparison it is assumed that the photocathodes are similar in sensitivity to x-ray diodes (XRD); the photocathodes will be high Z so high Z x-ray diode data is used for this estimation. The IP sensitivity is measured in milli-Photo stimulated luminescence per photon:

$$IP_s = \frac{mPsl}{Photon}$$

Equation 3.2

The XRD sensitivity is measured in Amps per Mega Watt:

$$XRD_s = \frac{A}{MW} = \frac{Current}{Power} \times \left(\frac{time}{time} \right) = \frac{Charge}{Energy}$$

Equation 3.3

where energy is the total energy (number of photons multiplied by the quantised photon energy).

Calibration has been performed [25] that gives a common reference point between the total charge on an x-ray diode and the Psl seen by the Image plate at 6keV. This calibration found that the total charge on the XRD is 200 pC and the corresponding IP reading is 1.6 Psl.

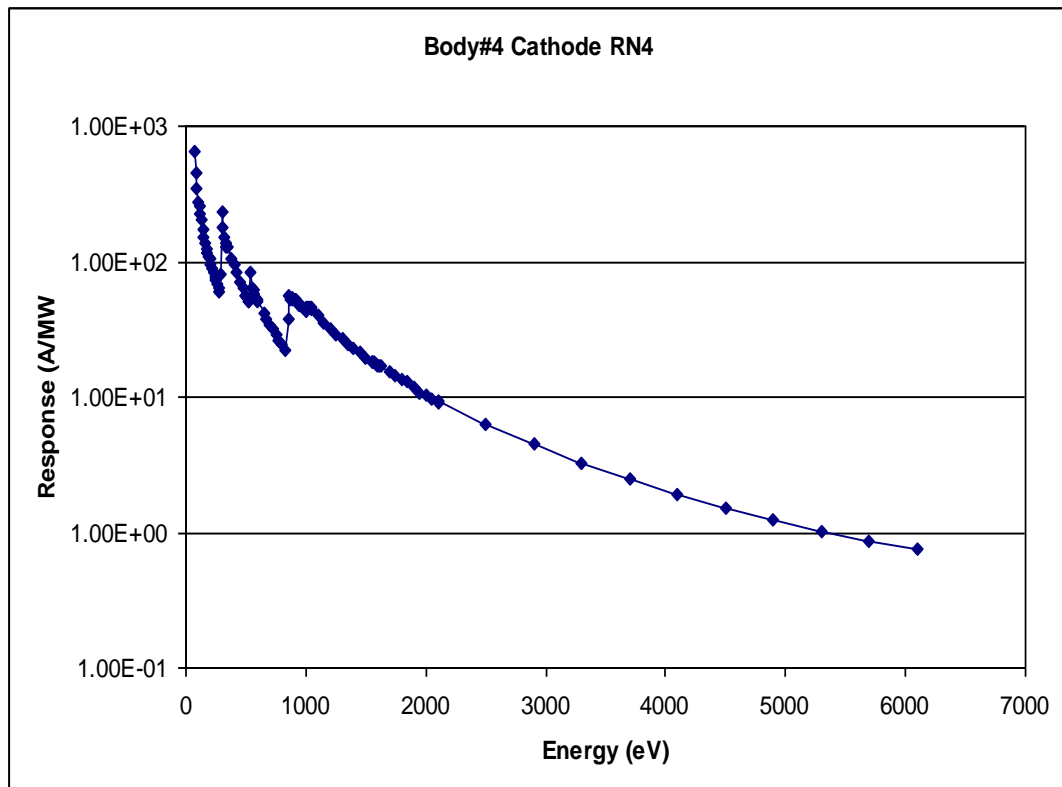


Figure 3.7 Nickel Photocathode Response Curve

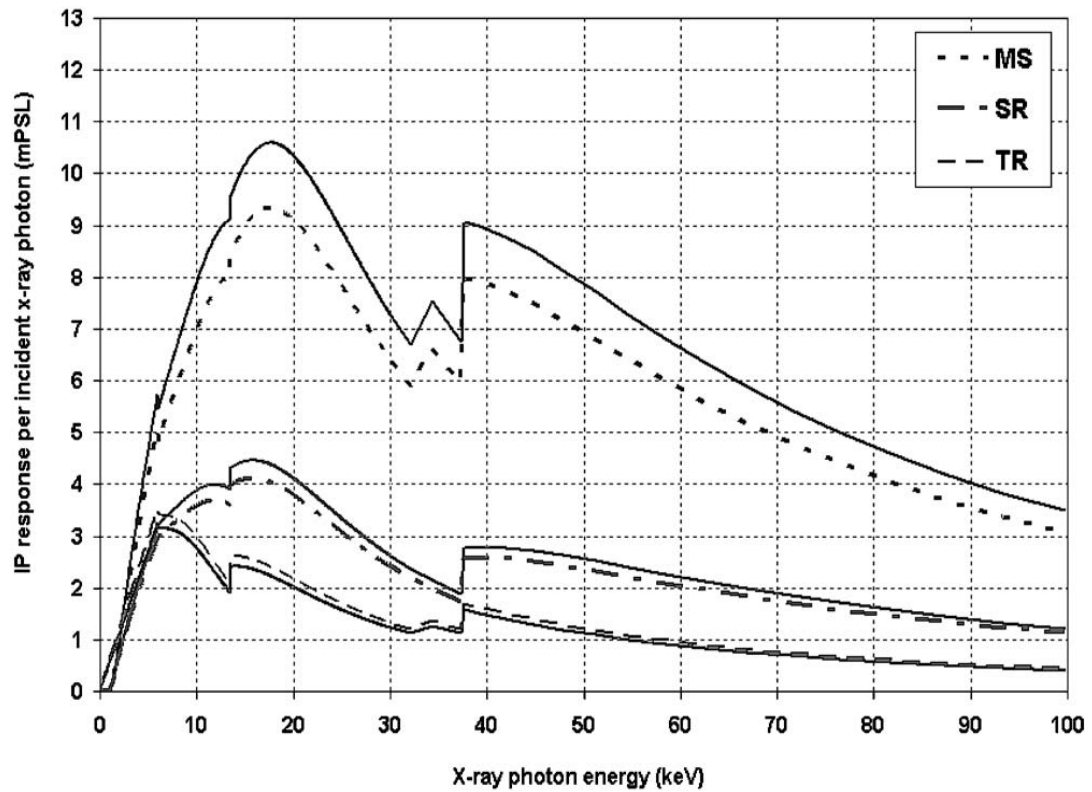


Figure 3.8 Fuji BAS Image plate Response Curve

Using two response curves common reference points R_{IP} and R_D are found at 6 keV, in order to find the number of photons detected by each device the following equations are used:

$$\frac{C_{IP}}{R_{IP}} = N_{IP}$$

Equation 3.4

$$\frac{C_D}{R_D} = E_T = N_D \times 6keV$$

Equation 3.5

Where C_{IP} = the calibration point of the IP (1.6 mPSl), C_D = calibration point on XRD (200 pC), R_{IP} and R_D = the reference points from the responsive curves at 6keV for the image plate and x-ray diode respectively, and E_T = total energy

Therefore the relative sensitivity per unit area can be found as:

$$\frac{N_{IP}}{N_D} = S_R$$

Equation 3.6

From figures 3.7 and 3.8 and the reference points can be established as $R_{IP} = 0.002$ Psl and $R_D = 0.8$ A/MW. Therefore the relative numbers of photons to produce equitable signal are: $N_d=260.06E-3$ photons and $N_{IP}=800$ E-3photons. So the XRD is ~3 times as sensitive as an image plate which seems a little low but suggests that the sensitivity reduction from a decreased area should be compensated by an increase in sensitivity.

3.3. Time resolved Point Projection Spectroscopy (PPS)

Fast time resolved 2D point projection spectroscopy is used for opacity measurements. PPS provides a measure of the radiative opacity by recording the absorption spectrum. Opacity plays an important part in creating radiation diffusion models in astrophysics and also is a critical component when trying to achieve indirect drive ICF.

When using a holraum (or other black body cavity) the high powered lasers ablate the inside of the cavity and that radiation is used to drive a fusion reaction.

Knowledge of material opacity is important because radiation from the plasma surrounding the capsule (which may have temperatures of the order of 10-200 eV) can be absorbed by the capsule shell, causing preheating.

The opacity of a material is a measure of its impenetrability to radiation. Opacity is a critical factor in ICF as the amount of energy absorbed by a D-T capsule shell must be accurately determined. In particular, it is important to observe how opacity changes over the very short time scales (10s of picoseconds) of the ICF implosions as even a small increase in opacity can have a drastic effect on the target performance and neutron yield [26].

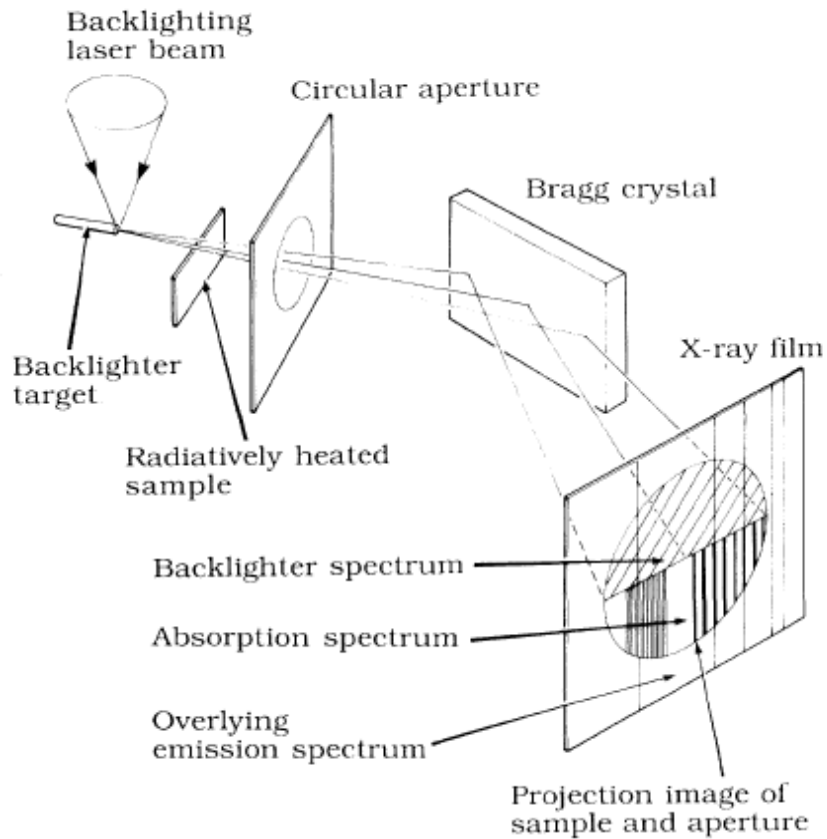


Figure 3.9 PPS with a flat dispersion crystal [27]

PPS involves backlighting a target with a laser beam to produce a well defined point source of x-rays which then pass through heated warm sample (often also allowing a portion of the x-rays as an un-attenuated backlighter spectrum). The x-rays are then spectrally dispersed, usually by a Bragg crystal, before being incident on a detector the position of which defines the magnification of the image and hence the spectral resolution.

Figure 3.9 displays an arrangement with a planar crystal and x-ray film for non-time resolved measurements of the absorption spectrum. This would be no good for observing dynamic effects which is the aim of these experiments.

Planar crystals are not the only dispersive element available. Using convex or elliptical crystals can bring the spectrum to a focus which could be placed at an

aperture in order to remove a substantial portion of the background emission spectrum noise.

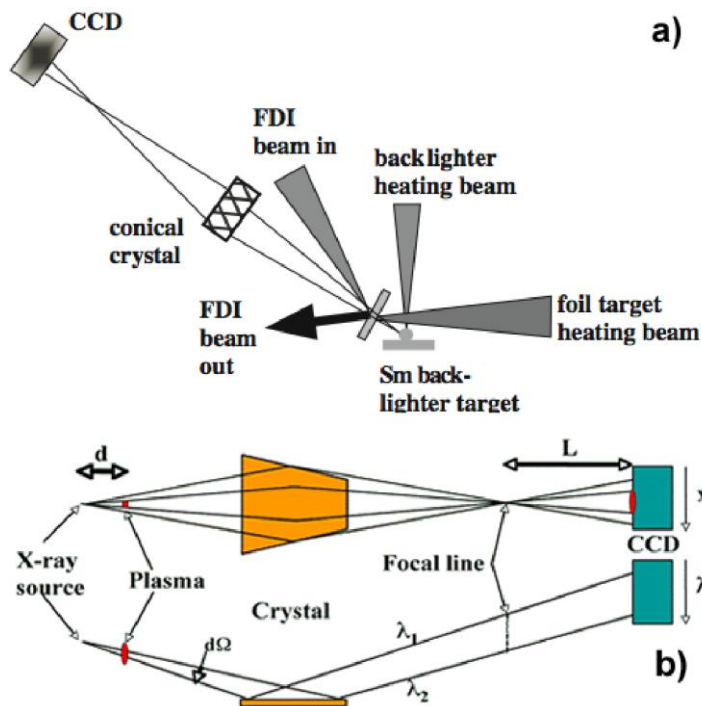


Figure 3.10 PPS with curved dispersion crystal causing a focus in the spectral output [28]

Figure 3.10 is taken from reference [28] which reports a study into the ionisation and recombination dynamics of transient aluminium plasmas over a picoseconds time scale. This was done by using two ultra short pulse lasers, one to pulse the backlighter and produce an ultra short pulse of x-rays, and one to create the thin dense plasma. The temporal information is probed by a frequency domain interference beam. The bent crystal allows for magnification (adjusting the position of the detector) while retaining the same wavelength range.

A curved dispersion crystal will probably be used with the Orion TIDI. The intermediate focus point will allow for pinhole filtering to protect the photocathode. The longitudinal movement of the TIM can then allow for an adjustment to the spectral resolution to suit purpose, see figure 3.11.

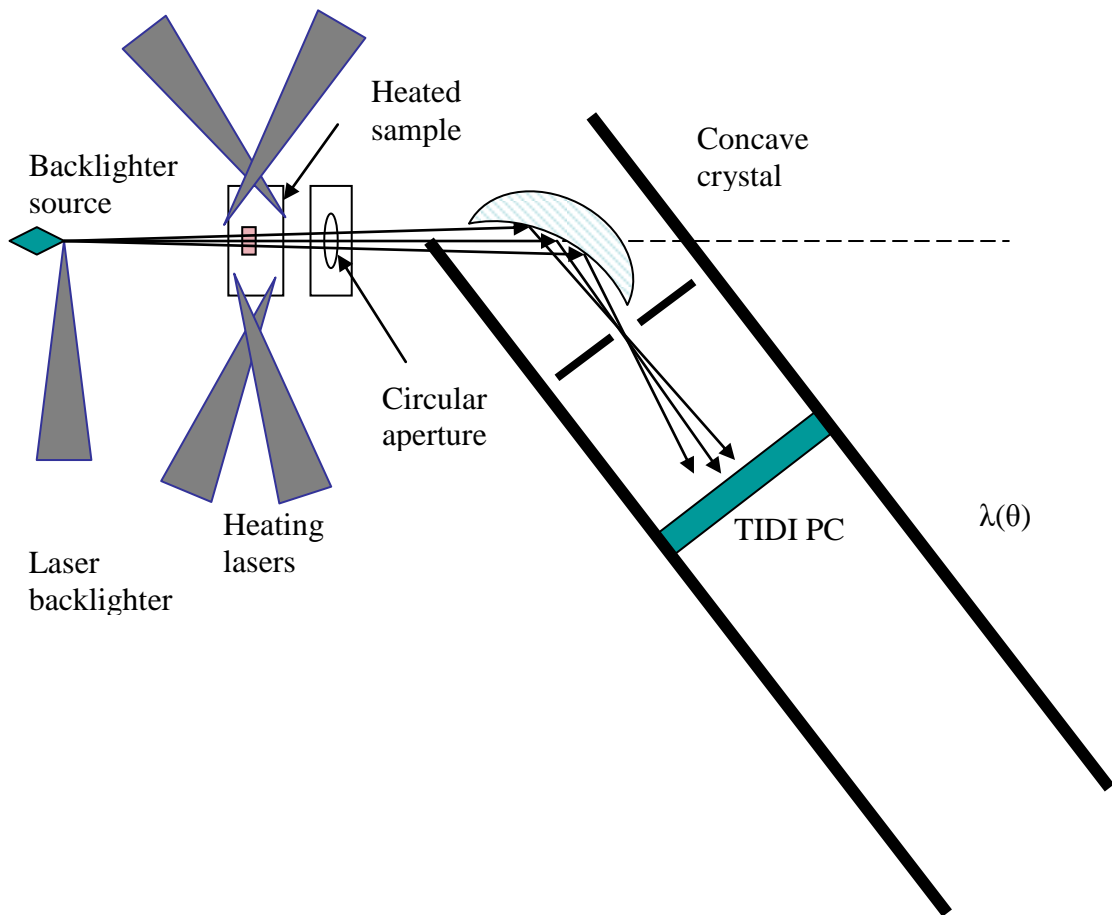


Figure 3.11 Potential PPS set up for TIDI with aperture

3.4. UV colour temperature Pyrometry

Laser driven shockwaves are of interest to HED physics as they are used to compress and heat material to high temperature and pressure states. The equation of state of a material is defined by the relationship between the state variables; the thermal state variables (temperature, entropy) and the mechanical state variables (pressure, density and internal energy) of a system in equilibrium. Shock wave experiments can be used to relate the mechanical state variables through measurement of shockwave and particle velocities. [29] [49]

As the material is heated it can undergo transitions, such as ionisation or phase changes. These transitions may lead to significant change in the thermal properties of

the system. Performing temperature measurements on shocked materials enables these transitions to be characterised. [48]

Optical and UV-XUV self emission from a shock wave can provide the thermal information needed in order to properly characterise the equation of state of a material. The shockwave temperature can then be inferred from this emission by comparing it to an equivalent Planckian radiator. The emission will occur over a very short period of time and will need a diagnostic capable of 1-10 picoseconds temporal resolution and a high dynamic range. The requirement for such high temporal resolution comes from the fact that emission can become shielded by surface blow off so the emission needs to be recorded before that point. The requirement for high dynamic range comes from the desire to be able to record preheating effects (on the order of 1 eV), as well as the main emission. 2D imaging would be valuable for the recording of hotspots on the surface. Such experiments are currently performed on Orion with a velocity interferometry system coupled with pyrometry in order to provide velocity and temperature measurements.

3.5. Summary of Application Requirements

Consideration of the performance of DIXI, the SLOS requirements, and potential applications of the TIDI summarised in table A.4 (appendix) have led to a set of achievable user requirements:

- X-ray sensitivity of 2 keV-60 keV interchangeable with a UV sensitive mode (covering spectral range required from user applications)
- High spatial resolution with up to 30 μm desired (especially for observing thermal emissions from microwire targets)
- Very high temporal resolution for 2D imaging with <10 ps
- A high dynamic range
- Compatible with a Ten-Inch Manipulator (TIM)
- Pointable to protect against straight-through x-rays striking CCD/CMOS
- Vacuum compatible
- Sufficient shielding to mitigate background signals and debris.

Chapter 4

Design limitations for the Orion Time-Dilation Imager

An analysis of the limitations of a time dilation device needs to be performed in order to establish that the experimental requirements set out in Chapter 3 are achievable. Using the equations from Hilsabeck et al [19] the fundamental limitations to the framing capability, temporal and spatial resolution of a pulse dilation device are estimated and presented.

4.1. Design limits to the Temporal Resolution

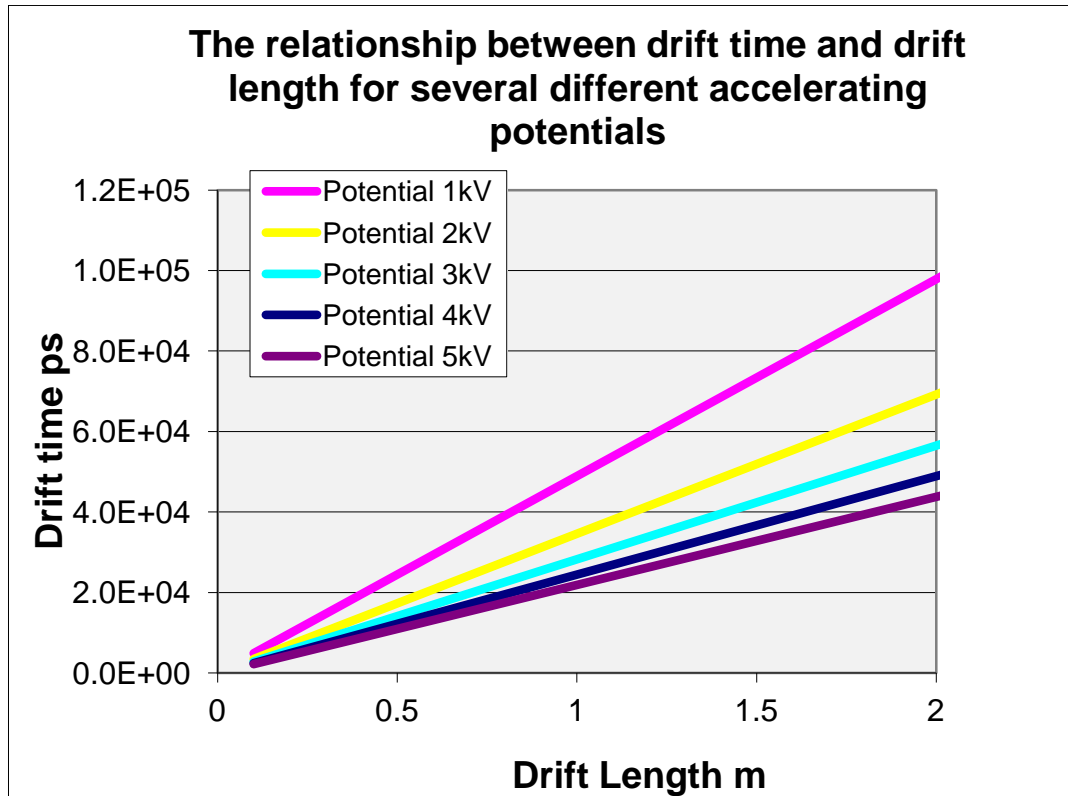


Figure 4.1 The accelerating potential's influence on a photoelectron's time of flight

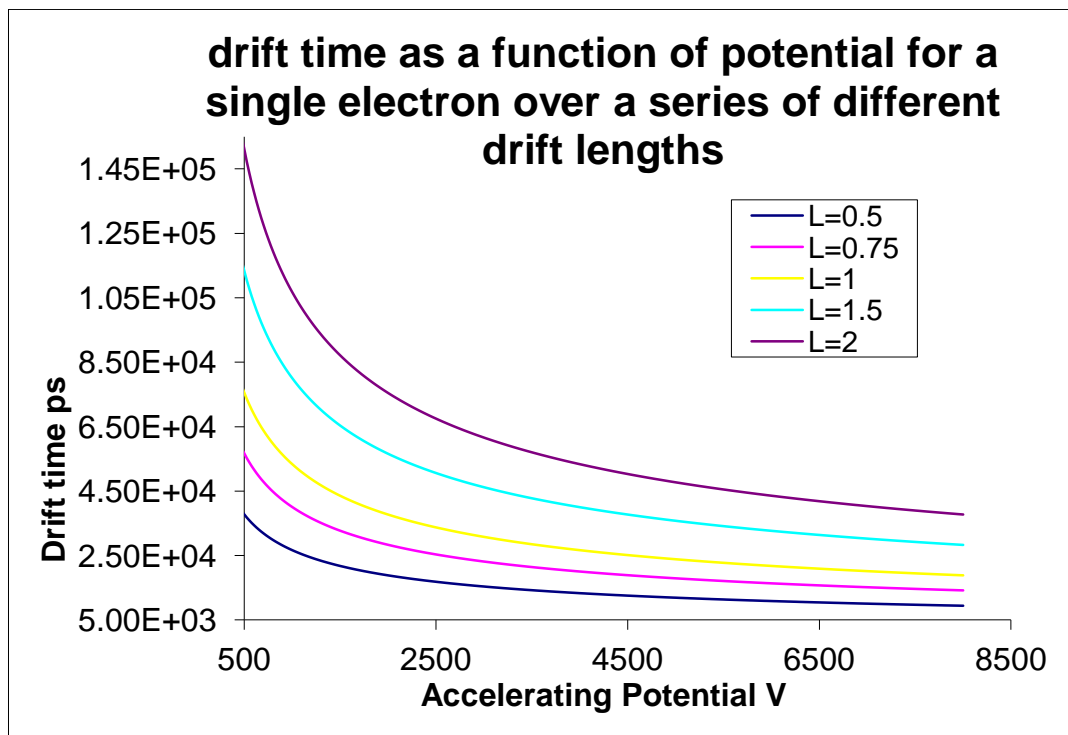


Figure 4.2 drift time as a function of Voltage for a series of drift lengths

Figures 4.1 and 4.2 show that a sweep at lower potential would lead to a larger disparity in the drift times as would a longer drift length. So we can conclude that one of the limitations will be a low voltage limit to electron drift and another will be a mechanical limitation in length. The lowest attainable sweep voltage is limited by space charge effects. A PIC code simulation ascertained that the lowest available sweep voltage is 100 V [23].

Ultimately the limit to the temporal magnification comes from the sensitivity of the detection end of the device; this will depend on the efficiency of the phosphor used and the number of photons required per pixel on the CCD/CMOS to record an image. Once a sufficiently sensitive enough detection end is used the temporal resolution becomes limited by the available space for a drift length and the gradient of the sweep across the photoelectron pulse.

4.2.Design limits to the Spatial Resolution

The Spatial resolution of a diagnostic device is the quadratic sum of the limiting resolutions of the individual components within the diagnostic [21] (see equation 4.1). Once the instrument's inherent resolution was established we also looked at how the resolution would be affected by the addition of front end optics.

$$\delta_{instr} = \sqrt{\delta_{PC}^2 + (\delta_{MCP} \times Mag_B)^2}$$

Equation 4.1 Instrument resolution [21]

Where δ_{instr} = the spatial resolution of the entire instrument, δ_{PC} = the spatial resolution at the photocathode, δ_{MCP} = the spatial resolution at the MCP, and Mag_B = Magnetic field component. In this equation the δ_{MCP} term is multiplied by a magnetic field component which takes account of any de-magnifying caused, in a 1:1 style diagnostic, $Mag_B = 1$

In the drift length the electrons are focused using a magnetic field, the transverse excursions of the photoelectrons therefore is what limits the spatial resolution at the PC (δ_{PC}) which is therefore limited to:

$$4r_L[\mu m] = 9500 \frac{\sqrt{T_e [eV]}}{B[Gauss]}$$

Equation 4.2

where T_e is the characteristic energy spread which is dependent on the material properties of the photocathode, and r_L is the Larmor radius.

And the system resolution will be:

$$\delta_{tot} = \sqrt{\delta_{instr}^2 + \delta_{Opt}^2}$$

Equation 4.3

where δ_{Opt} represents the resolution of the front end optical system, for example a pinhole. I performed work characterising an optical arrangement (see section 6.5) which would be a potential analogue for an arrangement used on a Orion TIDI. The spatial resolution of a potential front end optical system was established as $\sim 1.7\mu m$, when coupled with a time dilation imager with a 1:1 geometry this allows us to estimate the resolution of the entire diagnostic:

$$R = \sqrt{(1.7[\mu m])^2 + (\delta_{PC}^2 + \delta_{MCP}^2)^{1/2}}$$

Equation 4.4

Assuming a typical spatial resolution of the MCP to be $\sim 45\mu m$ [21] an estimation of the resolution of this instrument as a function of magnetic field strength can be found:

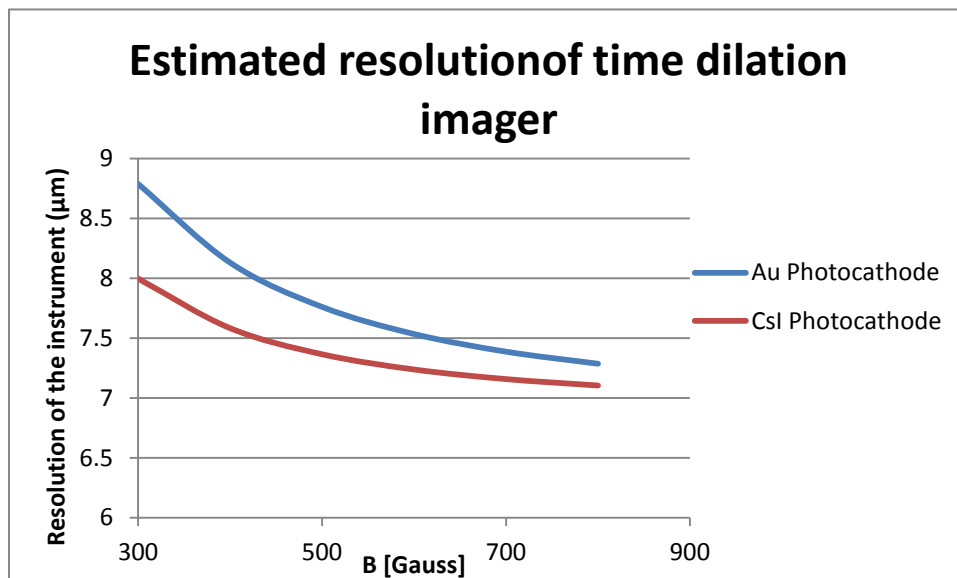


Figure 4.3 Resolution of the total system as a function of the Magnetic field

These are overestimations of the devices ability. In reality the front end arrangement of this system will be slightly different (see fig 6.22) with a 10x magnification as opposed to 12.5x. Therefore the resolution would need to take that into account. There is also the fact that this particular front end arrangement would only be applicable to UV imaging, however it acts as a good indication that the total resolution at the TCC could reach $\sim 10\mu\text{m}$.

In a paper by S. Nagel et. al. [20] detailing the characterisation of the DIXI a theoretical limit to the spatial resolution is postulated to depend on the electrons transverse excursions which in turn relies on 4 times the cyclotron orbits, this is dependent on the magnetic field, which we can vary, and the characteristic energy of the secondary electrons released at the photocathode, which depends on the material used for the photocathode. Displayed below are two dependences of spatial resolution on the magnetic field at the MCP for different PC materials. So limitations are also going to include the characteristic energies as produced by certain PC materials and the magnetic field that it is possible to obtain/maintain within a TIM/DIM.

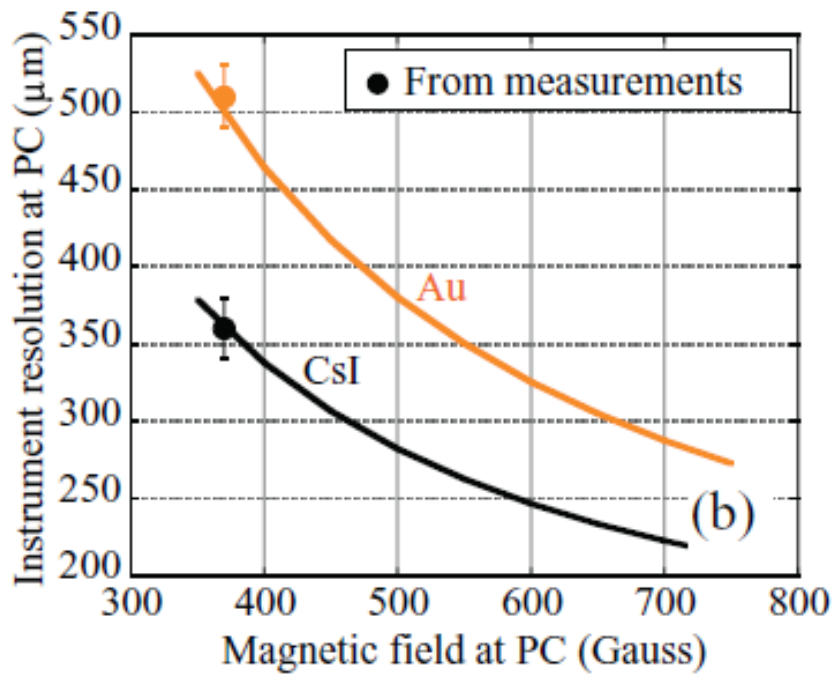


Figure 4.4 Resolution at the Photocathode as a function of the Magnetic field at the PC [21]

4.3.Design limits to the Framing Capability

A limitation particular to the single line of sight imager will be the efficiency of the phosphor. When the phosphor receives a frame it will take a certain amount of time to flash that frame out (around 50ns) so each frame must arrive at the MCP with an interval of ~50 ns to ensure that the phosphor is ready to receive the next frame. Therefore the efficiency of the fast phosphor is a limitation on the framing capability as well as the temporal resolution.

Consideration will need to be given to the voltage sweep. For a DIXI like instrument a smooth sweep in the potential would be used in order to dilate a single electron bunch:

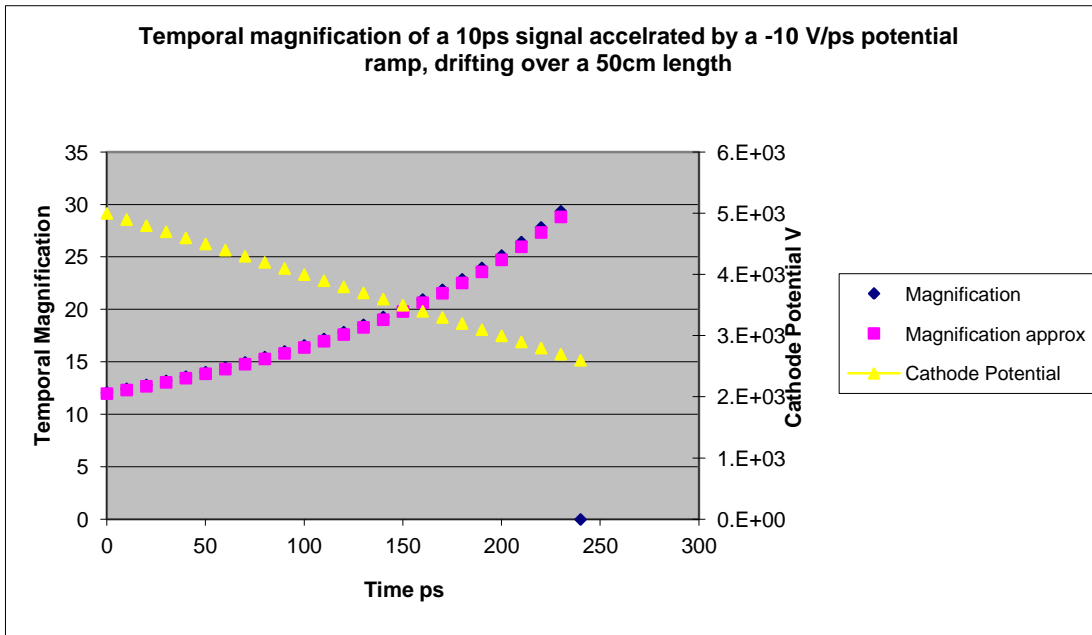


Figure 4.5, The temporal magnification provided by a -10V/s potential ramp over a 50cm drift space

If the dilation imager needs to separate frames in a manner similar to that of the SLOS then the pulse will need to be stepped. The pulse sweep then becomes dependent on the drift length; the SLOS was designed to produce four frames (50 ns apart for arrival at the MCP) in a 2 m drift length. However to increase the flexibility of the diagnostic it may be useful to install it in a DIM. The dimension then become slightly more limited. It is possible however to fit 3 frames into a 1.5 m drift length and may even be possible to have a fourth, although the gradient is becoming steep at that point and may lead to an unacceptable level of error:

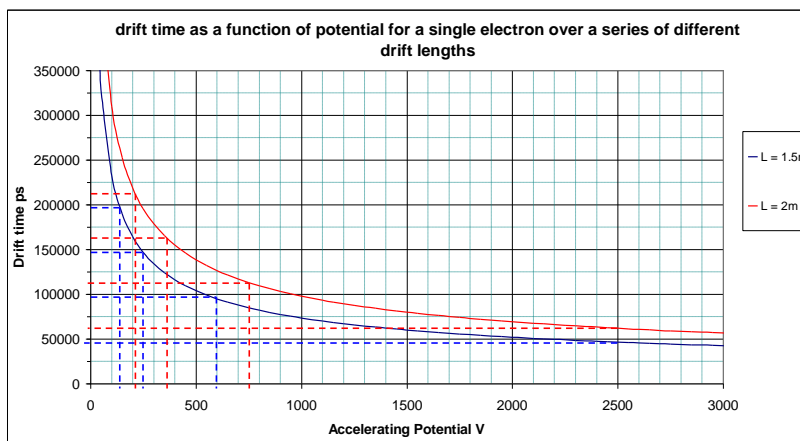


Figure 4.6 Prediction of the voltages needed for frame spacing for a given drift length

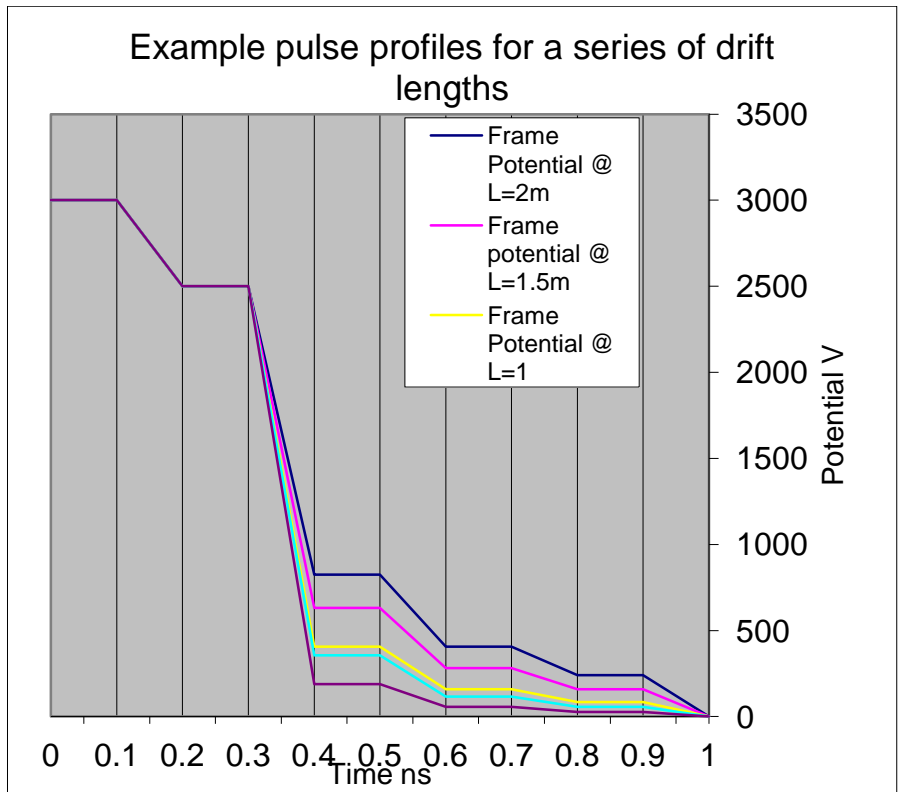


Figure 4.7 Example of several potential pulse profiles that achieve ~50 ns separation between frames at the phosphor

Taking an assumed maximum sweep gradient of -10 V/s, the maximum number of frames for a given drift length can be calculated:

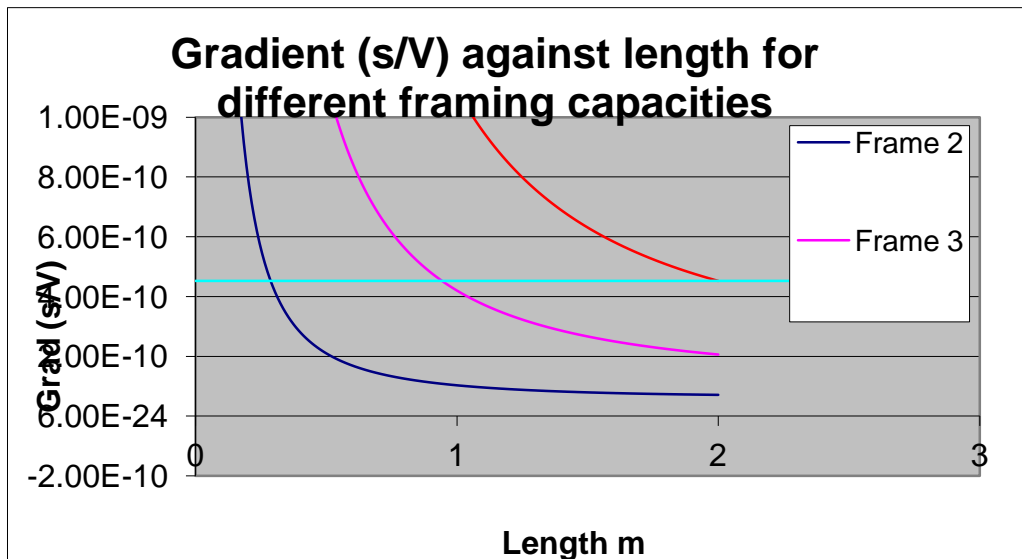


Figure 4.8 Minimum lengths required for number of frames due to the constraints of drift length, sweep gradient and minimum drifting voltage

This demonstrates that the minimum length for a 4 frame SLOS camera is 2m, 3 frames can be achieved in ~1m drift length and 2 frames in < 50 cm. This is based on a frame separation of 50ns at the phosphor.

Chapter 5

Design of the Instrument

This Chapter details the design of the proposed pulse dilation imager, the Orion TIDI (Time Dilation Imager). A basic analysis of the most likely components that would make up the Orion TIDI is presented. Each design decision has consequences which impact several other areas of the diagnostic so it is important to understand the physics behind each component in order to achieve the right balance for a diagnostic optimised to the key experimental applications.

The development of the final proposed design for the Orion TIDI was performed in close collaboration with Kentch Instruments Ltd. (see Acknowledgments). Three of the designs are presented towards the end of this chapter, each was analysed for strengths and weaknesses and then used to inform a successive design until all the design requirements were satisfied.

5.1. Basic component description and analysis

This section is a breakdown of the individual components which are most likely to make up an Orion TIDI, the physics behind how they work is described and the potential problems that could be encountered are explored. A basic schematic can be seen in Figure 5.1.

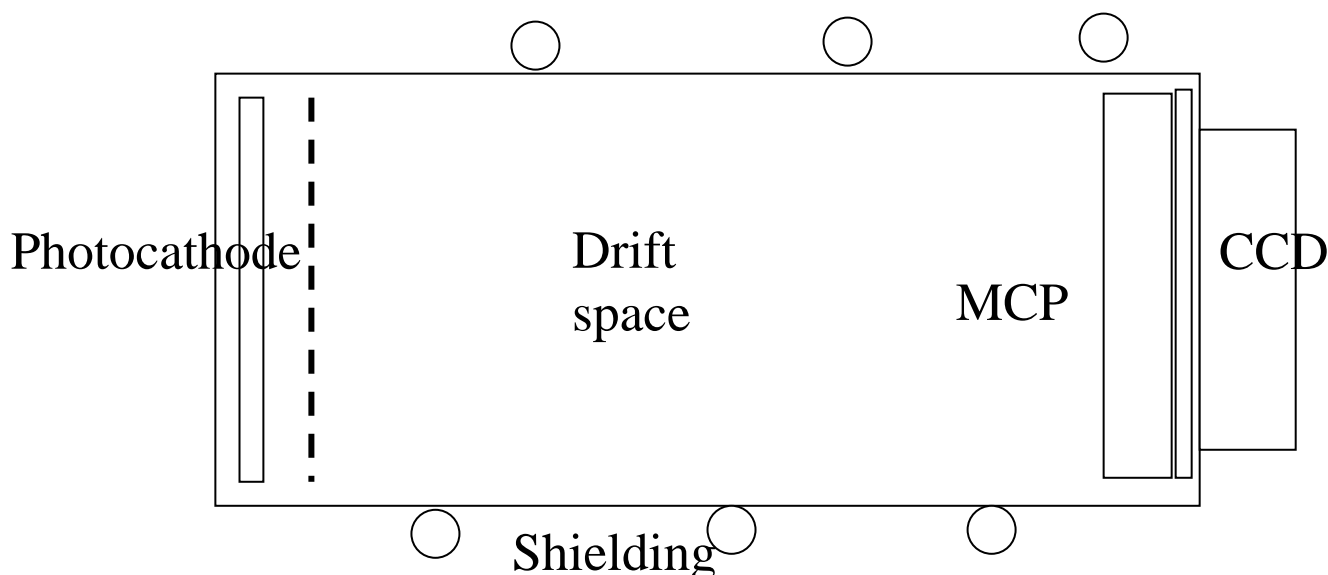


Figure 5.1 Schematic layout of a Time Dilation Imager

5.1.1. The Photocathode

The Photocathode is the first component activated in the diagnostic, it acts to capture the x-ray image and convert the photons into electrons so the image can be manipulated by electric and magnetic fields, all the while maintaining the image data.

Photocathodes work on the principal of the photoelectric effect which I will briefly recap here. The photoelectric effect is the phenomenon where high frequency radiation is incident on a metal and as a result the metal releases electrons. An increase in the amplitude of the radiation leads to a higher yield of electrons being produced, and increase in the frequency leads to more energetic electrons being released. This can only be explained by light arriving in quantised packets rather than a wave, this way an increase in amplitude = more photons and an increase in

frequency = higher energy photons ($E=hf$). If we progressively reduce the frequency of the incident radiation we reach a point where no electrons are produced (f_0), this allows us to characterise the material with a certain energy that is required before electrons can be emitted, this energy is known as the work function of the material. The work function is different for different materials and depends on the electron configuration, for example the alkaline metals have a low work function as their outer electron is easily liberated.

The Photocathode is a light detection device which utilises the photoelectric effect. The construction is usually a photosensitive compound coating on a material which either allows transmission (i.e. a glass window) or is reflective such as a metal. PCs operate under a vacuum and have an electric field and nearby anode to ensure the emission of electrons. The process of photo emission can be thought of in three steps: (1) initial absorption of incident photon and the transfer of the energy to an electron, (2) the migration of said electron through the material and to the surface, and (3) the escape of the electron from the material. During step 2 some energy may be lost due to electron-electron collision; if enough energy is lost the electron will be unable to overcome the work function and escape the photocathode surface, the rate at which energy is lost during electron migration defines the escape depth of the material (i.e. how thick it can be to produce electrons for a given frequency). [35]

Sensitive enough PCs can be affected by noise from spontaneous thermal emissions (this is especially prevalent in semiconductor material PCs), this is the effect of electrons escaping due to the thermal energy spread at room temperature providing enough energy (in the extreme upper end of the distribution) for an electron to overcome the work function. [35]

The sensitivity of the PC is usually quoted in Quantum efficiency:

$$QE = \frac{n_{eE}}{n_{pI}}$$

Equation 5.1

where n_{eE} = number of electrons emitted, and n_{pl} = number of photons incident. The QE is usually found to be ~20-30% due to the limitations detailed above. The QE of a photocathode is strongly dependent on the wavelength of the incident light which is related to the quantum energy as:

$$E = \frac{hc}{\lambda}$$

Equation 5.2

The QE of photocathodes can be broken down into a 3 step model known as the Spicer model (see figure 5.2). The first step of the Spicer model is the probability of the excitation of the electron through the photoelectric effect, this will depend of the fraction of absorbed light which in turn relies on the reflectivity of the material. The second step is the transition of the electron to the surface of the material, this is dependent on the likelihood of electron scatter throughout the material. Finally the third step is the electrons ability to escape the surface which depends most dominantly on the work function of the material.

All three steps must be achieved before the PC can release an electron, therefore the probability of achieving each step will contribute towards the overall QE of the PC. Below each step are the main probabilistic weights as established from a mathematical analysis in Knoll [35]. The integral over the product of all probabilities over all electron energies capable of escape gives a value for the QE of the photocathode.

Three Step Model of Photoemission

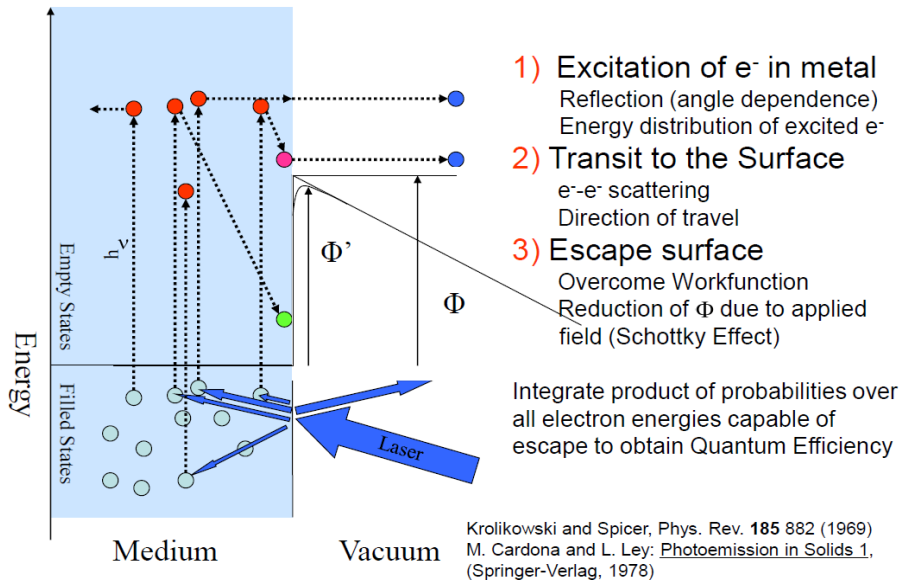


Figure 5.2 Photoemission schematic, Φ is work function [36]

The fraction of absorbed light:

$$\frac{I_{ab}}{I_{inc}} = (1 - R(\nu))$$

Equation 5.3

where I_{ab} =absorbed light, I_{inc} =incident light and $R(\nu)$ =optical reflectivity of metal

Probability of electron being excited to an energy E by a photon of energy $h\nu$:

$$P(E, h\nu) = \frac{N(E)N(E - h\nu)}{\int_{E_f}^{E_f + h\nu} N(E')N(E' - h\nu)dE'}$$

Equation 5.4

where $N(x)$ =number of electron states at an energy x , $E' = E - E_f$, and E_f = The Fermi energy.

Probability of reaching the surface without being scattered by other electrons

$$T(E, \nu, \theta) = \frac{\lambda_e(E)/\lambda_{ph}(\nu)}{1 + \lambda_e(E)/\lambda_{ph}(\nu)} C(E, \nu, \theta)$$

Equation 5.5

Probability of escape

$$D(E) = \frac{1}{2} \left(1 - \left(\frac{E_T}{E} \right)^{1/2} \right)$$

Equation 5.6

For small values of $E - E_T$, $D(E)$ is the dominating probability, so if we ignore the other two we can see:

$$QE(\nu) \propto \int_{\phi + E_f}^{h\nu + E_f} D(E) dE = \int_{E_T}^{(h\nu - \phi) + E_f} D(E) dE$$

$$\therefore QE(\nu) \propto (h\nu - \phi)^2$$

So the quantum efficiency is proportional to the square of the difference between the energy of the incident photon and the work function of the material [35].

The sensitivity of the photocathode is at one end defined by the work function as at sufficiently high wavelengths the energy imparted to the photoelectron is not enough for it to escape the PC surface. The limiting factor on low wavelength radiation (e.g. UV and X-ray) is usually not dependent on the PC itself but more on the window through which the light must travel before reaching the photosensitive area, for glass this is around 350 nm, for lower wavelengths special entrance windows must be made from fused silica or quartz. [35]

When assessing the potential of a photocathode there is generally a trade off between the photon interaction length and the electron escape distance (i.e. the thickness and thinness of the PC respectively). Another factor to consider is the skin depth; this is the ability of light of a certain wavelength to penetrate the PC medium, for shorter wavelengths this can be of the order of 10s of nanometers, so a thinner cathode is advisable for a short enough electron escape distance, however for longer wavelengths a thicker PC is required to increase absorption of the incoming photons. A thick cathode would be extremely bad for shorter wavelengths as the majority of

secondary electrons created near the window would not make it to the surface to escape [37]. There are potential issues with making a cathode too thin as thin cathodes tend to be resistive which can cause charge depletion and signal intensity distortion. [37]

The spatial resolution of a PC separated from the MCP is dependent on two factors; the material of the PC and the magnetic field at the PC. The material defines the characteristic energy spread of the photoelectrons emitted; paper by S. Nagel et. al.[21] compared the energy spreads of Au and CsI, it was found that CsI has a narrower characteristic energy spread and higher quantum efficiency (especially for high energy x-rays), with CsI having a characteristic energy spread of 1.7 eV whereas the Au PC has 3.5 eV. Within the magnetic field the transverse excursion of the electrons (which corresponds to the overall spatial resolution of the PC) is limited to 4 times their cyclotron radius (i.e. we cannot resolve lower than 4 times the radius of the orbiting electrons within the B-field):

$$4r_L = 95000 \sqrt{\frac{T_e}{B}}$$

Equation 5.7

This inversely proportional relationship between magnetic field and cyclotron orbit means that at a higher B-field we get a proportionally improved spatial resolution. [20]

There are potential issues which may need to be overcome in order for the photocathode to satisfy the application requirements, for example simulations suggest that QE drops off rapidly at $E > 10\text{keV}$. Using the example of the DIXI device, radiometric calculations indicate that a DIXI x-ray imager will require high energy PCs with a secondary electron QE of 5% to attain a SNR of 80, this QE is greater than the QE of solid CsI in the range of 10-30keV[38]

The photon energies received are expected to be $>10\text{keV}$ (range of 2keV-60keV). Photoemission quantum yield measurement data and photoelectron energy spectrum data are not currently available in this photon energy range. High efficiency PC materials require a high Z in order to stop the incident photons.

Improving the overall QE can be done through geometric techniques

A design was proposed in order to have a structure PC which would minimise electron escape distance and maximise photon interaction length. During characterisation of the DIXI it was found that PC flatness was incredibly important in order to correlate the time of images across the strip on the MCP and an even gap should be maintained between the PC and anode mesh, given these considerations a structured photocathode is probably not fit for our purposes. [38]

Using a similar theory a paper by Frumkin et al [39] found a sweet spot for PC thickness. Their study found that the QE of a CsI PC reached a maximum value around 300-400 nm for a range of 5.9-8 keV photons. It is hypothesised that this is due to the photons travelling a substantial distance into the PC and minimising the electron escape distance, too thin and the photon may pass through without absorption, too thick and the electron may struggle to escape without collision.

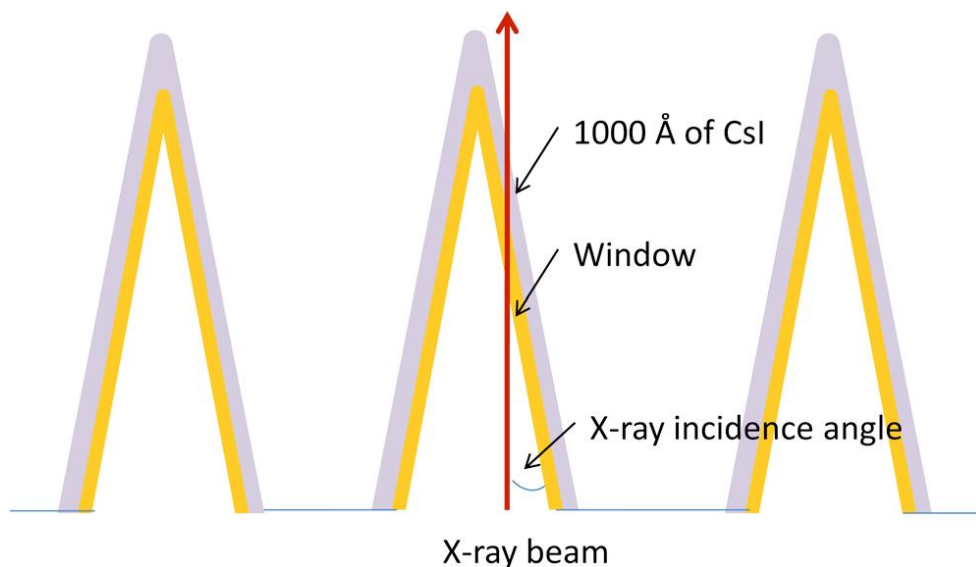


Figure 5.3 Potential enhancement of QE of PC by structuring in order to have an increased photon interaction length and minimised electron escape depth [38]

Another potential problem could stem from finite wavelength effects. The time varying accelerating potential causes a temporal spread in the photocathode output signal across the image plane. The effect is not present for static potentials (e.g.

streak cameras) and is a product of the RF excitement of the Photocathode. A simulation was performed to see how a pulse dilation imager would be affected by this effect. When the accelerating potential is at around 4150 V it was found that there would be a 48 V potential spread over a 5mm diameter circle on the surface of the photocathode, with a 10 V/ps ramp this corresponds to a temporal spread of around 5ps.[19] The design has to be constrained to minimise this effect: Image plane aperture size, the rate at which accelerating voltage can be ramped, and the maximum temporal magnification per unit drift length of the instrument all have to fall within certain parameters.[19]

In order to maintain an acceptable spatial resolution the transverse energy of the electron cloud is not too large, the magnetic field component of the RF electromagnetic wave can reach significant strengths which are able to impart transverse energy on the electron signal during the acceleration period. [19] In order to combat this one way of preventing the outcome is to reduce the magnetic component of the EM wave through deconstructive interference. There are several ways of achieving this, you could use an open transmission line or reflect the incident wave back on itself with the correct phase and polarisation to cancel out the magnetic component. Another way would be to use a duel injection set up and have the Photocathode excited by colliding pulses. Alternatively use an RF excitation signal that has zero net current at the gating time, this can be achieved by the capacitive coupling of a monocycle onto a static dc voltage that is equal to that of the drift voltage [19].

The TIDI will be fielded for a wide range of experiments, some of which extend into the UV spectrum; the CsI cathode which would be used for x-ray detection would have little effect in this range, therefore it will be necessary to have more than one photocathode material available. An interchangeable photocathode or a multi element PC would be needed to cover the full spectral range set out in the desired specifications. Au would be suitable for UV measurements while CsI is a well tested and reliable PC for x-ray detection.[40][38]

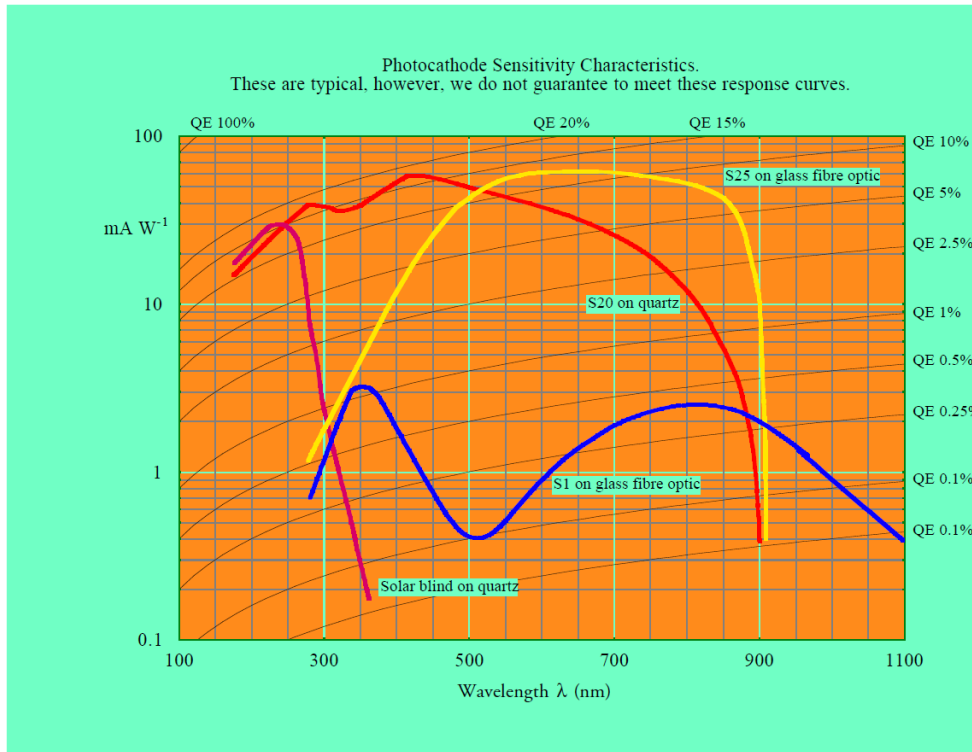


Figure 5.4 Example of QE for a selection of PC materials [12]

5.1.2. MCP-Phosphor as an image intensifier

A microchannel plate can be considered as a planar array of photomultiplier tubes. It acts to intensify single photons through the conversion to and multiplication of electrons through the photoelectric effect and secondary emission effects respectively. The design of the channels can be straight (which has a danger of letting electrons pass un-intensified), curved/slanted or chevron design. The chevron design is useful as it gets a significantly higher gain than the other two designs, however this comes at the cost of an increased transition time. The multiplied electrons are then incident on a phosphor. A phosphor is a planar scintillator which acts to convert the electrons in to a visible/detectable photon signal.

The spatial resolution depends on pore diameter, C-C spacing (centre to centre) and electrode depth penetrating into the MCP. Spatial resolution also is highly dependent on the gap between the MCP and the phosphor, the radial spread of electrons out of the back of the MCP is far higher than out of a photocathode and is one of the largest

contributors to degrading the spatial resolution. The temporal resolution of an MCP depends on the transit time of the electron through the pores and the thickness of the plate, more specifically the ratio between pore length and pore diameter and the applied voltage. [41] From earlier defined values; the Orion TIDI will require a spatial resolution of $\sim 30 \mu\text{m}$ and a temporal resolution of $< 10\text{ps}$. The device will need to be sensitive to x-ray light in the range of 2-60 keV and also be sensitive to the UV light region.

For an SLOS imager the flashing out of the frames must be temporally separated by at least the transit time of the electron bunch through the MCP, pulse dilation is used to separate frames taken 100ps apart to higher than the MCP transit time, the longer the transit time, the more dilation required. A small transit time is highly beneficial as it would allow us to slightly reduce the drift length (necessary for compatibility with DIM) and decrease the required pulse dilation time (which should increase the spatial resolution).

The MCP-Phosphor component will be the limiting factor in resolution and if the pore size or transverse energy spread is too large the spatial resolution of the diagnostic will never be any better than that. The gap between the MCP and phosphor is crucial and the smaller it is made the better the spatial resolution as this would allow less time for signal spreading before being recorded by the CCD.

The temporal response of the MCP-phosphor is also important as it will define the framing capability of a single line of sight imager. The phosphor has to be efficient enough to detect single photoelectrons but also be fast enough to process a signal and be ready for the next within 50ns. In general fast phosphors tend to produce short wavelength light, a CCD will couple less efficiently with these wavelengths which would lead to a reduction in the dynamic range of the diagnostic. Estimations made by J. Hares at Kentech [23] predict that a 40ns phosphor would require $64 \times 8\text{keV}$ electrons to guarantee the CCD records a signal and that around 22000 electrons can be produced per resolution element (from the MCP) this leads to an estimated dynamic range of 300.

Research has been performed into reducing the transit time through an MCP to produce a camera with 30-40 ps framing times [13]. This was done by reducing the thickness of two MCPs, one with a standard pore aspect ratio ($L/D = 40$) and one with a reduced pore aspect ratio ($L/D = 20$), L = length of the pore, D = diameter of the pore. The transit time through an MCP has been shown to scale as:

$$T = \left(\frac{m}{eV} \right)^{0.5} L \left(\frac{L}{D} \right)^{0.5}$$

Equation 5.8

where m =mass of electron, and V =applied voltage. The transit time, and hence the minimum gate width, can be reduced by decreasing the aspect ratio or increasing the applied voltage. It must be noted however that decreasing L/D will lead to a decrease in gain; this puts a limit on how thin you can make the MCP and still get useful gains.

Modelling predicted that the $L/D=40$ would not give sufficient gains when coupled with a lower voltage pulser, for similar voltage pulses the gate times for $L/D=20$ are longer than those for $L/D=40$, this is down to the reduction in L/D being offset by the reduction in the gain narrowing caused by a non-linear gain/voltage curve. The modelling predicts achievable gating times of 30-40 ps. These gating times were demonstrated in practice by measuring the temporal response (FWHM) of each detector pulser combination using a ~200nm, picosecond-duration laser pulses. As predicted the gate widths decrease with bias voltage and the shortest gates are achieved using $L/D=40$, although both aspect ratios are shown to be able to reach 30-40 ps resolution. [42]

One very simple way to remove any issue associated with the MCP is to find a way that the device can function without it including any reduction in spatial resolution. Recently a group at Sandia labs has developed a CMOS capable of ns interframe spacing and direct electron detection. This is achieved by storing the image in capacitors just behind the pixels allowing that pixel to be ready to receive the next

signal before the preceding one has been processed. This would allow more frames with a shorter drift length, the drift length available in the TIM is too short to separate frames by the 40-50 ns required by an MCP-Phosphor, however if the frame separation at the detector need only be a few ns then a TIM based diagnostic could easily support a 4 frame single line of sight mode. This is still in the early stages of development but if this technology comes to fruition then it will likely replace the entire back end of the TIDI diagnostic.

Another option, and one which could potentially act as a placeholder while the ns framing camera is being optimised, is to have just the phosphor and a accelerating region just before it. This region of acceleration will act as the gating mechanism by ensuring only signal that is desired will be accelerated to above the phosphors threshold for detection.

5.1.3. CCD/CMOS sensor

A CCD (charge-coupled device) works on the principle of the photovoltaic effect (much like a solar cell), pixels convert light into electrons and the charge is then carried across the chip and read in the corner of the pixel array. An analogue to digital converter produces a digital signal for each pixel.

A CMOS (complimentary metal-oxide-semiconductor) also works on the principal of the photovoltaic effect, by converting light into electrons, here though each pixel has several thousand transistors and the charge is moved through wires.

In order to establish that a CCD/CMOS detection end was the optimum arrangement I had to consider the benefits when compared to other methods, such as x-ray film or image plate. I considered efficiency (which is reliant on sensitivity, signal capacity and noise susceptibility), sensitivity range (largely dependent on material), and image quality (in its ability to reduce the effects of motion blur via high speed shuttering and exposure control). Within these categories CCD/CMOS devices are generally of a similar standard to x-ray film and image plate. Taking into account the

added convenience of receiving an instant image (no need to spend time developing film or scanning plates) CCD/CMOS devices seem a much more favourable choice.

CMOS and CCD are both silicon based constructions with pixel based architecture; therefore the sensitivity range is very similar. CMOS is able to integrate circuits that perform other camera functions (e.g. noise reduction) directly onto the chip, this reduces cost and power consumption but it also can reduce the fill factor (which is 100% in a CCD). [43]

The dominant source of random noise tends to be the pixel itself, this is increased in CMOS when any additional transistors are added, however the functionality of this extra circuitry often outweighs the detrimental effects of extra noise. [44] CMOS also has an advantage in that it has excellent anti-blooming properties with the transistor at each pixel offering a path to remove excess charge which would cause a blurred effect on the image.

5.1.4. Drift region Manipulator

The purpose of the drift length is simply to allow the pulse time to dilate, it is not a necessary component for imaging and will only act to degrade spatial resolution. To combat degradation in signal the drift length needs to be held under a vacuum, while traversing the drift space transverse electron motion will be kept to a minimum with a strong magnetic field produced by solenoid coils.

The Length of the drift length is the key parameter for this section, it will need to be long enough to accommodate the required spreading of the signal, but not be so long to either not fit in the TIM or cause the signal to become dominated by space charge effects.

The dimensions of the drift length are mainly set by the dimensions of the Orion TIM payload. The TIM length is ~1538 mm with a square cross-section of 180.2wx169h mm. Given room required for solenoid pulsers and other electronics this leaves a maximum drift length of around 40-50cm with a lateral geometry. The dimensions

are fixed and along with the limitations of the pulser (due to space charge effects, see section below) will go on to define the number of frames and temporal resolution available.

In order to produce a good quality image there needs to be sufficient signal per pixel. One of the effects of high photocurrent density is the presence of space charge effects (repulsion within the electron cloud) which will cause axial as well as temporal spreading. If this spread becomes comparable to either the inter-frame spacing or the period between gates then the frames could overlap. Also the transverse repulsion could lead to a reduction in signal per pixel and hence the dynamic range of the device. An analysis of the DIXI suggests that a dynamic range of around 300 counts is required [21], a PIC simulation performed by Kentech found that ratio of the dispersion caused by space charge ($Dt_{\text{space charge}}$) over the dispersion caused by the applied velocity gradient over the signal (Dt_{frames}) is a figure of merit which is independent of drift length which can be used to assess the maximum dynamic range for a given drifting voltage. For a pixel size of $20\mu\text{m} \times 20\mu\text{m}$ and a pulse of 100ps, a dynamic range of 300 counts can be achieved if the accelerating voltage remains over 100 V. [23]

5.1.5. Shielding

Electromagnetic pulses (EMP) are a result of high power laser integrations with matter causing a charge imbalance across the chamber. When high powered lasers are incident on a material that material will release electrons, if a direction of electron emission is favoured this can lead to a charge imbalance, since the EMP is proportional to the number of electrons emitted we can predict how much of an issue this is going to be based on the energy ranges proposed. If the energy range remains 1-100 keV then only a small number of electrons should be produced and EMP should not become a problem.

Any TIM based diagnostic will be subject to a radiation field due to close proximity to the target chamber centre (TCC), and will also have to contend with debris and

high energy photons. The neutron yield for the experiments proposed at the Orion laser facility is not expected to be large enough to damage the electronics so they can be housed within the TIM without much concern.

Apertures can be used to limit damage from debris.

Electromagnetic (EM) interference may cause an issue with the electronics on the device. To date no EMP issues have arisen in the fielding of the DIXI at LLNL (Lawrence Livermore National Laboratory) which has been subjected to a far higher EMP environment than would ever be expected at the Orion laser facility. However if EMP does become a problem it would be advisable to encase the entire diagnostic in a conductive material (e.g. Aluminium) to act as a Faraday cage in order to protect the electronics.[45][46]

5.2.Development of the Orion TIDI

The schematic below (fig 5.5) displays the number of design variables which have an impact of certain areas of performance. Table A.5 (appendix) provides details of key variables on the design of the TIDI, the benefits and drawbacks of which have been determined through a number of discussions with Kentech Instruments Ltd.

Discussions are ongoing with both General Atomics and Kentech on full layout for the TIDI diagnostic.

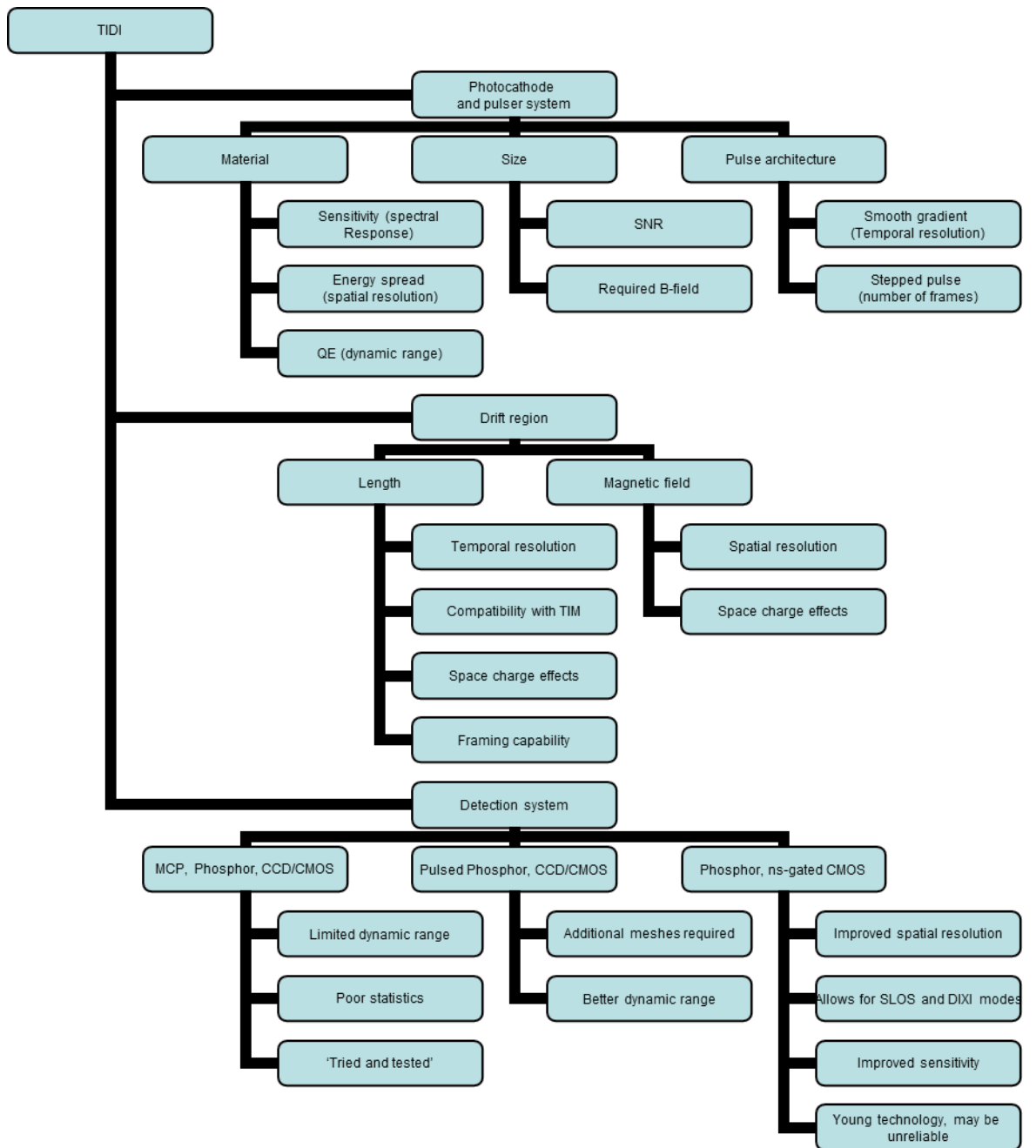


Fig 5.5 Variable-Design dependent

The TIDI has been through a few design iterations following research on the key variables for a pulse-dilation instrument as outlined in table A.5 (appendix), and identification of the techniques that would be used in the key experimental applications for the TIDI. The reasoning and progression of each stage up to the latest design will now be described.

5.2.1. TIDI 1: SLOS design with oblique transmissive photocathodes

The motivation behind TIDI 1 was to make a device compatible with the TIM. In addition to there being a lack of space on Orion for a port-mounted diagnostic (as mentioned in intro), the benefits of fitting a diagnostic within a TIM include; increased portability, pointing accuracy and the ability to point off TCC, lateral movement which can help adapt to a range of applications, and ease of access for changing components (for example the photocathode).

This design is a development of the basic SLOS design (see literature survey) which utilises two staggered transmissive photocathodes arranged to intercept a single line of sight x-ray signal. The four meshes will provide four different potential differences which accelerate the four frames at different speeds in order to separate them at the MCP/Phosphor. The pulses could be ramped in order to provide temporal magnification but as it stands in this design the temporal resolution is four frames separated by 100ns

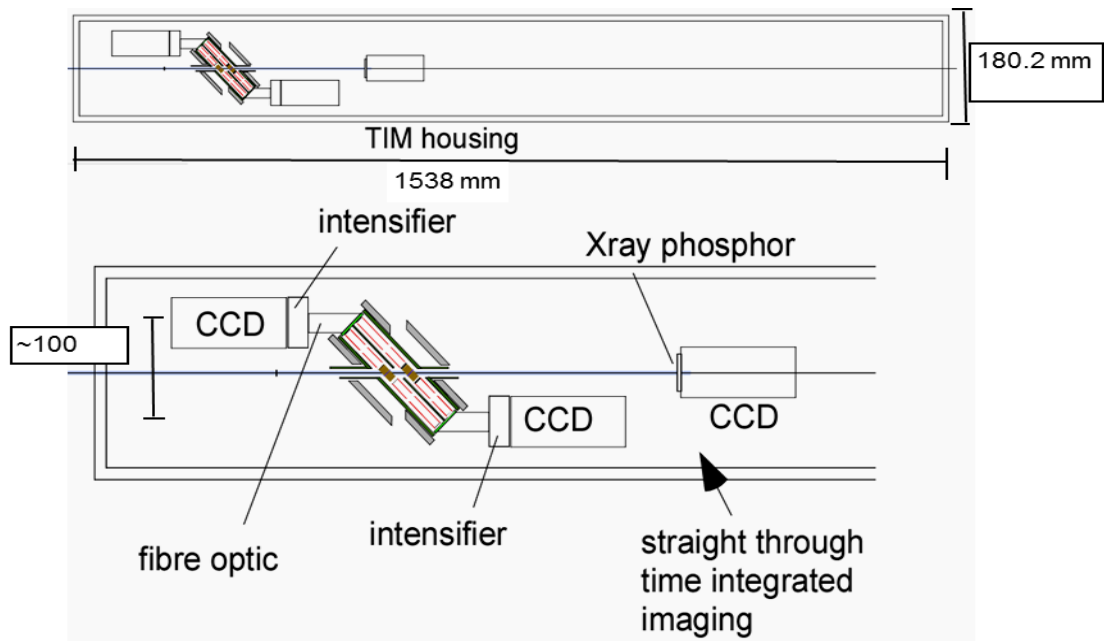


Figure 5.6 TIDI 1 design

This design is proposed for a time dilating diagnostic that will be compatible with a DIM, a DIM has a substantial larger cross section than a TIM so the drift length and photocathode size would be more limited for the TIDI. The maximum drift lengths would be limited by the width of cross-section of the TIM, using TIM dimensions and estimations of the size of CCDs and other components we can establish roughly how much space would have to be given up within the TIM for a certain drift length:

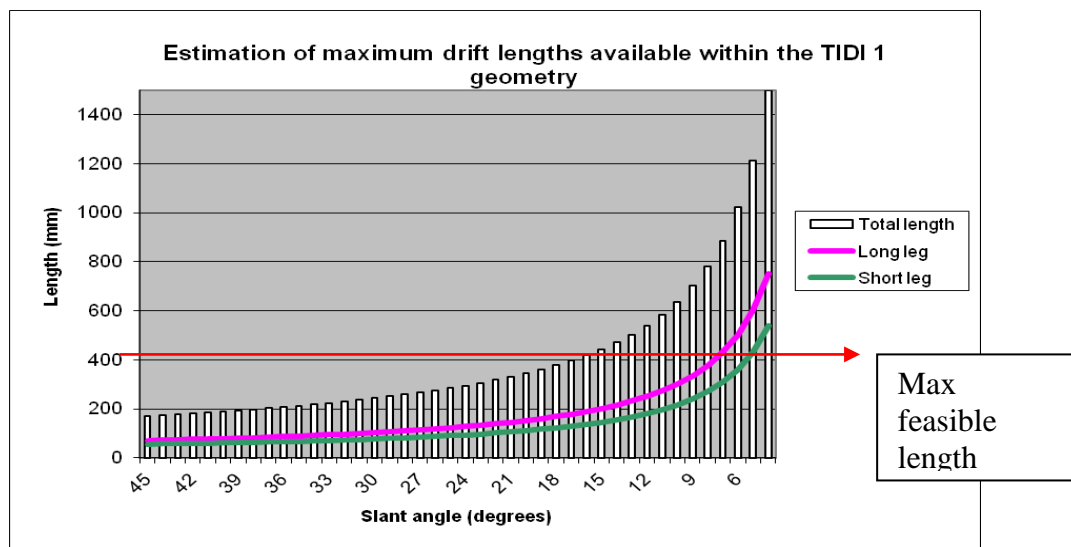


Figure 5.7 'Short leg' refers to the shorter of the two slanted drift regions, and 'long leg' the longer.

The drift time can be calculated for these lengths as a function of voltage and it can be shown that a frame separation of 50ns at the phosphor is possible within small lengths:

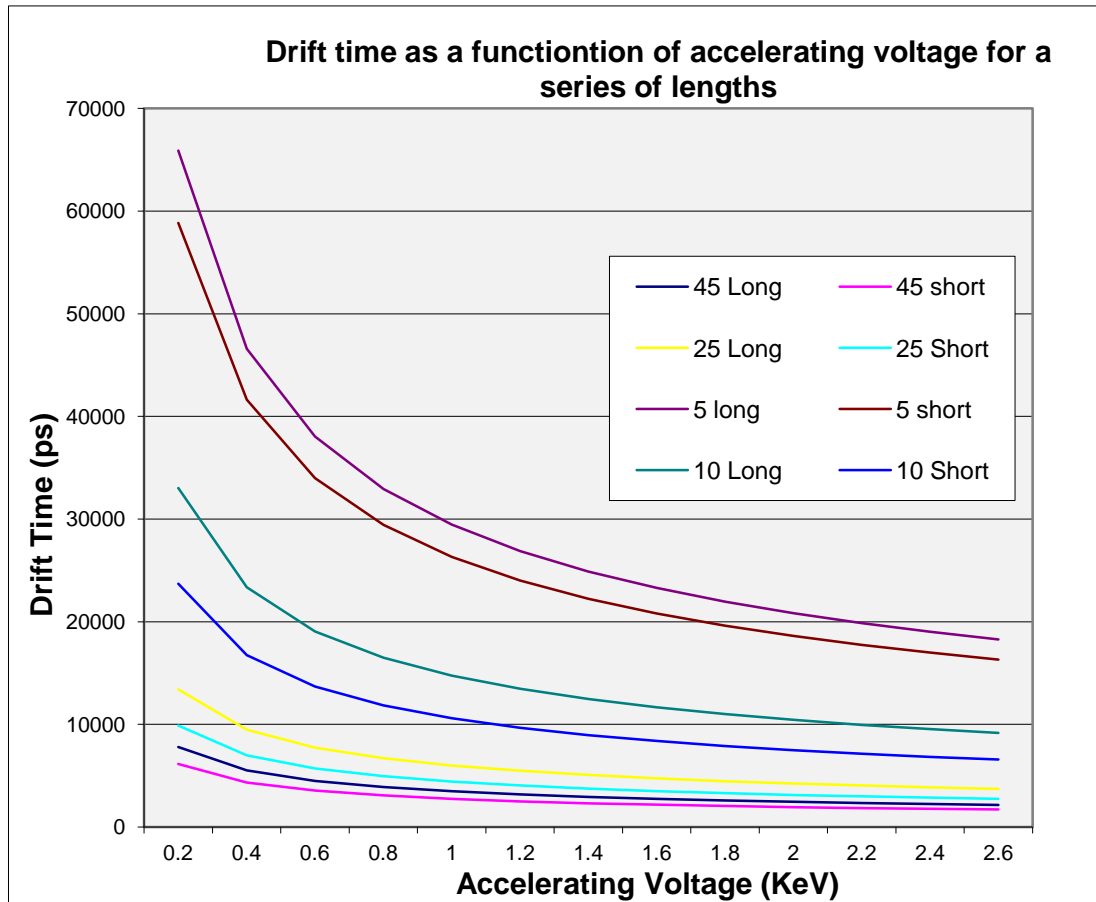


Figure 5.8 TIM 1 potential drift times

The design would require optics with a large depth of focus for the image to stay in focus over all the photocathodes, this can be achieved with a K-B microscope and this is the method proposed for implementing this design at NIF 12]. For the UV application of the TIDI the optics used will have a relatively shallow depth of focus (of the order of 10s of microns) and hence this arrangement would not be suitable.

The design also limits the size of the photocathodes to such an extent that it may not provide a large enough image size for the BBXRD application which requires enough space to observe the translation of diffraction spots. Due to the narrow aperture (a result of placing the solenoids at an oblique angle) a small FOV is predicted with this design which could cause a problem for all of the experiments

unless front end optics are carefully considered. The design relies on transmissive photocathodes so would be difficult to modify for UV sensitivity. The design is rather space inefficient (the photocathodes need to be at that oblique angle in order to stop the photoelectron bunches passing through a subsequent photocathode before entering the drift region) which may make the device incompatible with the TIM, especially consider there needs to be space to house the pulser, the CCD and MCP electronics and the stored energy for the solenoids.

5.2.2. TIDI 2: SLSO single shot

The TIDI 2 is a more DIXI like instrument; this was chosen in order to gain a high temporal resolution (~ 5 ps) and a large FOV as a result of a large photocathode. It has a 4 cm diameter photocathode (interchangeable between Au and CsI for UV and x-ray detection respectively), a 40 cm drift space with solenoids providing a magnetic field throughout. The detection end consists of an MCP-phosphor however this will most likely become a pulsed mesh-phosphor which will give us improved spatial resolution limited mainly by the cyclotron orbits of the photoelectrons. This will provide ~ 6 ps temporal resolution in UV and ~ 10 ps in x-ray regimes, a spatial resolution of up to 50 microns at the MCP and a high dynamic range.

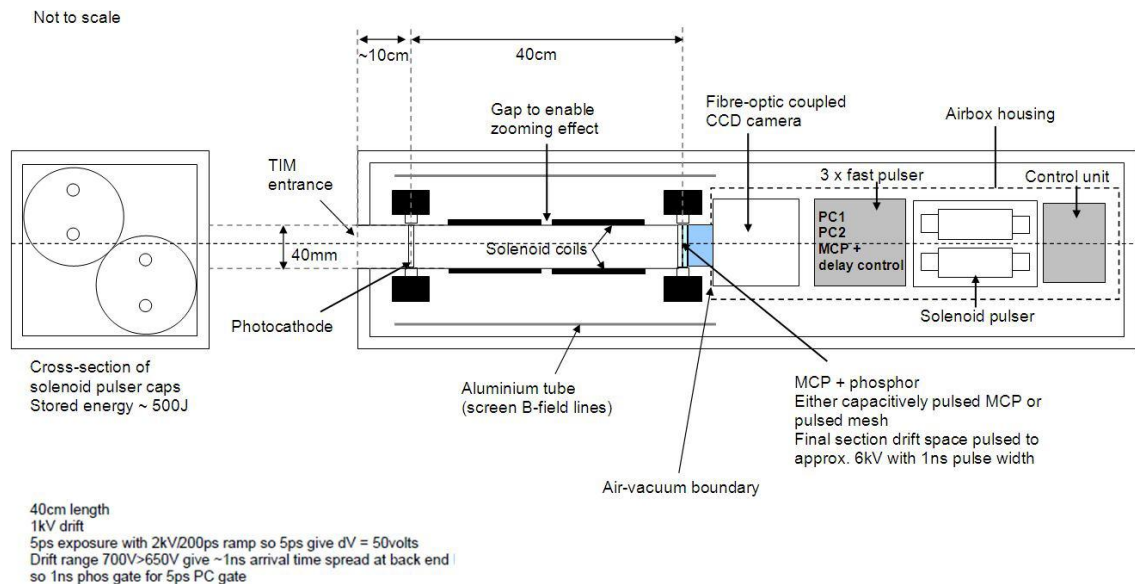


Figure 5.9 TIDI 2 design schematic for TIM compatibility

This device is essentially a DIXI but with 1:1 imaging between the photocathode and MCP which avoids the focusing geometry which was detrimental to the spatial resolution of the DIXI. The focusing geometry can be avoided by using the TIM to move the TIDI payload such that the photocathode is sufficiently close enough to the TCC. The sensitivity is then not an issue and a large photocathode to compensate for sensitivity loss (as for the DIXI). This design took account of the TIM dimensions.

It has a modular photocathode; CsI for x-ray imaging and Au for UV. The UV will not have as good spatial resolution due to the spread of photoelectron energies [47] The PC is 4 cm diameter which is the upper limit of PC size due to the size of the B-field and amount of stored energy in the coils (Doubling the area of either the PC or the MCP will lead to a required quadrupling of the B-field to keep the same spatial resolution)(see equation 4.2).

The spatial resolution is primarily determined by the gap between the MCP and the phosphor (this is due to the radial spreading from the MCP being much larger than the radial spread out of the PC). Since the MCP/phosphor gap is in a non-sealed off tube the spacing can't be as tight as in a sealed off design, therefore this design will suffer slightly in terms of spatial resolution and it is estimated to be around 50 μ m at the MCP.

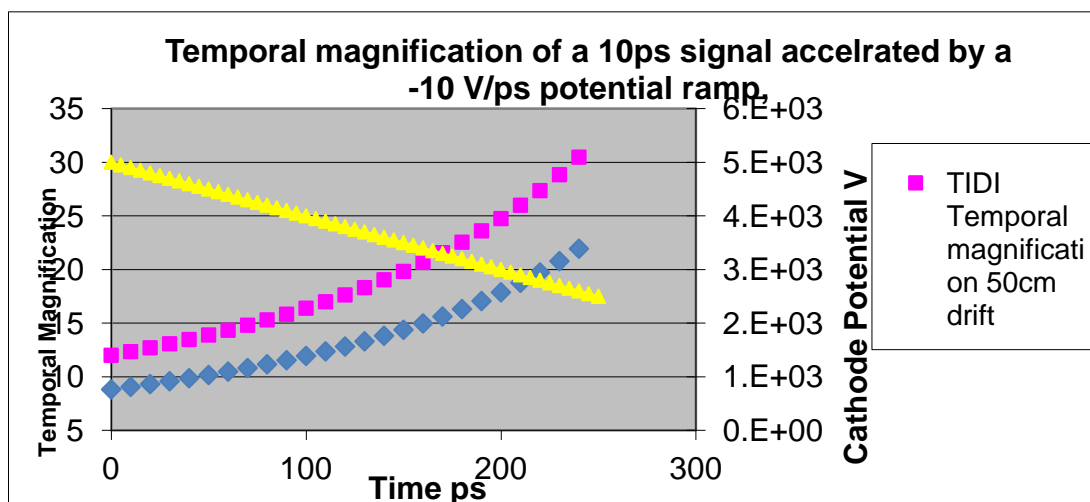


Figure 5.10 Temporal magnification for TIDI 2

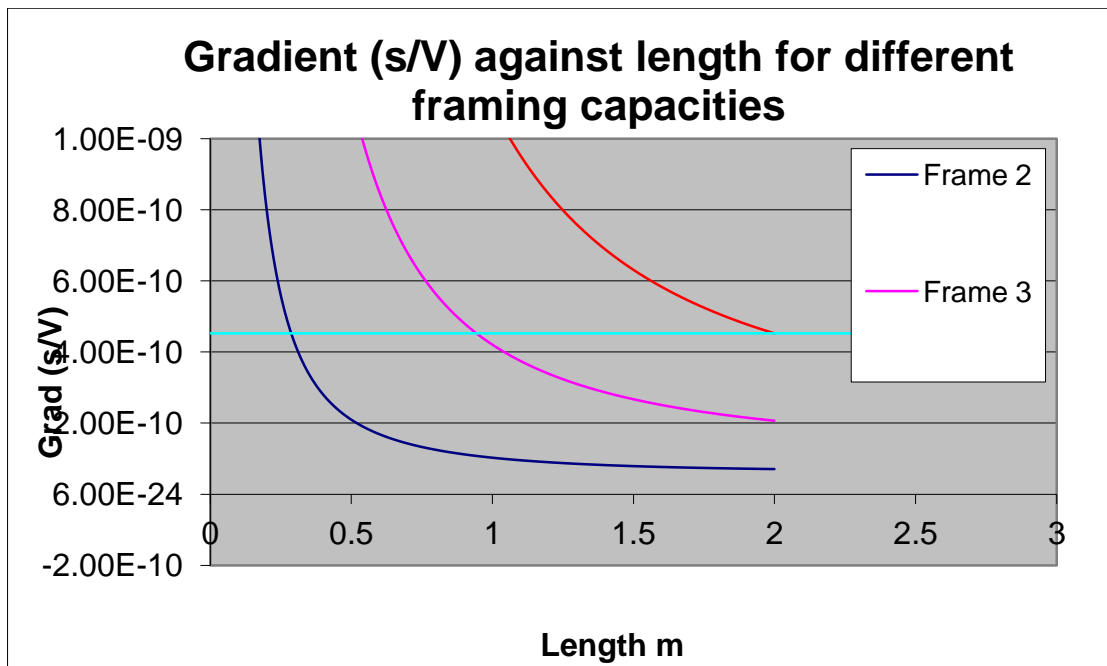


Figure 5.11 40 cm drift length is around the limit of a two frame device

The drifting voltage is limited to 100V by space charge effects so this device would be limited as a two frame single line of sight imager or would function with a strip line gated MCP much like the DIXI.

This design is able to produce the desired temporal resolution for the experimental applications and it can provide a large enough field of view for time-resolved x-ray diffraction. However, the spatial resolution is insufficient for viewing the thermal emissions from micro-wires (which requires $<50\mu\text{m}$).

5.2.3. TIDI 3: Multiple lines of sight, segmented PC, no MCP design

TIDI 2 fulfilled the design specifications in all but the spatial resolution. To improve the spatial resolution it would be useful to remove the MCP. Photoelectron counting could be achieved with a suitable phosphor placed in front to detect photoelectrons of sufficient energies. This way the spatial resolution would be mainly defined by the cyclotron orbits of the electrons in the B-field, there may also be some effect from E

x B drift towards the outer edge of the electron cloud as a result of the curvature of the B-field. Based on experiments with DIXI these drifts could be significant.

The ExB drift is a guiding centre drift in a direction perpendicular to the B and E field, it comes about as a result of the non-uniformity of the B-field, causing an uneven Lorentz force to be applied to the electron in orbit resulting in a gyro motion. Other guiding drift such as due to gravity should not have an effect.

Without an MCP, another method of framing and gating is required. Since the drift length is too restricted by the TIM to separate frames in the drift space, the framing will be performed by a repetitively pulsed PC (as for the SLOS diagnostic), which is sectioned and each section is triggered separately. Although this won't define a single line of sight, it will suffice for the experimental applications intended (see fig 5.12). Given the small drift length than the SLOS, gating and recording of images must be performed on a ~1ns timescale (as opposed to ~50ns). The gating can be done with a pulsed, very fast phosphor (~1ns decay time), combined with a mesh to provide a small acceleration region at the end of the drift length. The acceleration region acts to boost the incident photoelectron energy in lieu of an MCP intensifier. Any signal not desired will not be accelerated, and it will be below the threshold to be picked up by the phosphor. If the signal is wanted, the electrons are accelerated to $\geq 5\text{kV}$. Recording of the image is then performed by the ns framing CMOS camera mentioned earlier

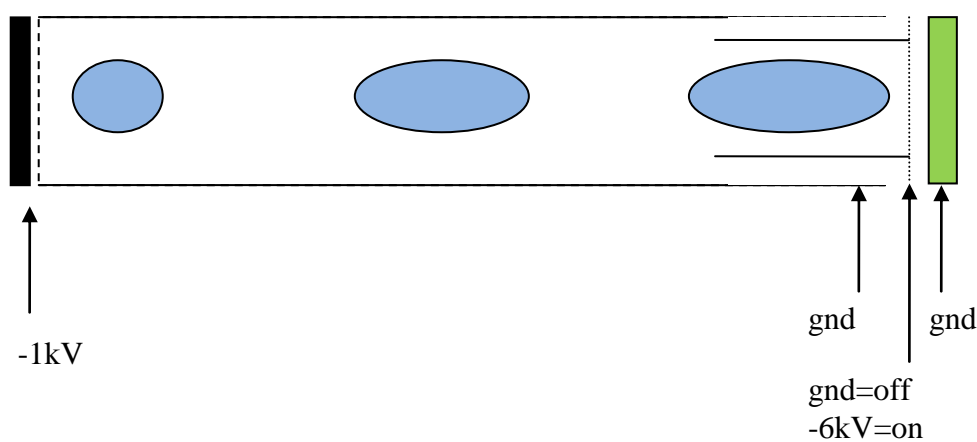


Figure 5.12 Gating using the threshold of the Phosphor and a short accelerating region

In this design the segmented photocathode does not give a single line of sight, but it will be particularly useful for the time-resolved x-ray diffraction application. This application requires measurements of the shifts of diffraction spots that result following relaxation processes of laser-driven shocks in crystals. Figure 5.13 shows one design which would drift four frames. The photocathode would be provided with a single ramp from the electronics and each section/frame can be off- set by an independently controlled bias. This would allow for the timing separation in the drifting frames. Since the photocathode will be interchangeable, different photocathode geometries could easily be explored to better suit the diagnostic to the experiment. For example in time-resolved x-ray diffraction the direction of diffraction spot shifts are not necessarily known. A better design might therefore be concentric circles as shown in Figure 5.14.

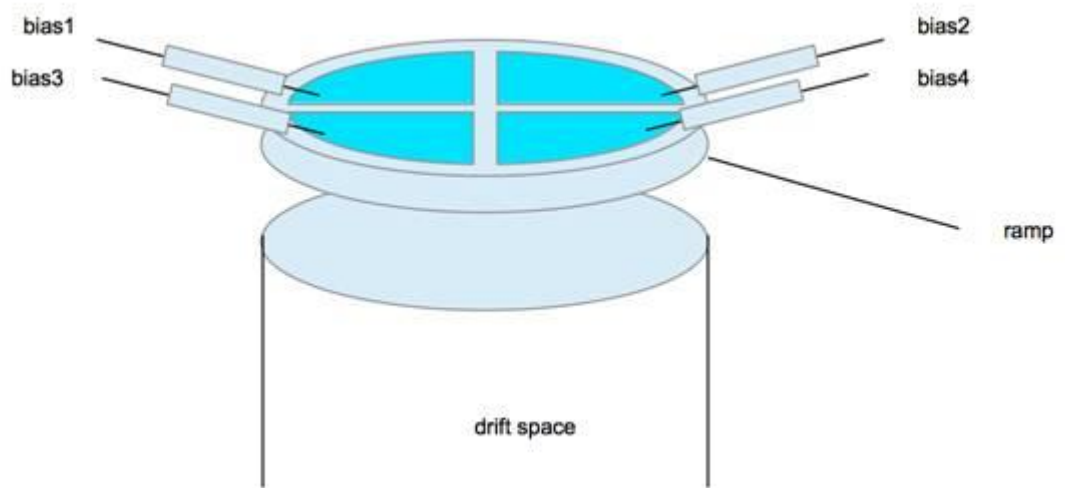


Figure 5.13 Example of segmented PC

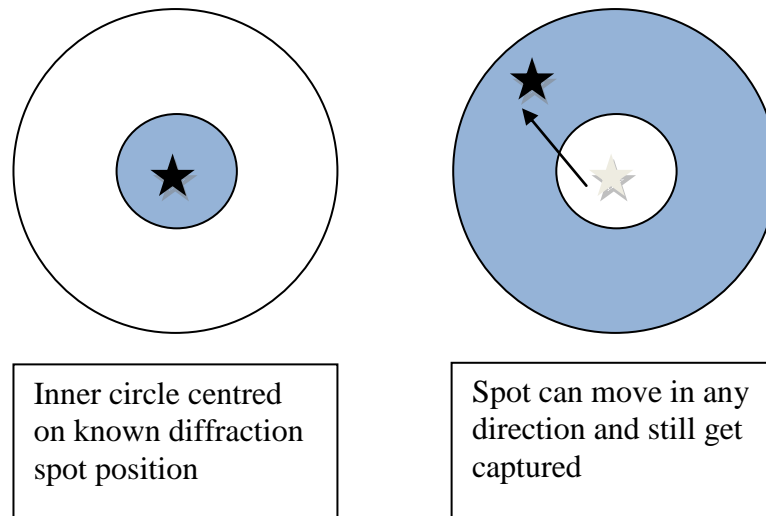


Figure 5.14 Benefit of a concentric circle PC for BBXRD demonstrates the flexibility of this design

The design provides different gating times from different parts of the cathodes by having a single ramp over the entire cathode (provided by a mesh coupled to the PC) and having a bias on different parts, in effect, the segmented photocathode now separates frames out both spatially (according to photocathode geometry exploited) and temporally.

Straight through hard x-rays could potentially be an issue (This is one reason an MCP would be a beneficial component as it offers some protection against straight through x-rays striking the CCD). One way of avoid this issue is to use the front end optics to discriminate the desired wavelength(s) for observation and using the TIM pointing ability (a 30x30 mm square at the TCC) in order to point off axis. TIM pointing can be utilized along with a lateral offset with the TIM itself

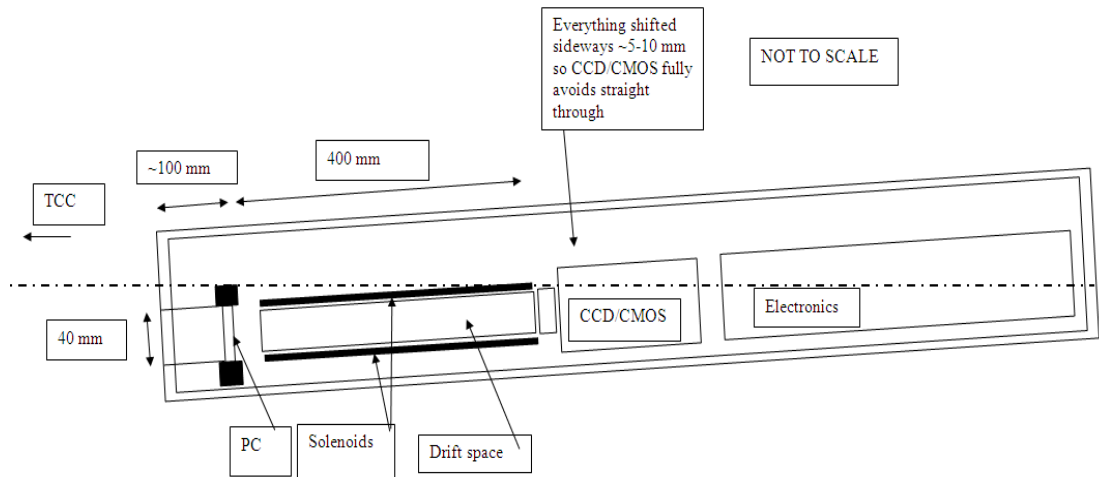


Figure 5.15 to scale schematic for pointing off centre and avoiding straight through

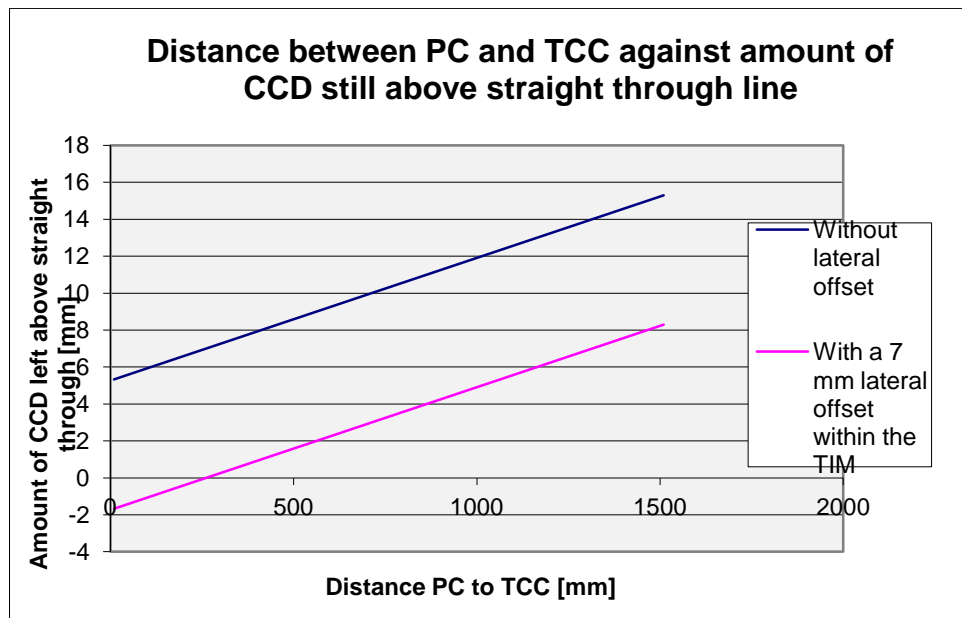


Figure 5.16 Protecting the CCD against straight through

Figure 5.16 shows that if the entire CCD area is to be protected then the Photocathode can be no more than 300mm away from TCC, however some active area on the CCD may be sacrificed in order to make more space for the front end optics. The gradient is not too steep so even at 1m away only ~ 5mm of CCD is going to potentially be struck by straight through hard x-rays.

The spatial resolution will be limited by the 4x the electron cyclotron orbits which are defined by the magnetic field, this will easily reach the desired 30 μm .

Essentially we have <10ps resolution for each frame and ~ 100ps frame separation in line with requirements for time-resolved x-ray diffraction.

5.2.4. Summary of designs

The following table is used in order to summarise how the user requirements are satisfied by the three designs.

User Requirement	TIDI 1	TIDI 2	TIDI 3
X-ray sensitivity of 2 keV-60 keV interchangeable with a UV sensitive mode	Requires transmissive photocathodes, UV may not be an option.	Yes	Yes, with the option of having combination of materials on one PC, also flexible PC design
High spatial resolution with up to 30 μm desired	>50 μm	>50 μm	Limited only by B-field, <50 μm
Very high temporal resolution for 2D imaging with <10 ps	<10ps, 4 frames at 100ps frame separation	~5ps two frames at 100ps frame separation	<10ps with 4 ~100ps frame separation
A high dynamic range (predicted)	300 counts	300 counts	300 counts
Compatible with a Ten-Inch Manipulator (TIM)	Yes, but not in the most space efficient manner	Yes	Yes
Pointable to protect against straight-through x-rays striking	No need CCD's off axis	Yes + protection from MCP	Yes

CCD/CMOS			
Vacuum compatible	Yes	Yes	Yes
Sufficient shielding to mitigate background signals and debris.	Yes	Yes	Yes
General suitability for experimental applications	Not suitable for BBXRD, potentially difficult for UV sensitivity	Spatial resolution not suitable for imaging micro-wire targets.	Suitable for most applications, benefits from flexible photocathode design.

Table 1 Summary of TIDI designs to date

Chapter 6

Testing to inform design and predict performance

The following Chapter details the practical work done in support of this project. A test bed for a potential front end optical arrangement for the proposed TIDI was built and characterised. The Chapter contains a detailed prediction of the performance of the system and the methodology used in testing. The results are used to extrapolate the spatial resolution of the Orion TIDI (see Figure 4.3) and predict performance limitations which could be imposed by this front end arrangement (e.g. aberrations, field of view), as well as more practical limitations such as the space available in a TIM.

6.1. Introduction and justification for practical work

Due to the novel nature of the Time Dilation Imager the practical work is based on characterising a potential arrangement of front end optics similar to the set up which would be used for the UV colour temperature measurements made by TIDI. The optical arrangement in question is an optical pyrometry system which will be used on the Orion test chamber in conjunction with an optical streak camera. The aim of the practical work was to gain enough information about the optical performance of the pyrometry system so that it can be reliably fielded at the Orion laser facility.

A Gated Optical Imager (GOI) was used to act as a stand in for both the optical streak camera and the TIDI, it was intended that the gating mechanism of the GOI was also tested, however the timing was found to be unreliable and so has been omitted from this thesis.

The results of the testing were that the vignetting and magnification of the pyrometry system have now been successfully characterised, the chromatic performance was as expected and the aberrations were minimal. The native resolution of the optical system was sub-micron. The temporal performance of the GOI was found to be unreliable, the spatial resolution (when combined with an optical pyrometry system) was limited by the CCD rather than the MCP and found to be $<4 \mu\text{m}$.

The primary objectives of the practical work are as follows, test, against prediction, the vignetting, magnification, chromatic performance, and resolution of the entire optical pyrometry system. Test for any unforeseen aberrations in the pyrometry system, and to characterise the spatial resolution of the optical system and observe how it is degraded by the addition of the GOI

The pyrometry system will be used for two primary measurements; Colour temperature and Brightness. The colour temperature is a relative measurement of the IR and UV light in the system and the brightness measurement is an absolute measurement of the broadband spectrum. It is therefore very important for the brightness measurement to know the amount of light lost through vignetting.

The purpose of the approach was to simulate conditions at Orion closely enough that any data gathered can be reliably applied there. The approach was to first test the optical arrangement passively using a close to white light source and then to test it in conjunction with the GOI.

The method was to first use an incoherent light source to align the three main optical components of the pyrometry system (the microscope objective and two tube lenses). This small system was then characterised in terms of vignetting and beam divergence. The next step was to replicate the optical path that would be expected when fielded at the Orion Laser Facility (see Figure 6.1).

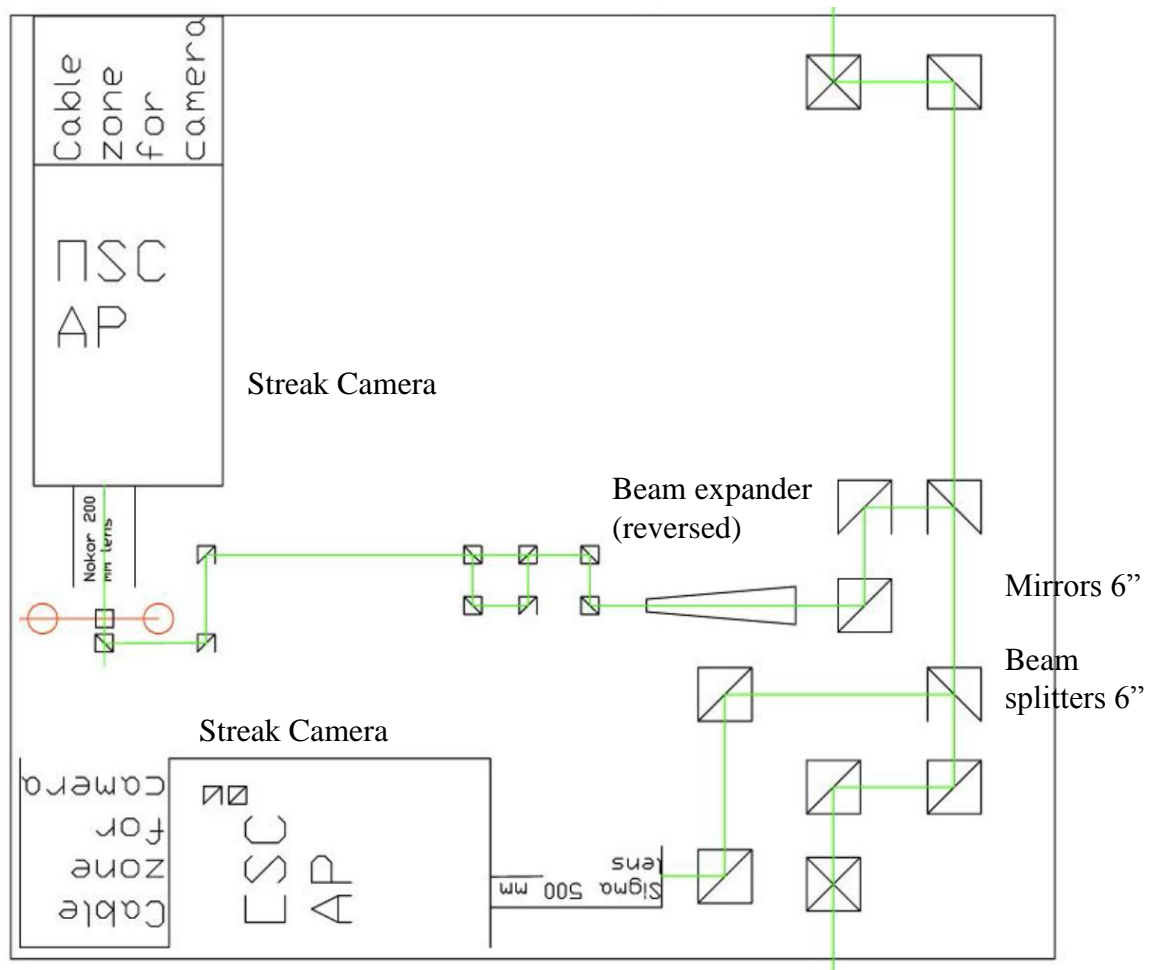


Figure 6.1 Table Layout for Pyrometry measurements [30]

Then the FOV, resolution and chromatic performance of the system could be well defined before it is transferred to Orion.

6.2. Theory

6.2.1. GOI

The GOI is an optical, time-resolved imaging diagnostic designed and built by Kentech. It is a microchannel plate intensified gated camera. Originally it was designed to work with standard Polaroid® film but has since been adapted (via the addition of collimating tubes) to work with CCDs. The GOI heads consist of a cathode and MCP. The cathode is separated from the channel plate by a gap of < 250 microns and the tubes are biased by a very high potential. This gives a very low electron transit time and enables fast gating. The cathodes are sensitive to 850 nm light. The gain on the MCP is controllable by adjusting the high voltage (in 50V steps). [31]

The Gated Optical Imager (GOI) works similarly to an x-ray framing camera, in that there is an input window followed by a gating mesh (driven by a high voltage pulser), after which there is an intensifier (Photocathode/MCP component) driven by a high voltage supply and outputting on to a phosphor.

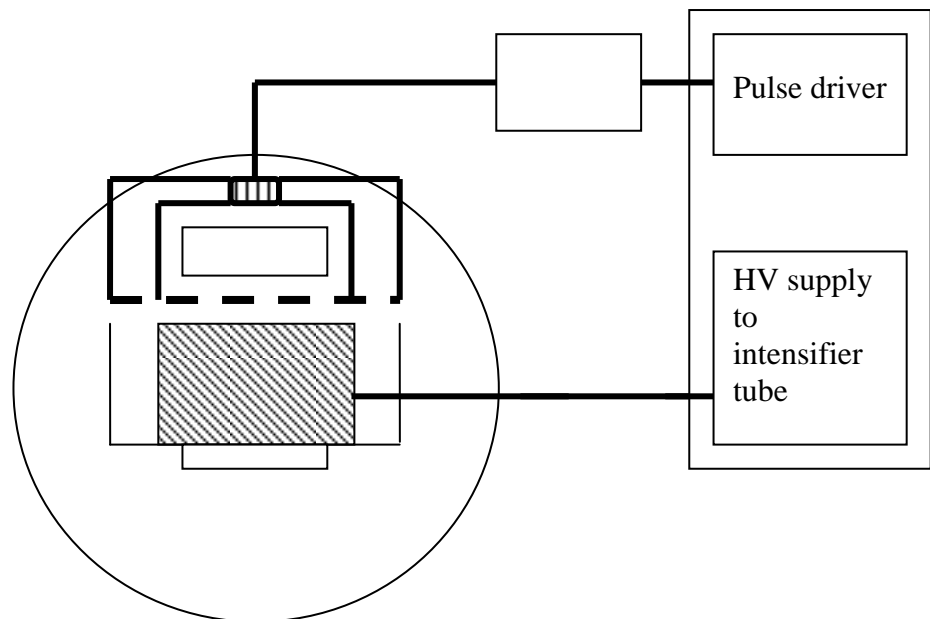


Figure 6.2 GOI head schematic

A small positive bias is applied to the PC and a short negative pulse is applied from the PSU to the PC in order to put the head in 'on' mode.

There are four distinct heads each with an individual power supply unit (PSU) which supplies the gating pulse, bias, and trigger for the CCD. The gain is also controlled at the PSU.

The GOI is similar in operation to the TIDI in the sense that it uses the same basic components (PC-MCP-Phosphor). However, it does not use the drift region between the PC and the MCP or a ramped potential difference to apply a temporal magnification to the signal.

6.2.2. Optical pyrometry

When performing optical pyrometry it is very important that we know how much light we are getting through the system and how much is lost as a result of off axis rays being stopped by apertures in the system. This is known as vignetting, if for example the rays from all points along a finite FOV fill the aperture stop without any loss then the system can be considered to have no vignetting.

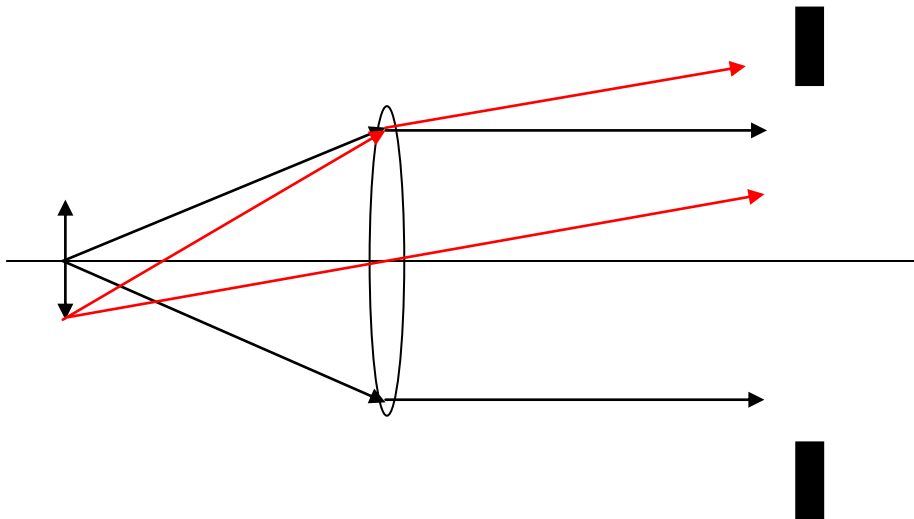


Figure 6.3 Vignetting example

Vignetting will appear as a steep darkening around the image edge and (along with magnification) will define the limit of the field of view.

As careful consideration of the vignetting was necessary, it was important to ensure the source had no additional collimation which would improve the vignetting performance. A Lambertian source is a finite source which follows the Lambertian cosine rule that the radiance of the source drops off as $\cos^4 \theta$ when viewed from a glancing angle compared to the normal in the same plane. This is as a result of the reduction in solid angle, and an increase in both the detection area and distance between detector and source. [32]

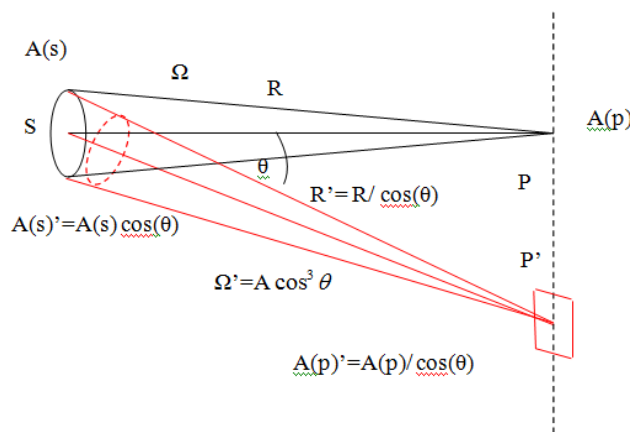


Figure 6.4 Depiction of a Lambertian Source

6.3.Method

Initial vignetting tests were performed as in Fig 6.5:

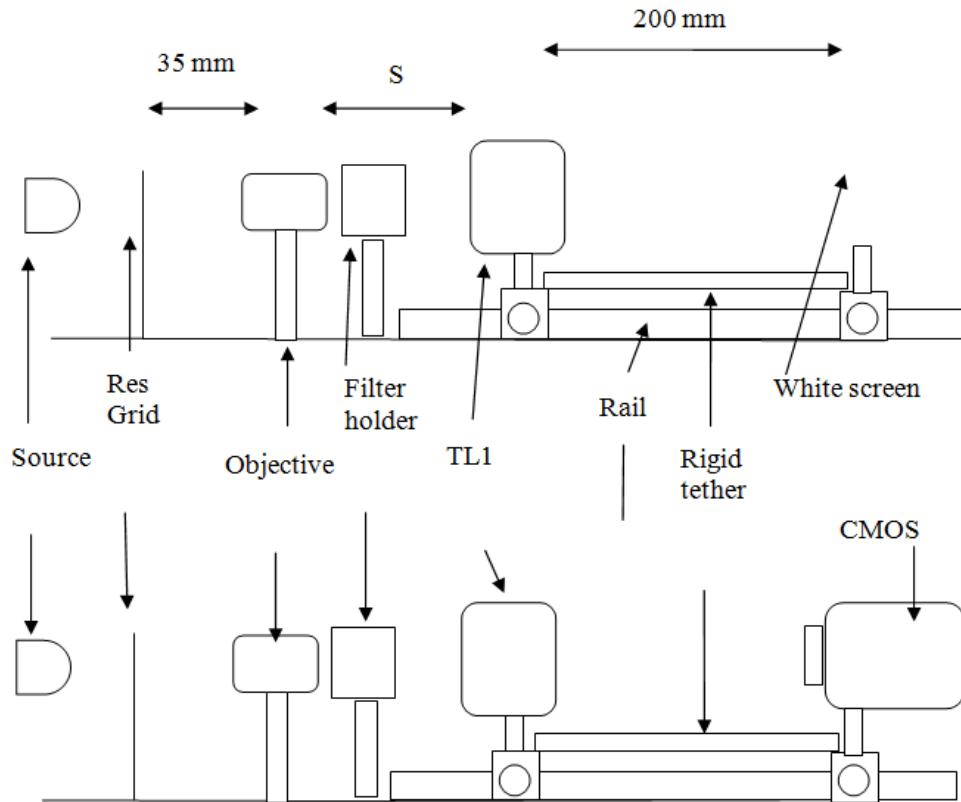


Figure 6.5 (a) set up for measurement of vignetting by eye, (b) same set up for measurement with a CCD

The separation S is increased incrementally in order to observe the effect on vignetting; all other dimensions are held constant.

As can be seen in Figure 6.14 the system outperformed the quoted figures from the Mitutoyo catalogue [33], slight over-performance would be expected, however the discrepancy is too large to overlook. The source position with a transmissive resolution grid could potentially be producing collimated light resulting in reduced vignetting. To test this, a fluorescent grid was put in place of the transmissive and front lit to produce a Lambertian source.

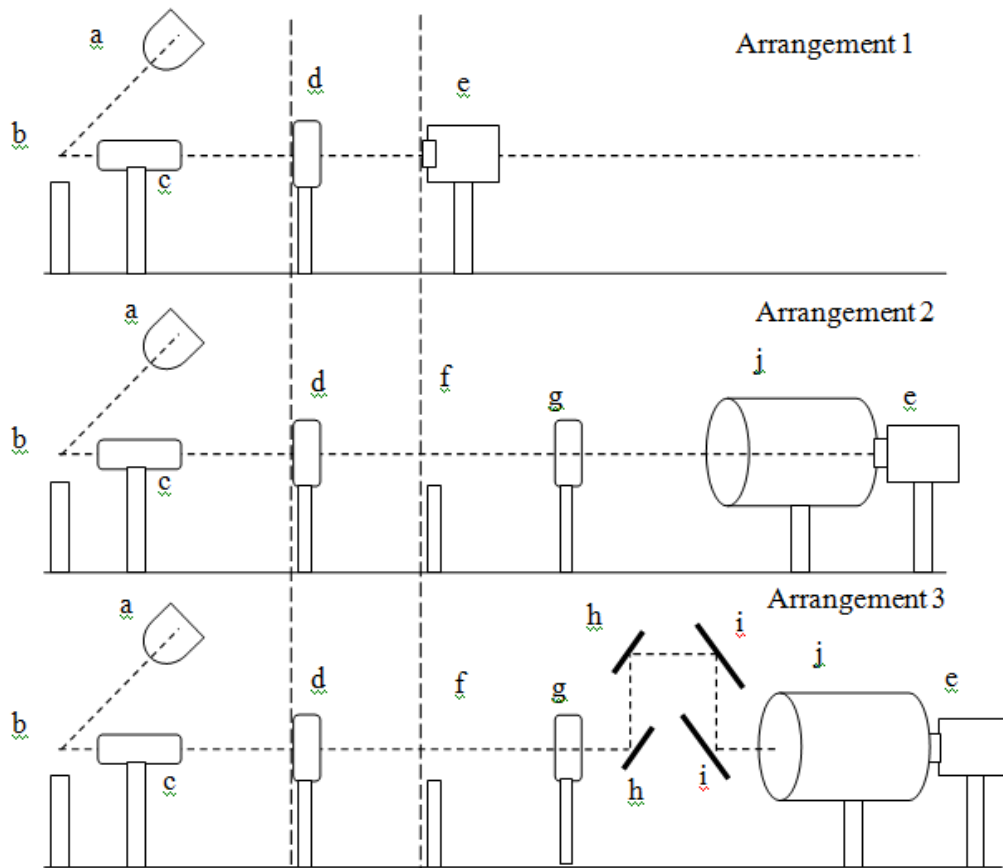


Figure 6.6 Schematic layouts for passive optics testing

Diagram reference	Description
a	White light source
b	Fluorescent Resolution grid (600 lp/mm)
c	Microscope objective (5x or 10x)
d	TUBE LENS1 (MT1 200f)
e	FireWire CMOS camera
f	Intermediate transmissive USAF resolution grid
g	TUBE LENS2 (MT2 400f)
h	4" Al Mirror
i	6" Al Mirror
j	Fast photography lens (Nikon 150f / Sigma 500f)

The next stage in testing was to mock up the optical path at Orion (see figure 6.1 and figure 6.12) with all apertures and distances (this includes the entire path from TCC to detector including a window at the end of the TIM and the apertures introduced by the mirrors used to periscope down from the TIM to the optical table) to see how the performance would be affected.

To check magnification and alignment a second resolution grid is placed at the focal point of the relay lens pair, this simultaneously allows for confirmation that all the elements are in focus and the magnification is as expected (see arrangement 2 and 3 in Figure 6.6).

Initial resolution tests were performed with a transmissive USAF capable of spatially resolving up to $4.3\mu\text{m}$, then with both a transmissive and fluorescent Ronchi grating to extend the tests to $1.67\mu\text{m}$. Finally, absolute limits for the optical systems resolution were determined using a series of bespoke grids of resolution $1\mu\text{m}$, $2\mu\text{m}$ and $5\mu\text{m}$. Band pass filters were used to find upper and lower limits to the visible spectrum within which the system can still perform adequately.

The smallest resolution that the Firewire camera can resolve is based on its pixel size; it has a cell size of $7\mu\text{m}$, a pair is needed to resolve giving a size of $14\mu\text{m}$, so with a magnification of 10x the CMOS camera is limited to a resolution of $1.4\mu\text{m}$ for the initial test, and $1.1\mu\text{m}$ for subsequent tests at 12.5x magnification.

For this test an attempt was made at replicating the Orion optical path with the GOI in place of the OSC, a 1Hz short pulse laser was used in place of the passive light source in order to characterise the temporal performance of the GOI. Some changes were necessary due to basic differences in functionality between the GOI and the OSC: The photography lens is placed behind (and focused onto) the phosphor as opposed to in front of the PC, the beam needed to be split in order to be incident on both heads as opposed to a single slit and in order to split the beam and steer it onto the heads while focusing a long focal length (250mm) macro lens was placed before the beam splitter.

Figures 6.7, 6.8 and 6.9 show the delays which need compensating for and the optical arrangement within the laser cavity and on optical tables 1 and 2

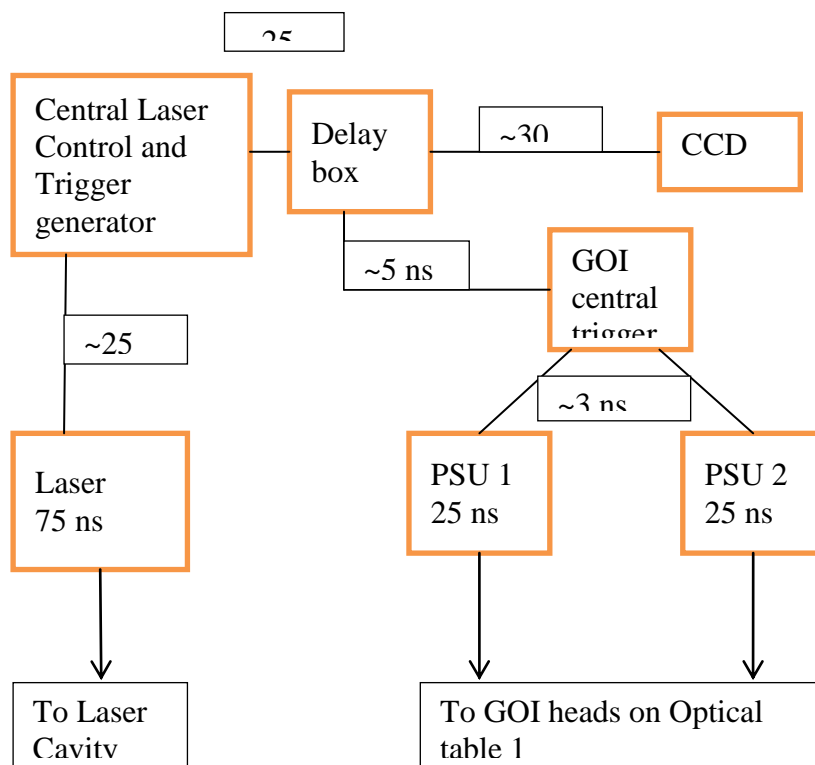


Figure 6.7 Schematic representation of delays

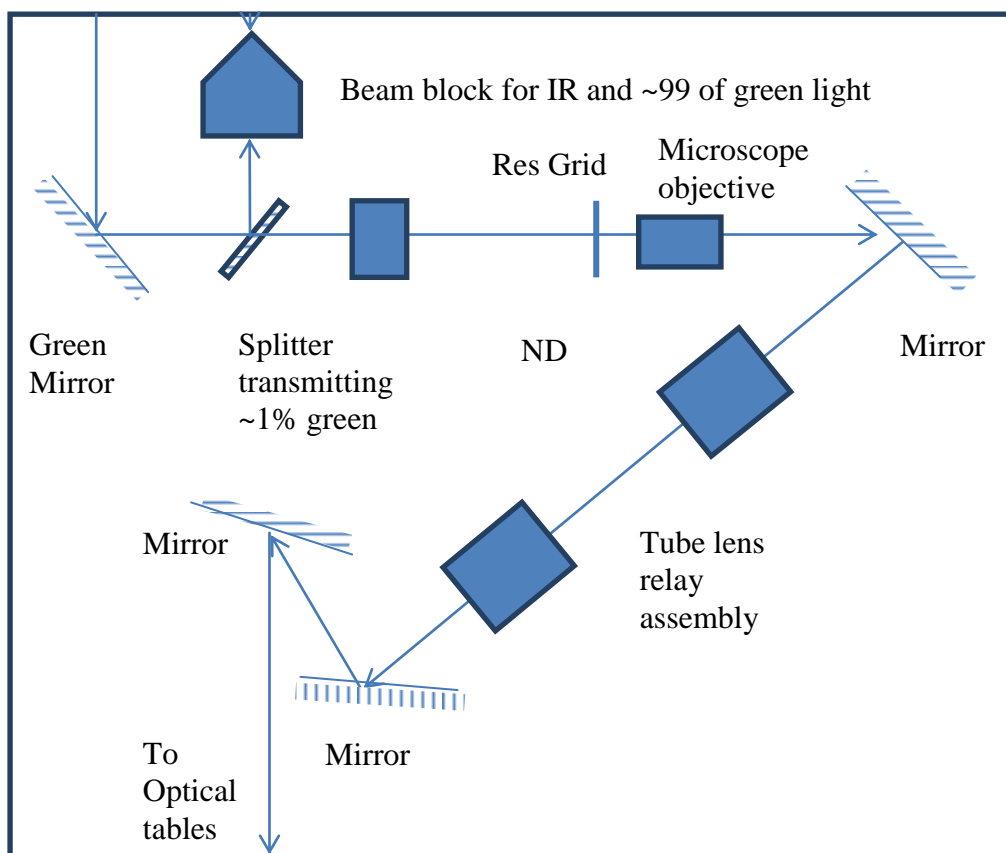


Figure 6.8 Laser cavity setup

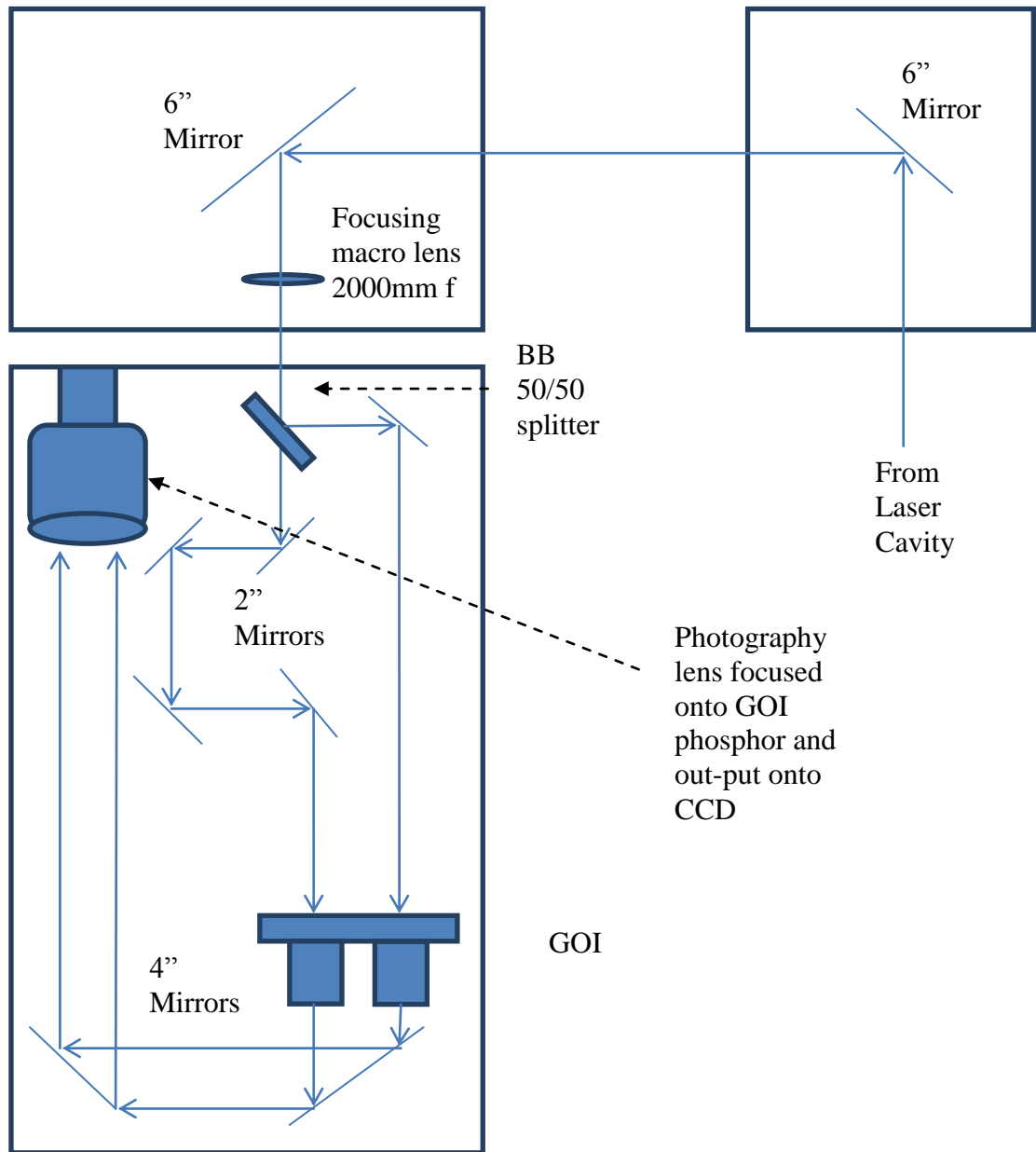


Figure 6.9 Optical table arrangement

During imaging tests with the pyrometry optics and GOI, the resolution, magnification and FOV were recorded for all gating modes and compared to the predicted values. In the following section a breakdown of the predictions for these parameters is given, before the experimental results are analysed.

6.4. Predicted performance of the system

6.4.1. Vignetting

The vignetting can be calculated at each stage by the approximation:

$$\theta = \tan^{-1}\left(\frac{d/2}{f}\right)$$

Equation 6.1

where θ = the maximum angle at which the off axis beam will leave the lens, d = the diameter of the object (effective FOV) and f = the focal length of the lens. In the pyrometry system the second tube lens is imaging the magnified image so if for example the requirement is for a 1 mm FOV unvignetted then the second tube lens (TL2) will be imaging an object that is effectively 10 mm in diameter, a quick calculation predicts that the beam from the edge of this FOV will leave TUBE LENS2 at an angle of 0.72° .

$$\theta = \tan^{-1}\left(\frac{5\text{mm}}{400\text{mm}}\right) = 0.72^\circ$$

This allows us to estimate the beam divergence for a given distance:

$$\text{Beamwidth} = r \times \tan \theta$$

Equation 6.2

where r = the distance the beam has travelled and θ = the maximum angle at which the off axis beam will leave the lens.

Over a distance of 1 m the beam width increases by 12.5 mm which is approximately $0.5''$; this means that for every meter travelled the optics need to increase in diameter by $1''$. This is quite a significant divergence especially considering the distances which will be involved in the optical set up at the Orion Laser Facility (approximately 8 m of travel from TCC to detector). One method of reducing the divergence would be to decrease the magnification through use of a different

objective; this would however limit the eventual resolution of the system and is probably not desirable. It would be helpful to reduce the path distance after tube lens 2 (TL2), theoretical approximations [33] suggest that the infinity space between the objective and tube lens 1 (TL1) (the tube length) can be increased to 230-240 mm.

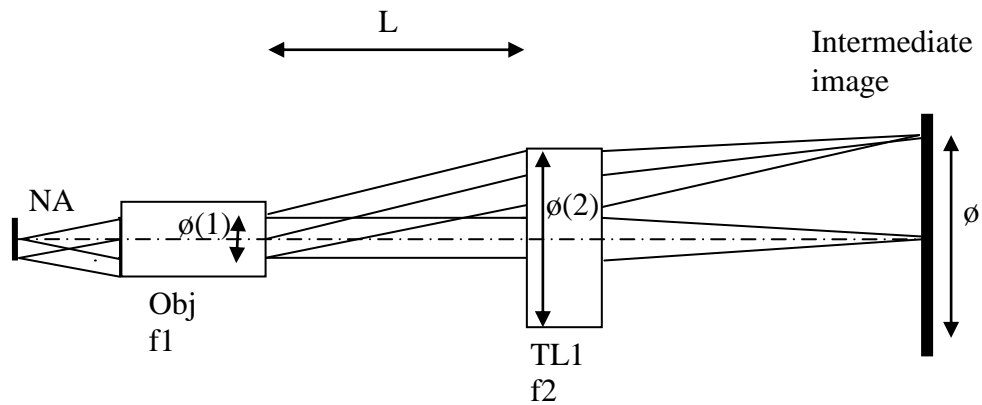


Figure 6.10 infinity corrected microscope and tube lens

The following equations are used in order to predict the image diameter as a function of the distance between the infinity corrected microscope objective and TL1:

$$L = (\phi_{(2)} - \phi_{(1)}) \cdot \frac{f_2}{\phi} \text{ [mm]}$$

Equation 6.3

$$\phi_{(1)} = 2 \cdot f_1 \cdot NA \text{ [mm]}$$

Equation 6.4

Where $\phi(1)$ = Objective exit pupil diameter, $\phi(2)$ = Effective diameter of TL1, f_2 = focal length of TL1, f_1 = focal length of objective, and ϕ = image field diameter[33].

Calculating for the whole system shows that an unvignetted FOV of around 0.45 mm should be obtainable:

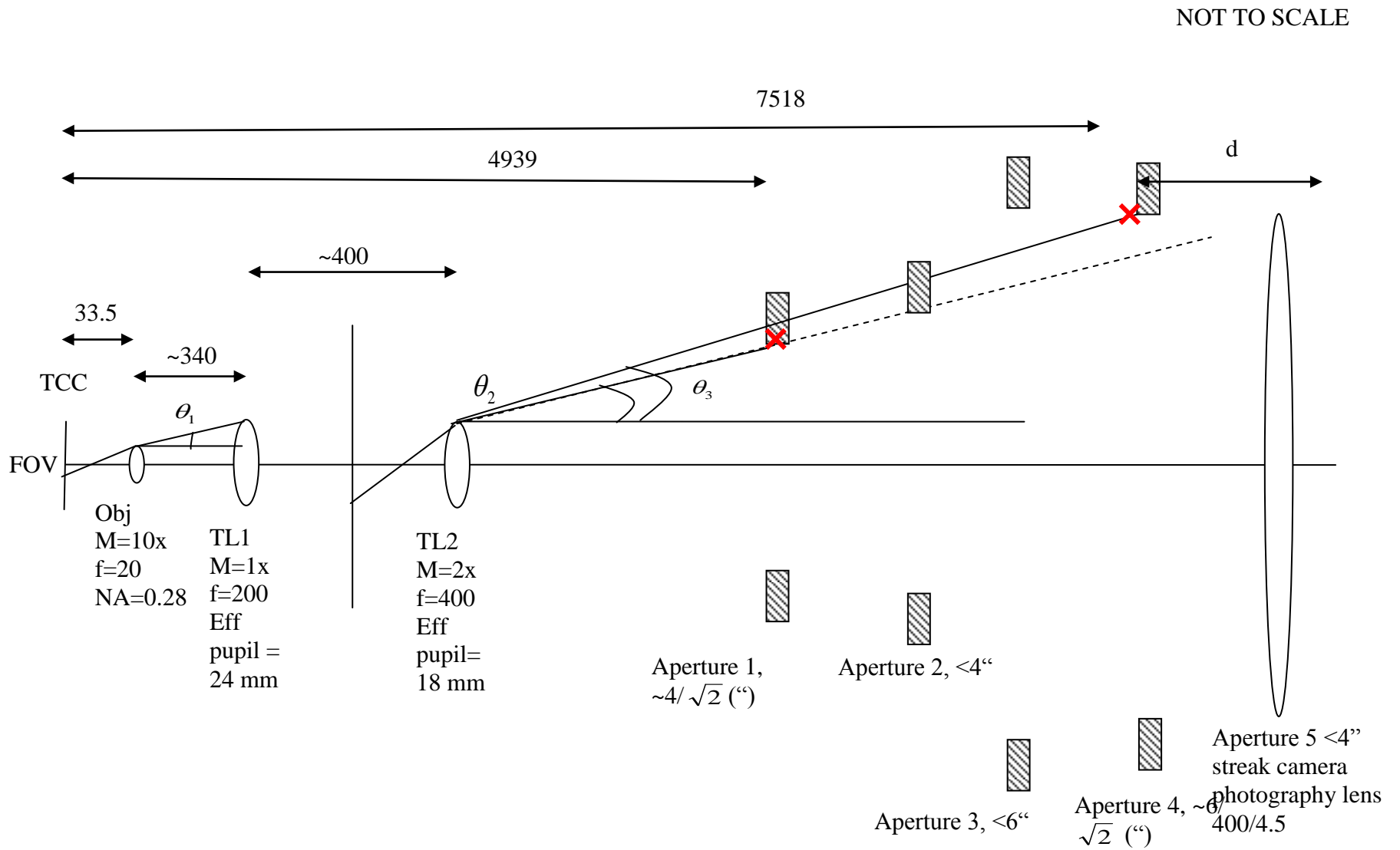


Figure 6.11 Full aperture layout for Orion optical pyrometry system

Apertures 1 and 4 are going to be more limited horizontally than they are vertically as they are mirrors at $\sim 45^\circ$, using equation (6.1) and basic geometry it is calculable that the limiting aperture horizontally is Aperture 4 which requires a broadening angle of $\leq 0.325^\circ$. The vertical limiting aperture is predicted to be Aperture 5 which requires a broadening angle of $\leq 0.323^\circ$.

The FOV can then be predicted as:

$$FOV = 2 * 400 * \tan(0.323) [mm]$$

$$FOV = 4.5 [mm]$$

This is the FOV at the Image plane between MT1 and MT2 which is a 10x magnified representation of the real FOV which is therefore predicted to be 0.45mm.

6.4.2. Chromatic performance

The pyrometry optics will be based in the TIM and the light will pass through a 10mm fused silica glass window of 4" diameter, measurement of the broadband spectrum through the window is necessary as the material refractive index depends on the wavelength of light:

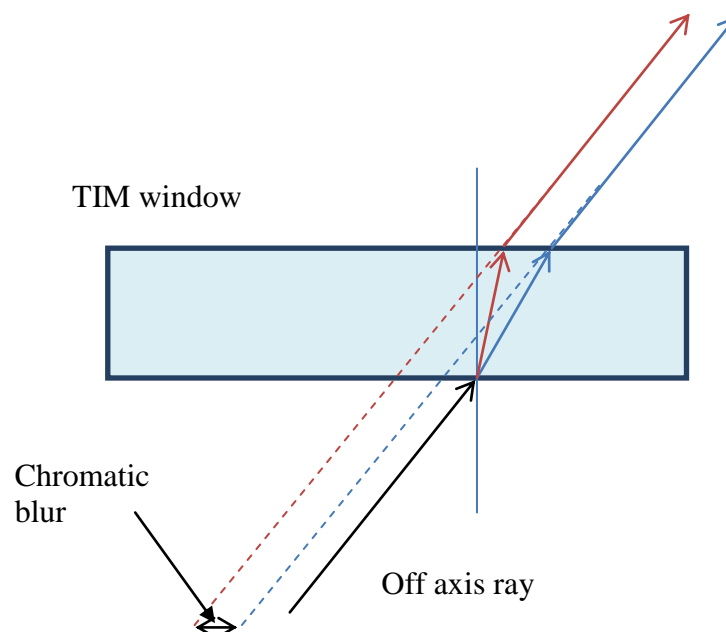


Figure 6.12 Chromatic blur due to window

Similarly, the sapphire entrance window on the streak camera is another source of chromatic aberration. It is important that a paraxial shift be predicted and properly characterised as the measurements require a comparison between the two wavelength groups, and that comparison can only be accurate if the light is focusing in the same plane at a well defined time. The focal shifts are calculated as follows:

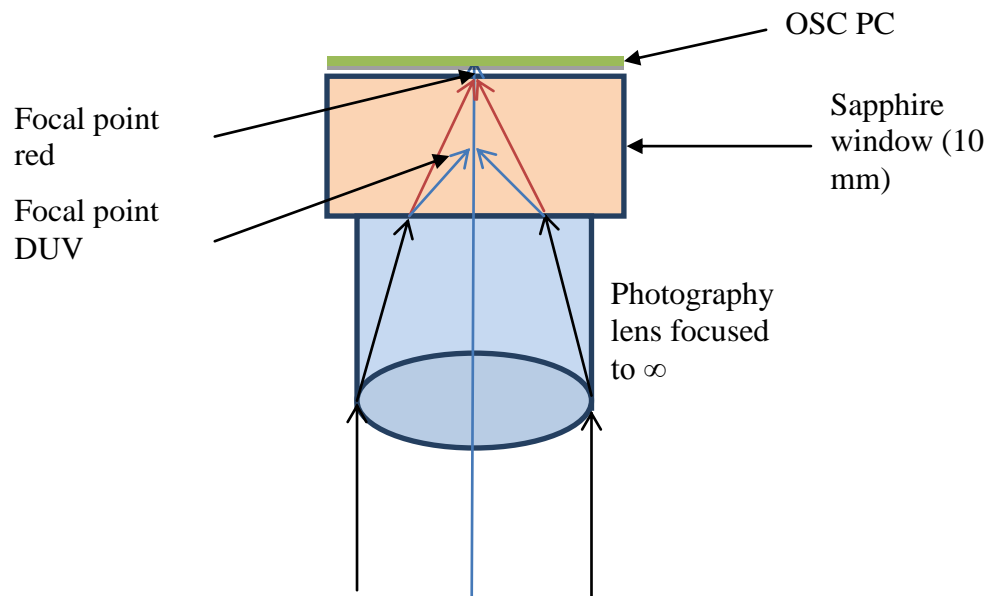


Figure 6.13 Chromatic defocusing through sapphire entrance window

For Paraxial rays the focal shift associated with the window is

$$\Delta v = \left[\frac{(n - 1)}{n} \right] * 'Window Thickness'$$

Equation 6.5

The lens is set to focus red light onto the photocathode, the paraxial shift is the difference:

$$\Delta v(violet) - \Delta v(red) \sim 60 \mu m$$

As the depth of focus of the Sigma 500 lens is estimated by:

$$t \approx 2Nc$$

Equation 6.6

Where t =the depth of focus, N the F# and c =the circle of confusion [34]:

$$t \approx 2 * 4.5 * 0.03 [mm]$$

$$t \approx 260 \mu m$$

Since this is larger than 60 μm the chromatic blur is not a problem for the brightness channel. However for the colour channel this may pose an issue. The colour channel records a relative measurement of the deep ultraviolet and the red light, due to the wider separation in the spectrum the focus shift is greater:

$$\Delta v(DUV) - \Delta v(red) \sim 210 \mu m$$

This begins to become a problem as the lens used will have a similar DoF as above. Two ways have been considered to correct this problem; firstly independent imaging optics could be used to re-image the red and the DUV, this way the focuses could be independently set, the other option is to keep the single optic but use a negative lens in the UV path in order to correct the difference in focus before reimaging.

6.4.3. Magnification, Resolution and sensitivity/fluence

In order to have a well characterised system it is important to establish as much of the performance as you can before fielding in an experimental environment. The need to know the vignetting and field of view (FOV) stem from the requirement to know exactly how much light is being received for the brightness channel on the optical pyrometry experiment.

The spatial resolution of the system needs to be high enough in order to account for the polarity of shock breakout. This is essentially referring to uneven emission over the surface, if over a small surface element one half of the surface element is producing emission but the other half is lagging behind, if the spatial resolution of

the detector is not able to distinguish these two spatially dependent events then the temperature measurement will be an incorrect integration over the two giving a mislead temperature reading [30]. If the spatial resolution is increased via a larger magnification then the signal drops off as the square of that increase, although this will allow for a better characterisation of the temperature in terms of uneven shock break out, it will be sacrificing signal to the point where hotspots are harder to identify on the surface. [30]

The magnification of the system is defined as:

$$M = M_{OBJ} \times \frac{f_{Nikon}}{f_{TL2}}$$

Equation 6.7

Where M_{obj} = magnification of the objective, f_{Nikon} = focal length of the fast camera lens, f_{TL2} =focal length of the tube lens.

The resolution of the system is defined as:

$$R = \sqrt{(R_o)^2 + (R_d)^2}$$

Equation 6.8

Where R_o = Optical imaging resolution and R_d = detector resolution. For the pyrometry system the limiting optical component is the final element (the fast photography lens) which has a resolution of 50 lp/mm, which is roughly 20 μ m, at 50% contrast, so R_o is:

$$R_o = \frac{25 \mu m}{M}$$

The detector (in this case an optical streak camera) has a resolution of 25 lp/mm (~40 μ m) at 50% contrast:

$$R_d = \frac{40 \mu m}{M}$$

If the setup is a 10x objective followed by an MT1 tube lens, then an MT2 tube lens to relay the image out to a 500 mm focal length photography lens the overall magnification will be:

$$M = 10 \times \frac{500mm}{400mm} = 12.5$$

Giving a resolution of:

$$R = \sqrt{\left(\frac{20}{12.5}\right)^2 + \left(\frac{40}{12.5}\right)^2} \approx 3.5\mu m$$

Better resolution could be achieved by increasing the magnification, for example if the positions of the 200f and 400f tube lenses were swapped the resulting magnification and resolution would be:

$$M = \frac{400}{20} \times \frac{500}{200} = 50$$

$$R = \sqrt{\left(\frac{20}{50}\right)^2 + \left(\frac{40}{50}\right)^2} < 1\mu m$$

However this comes at the sacrifice of fluence through the system and will degrade the sensitivity of the diagnostic potentially to unacceptable levels (for a magnification of 50x the beam divergence angle is 2.9° , greatly increasing light loss). Also this resolution actually exceeds the diffraction limit of the system so is unattainable anyway:

$$DL = F\#\times\lambda \times 1.22 = 1.8 \times 500nm \times 1.22 \approx 1\mu m \text{ [35]}$$

A third potential arrangement is to use two 400f tube lenses as the relay lens pair giving a magnification of 25 and a resolution of $\sim 2\mu m$.

As detailed above there are 3 potential arrangements (12.5x, 50x and 25x magnification), however taking into account that the signal drops off proportional to the square of the magnification means that a lot of signal will need to be produced to use anything other than the 12.5x magnification set up.

6.5. Results

6.5.1. Initial vignetting test:

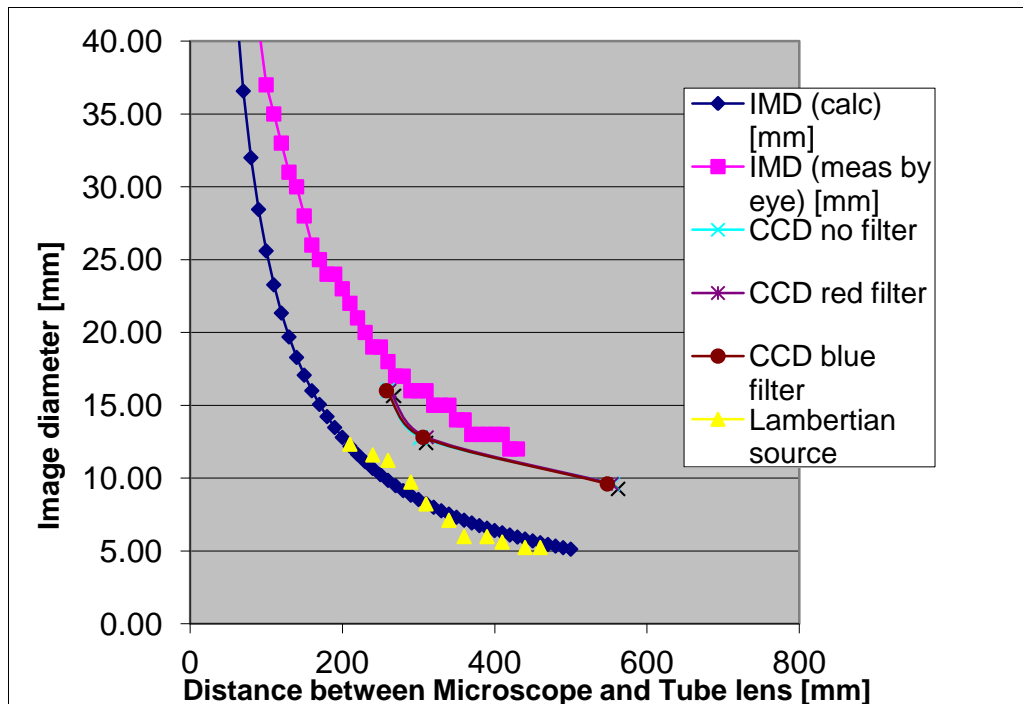


Figure 6.14 Image diameter as a function of microscope and tube lens separation, IMD=image diameter, the performance was unchanged by filtering between 450-700 nm and the Lambertian source points are from measurement using a CCD.

Testing was initially performed with a transmissive resolution grid; this gave an artificially greater unvignetted field of view due to collimation effects, once a Lambertian source was used the vignetting followed the expected trend (fig 6.14). That the Lambertian source gave the expected trend suggests that the source being used previously was subject to collimation effects.

6.5.2. Resolution of pyrometry system

A simulation of the optical path length and expected optical components that the pyrometry beam would traverse when installed at Orion is shown in Figure 6.15.

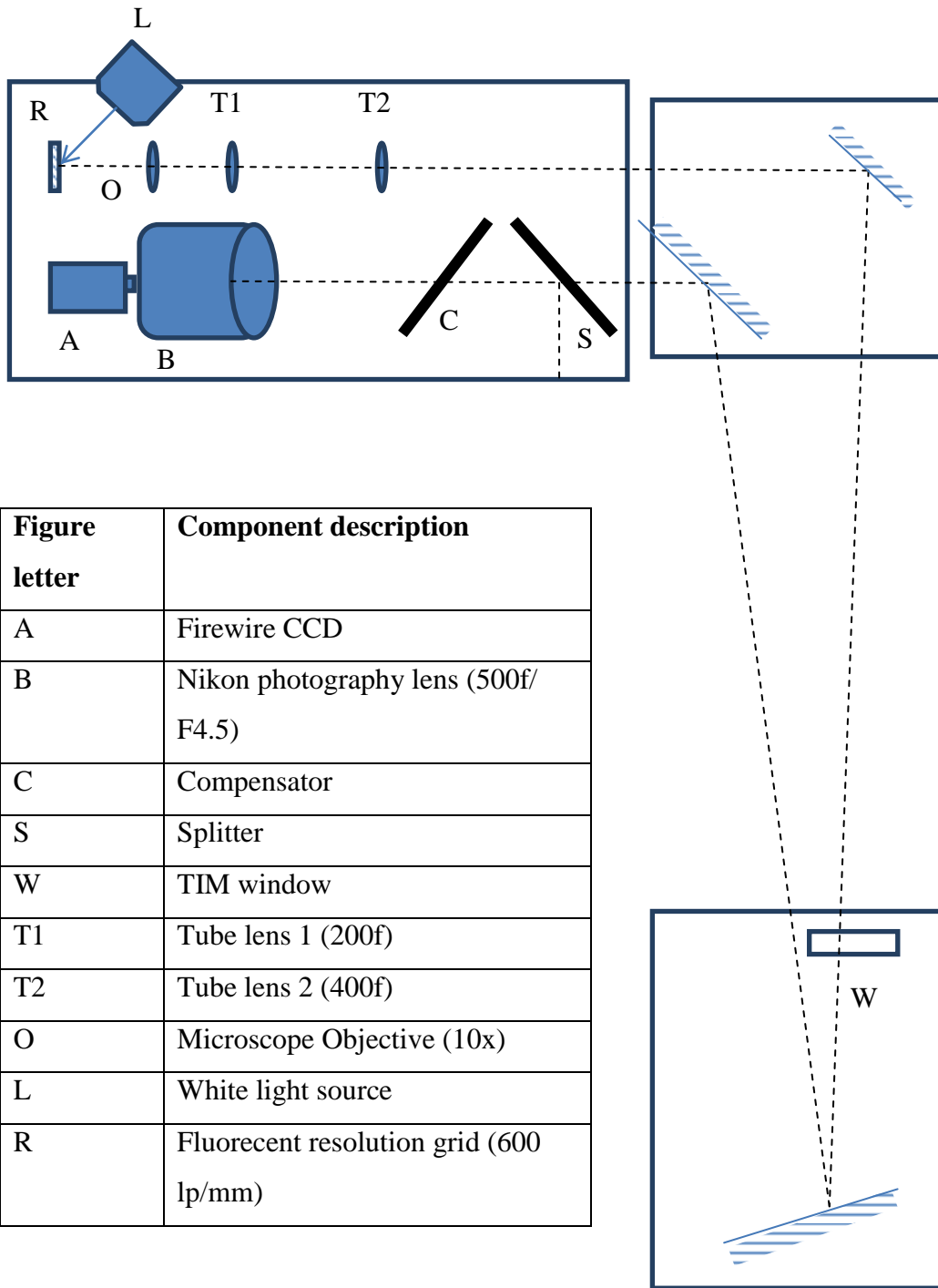


Figure 6.15 Passive testing with full aperture arrangement

Images in tables A.2 and A.3 (see appendix) show resolution down to $1\mu\text{m}$ which is around the predicted diffraction limit of the system, figure 6.16 shows the smallest element on a USAF grid (~ 4 micrometers) being easily resolved.

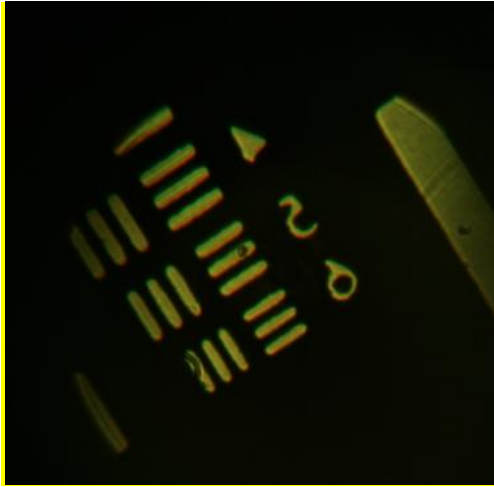


Figure 6.16

Filters were used in an attempt to degrade the resolution but the resolution performance remained unchanged; the system remained able to resolve the one micron wire at wavelengths $<400\text{nm}$ and $>750\text{nm}$ which is outside the operational parameters of the tube lenses, see tables A.2. and A.3[33].

The beam splitter and window were introduced into the path to see if there was any walk off or chromatic blur effects decreasing the resolution. Pictures **H**, **I**, and **J** in table A.3 show a walk off due to the splitter which is then corrected by an equally thick anti-parallel compensator. Images **L** and **N** show the effect of the splitter on resolution to be minimal. However images **M** and **N** show that the window does seem to degrade the $1.6\mu\text{m}$ resolution slightly. Since the overall pyrometry resolution will be limited to $3\mu\text{m}$ by the streak camera, the window's reduction of the $1.6\mu\text{m}$ resolution contrast can be considered negligible.

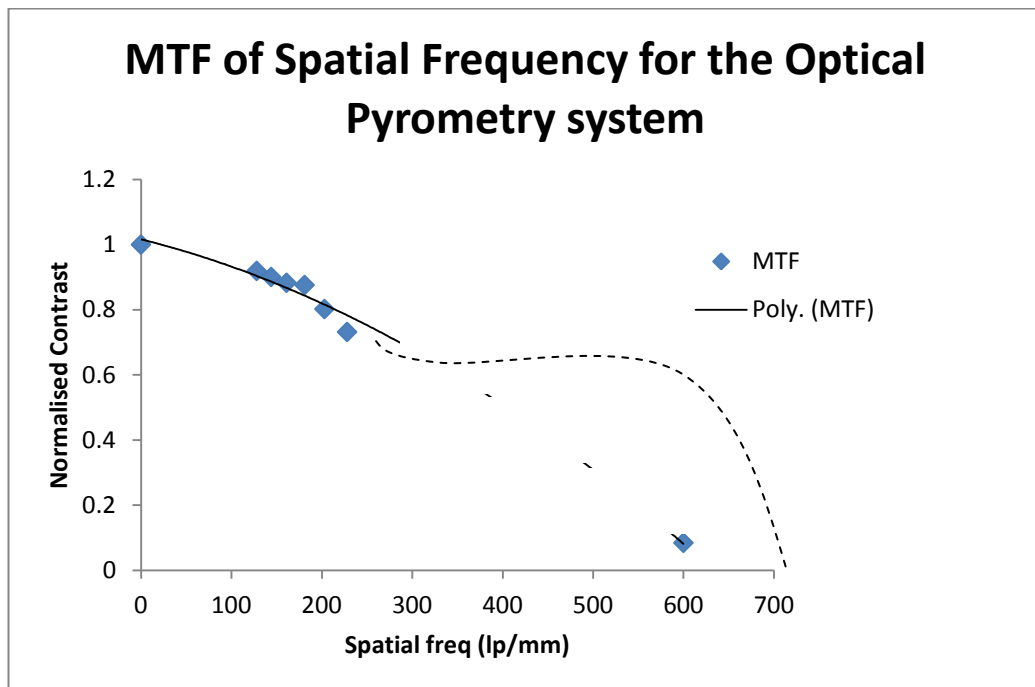
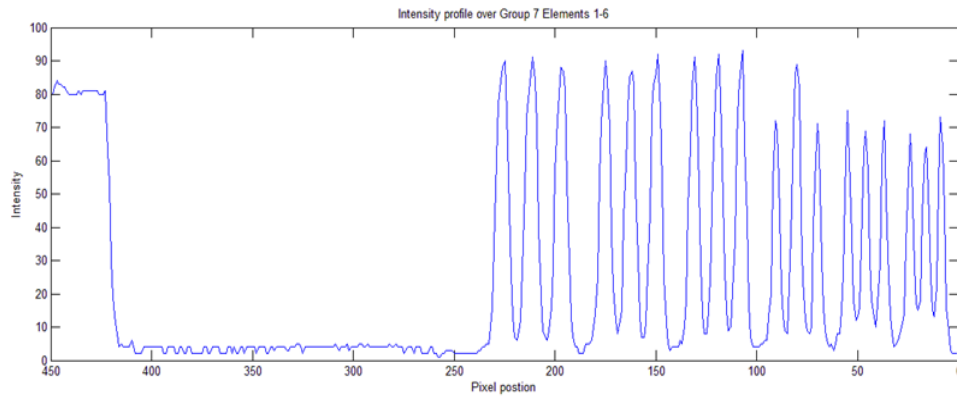


Figure 6.17 Contrast function for the Optical Pyrometry

The contrast profile shows an expected drop off in system performance towards the resolution limit and allows a prediction of the contrast at untested spatial frequencies. The dashed line is a free hand estimation of the untested resolution performance, this is based on the fact that the 5 and 2 μ m wires (images **A** and **H**) are both sharp whereas a softening appears in the image of the 1 μ m (image **E**) wire suggesting a sharp drop in contrast around this point. This would make sense as the system is diffraction limited to \sim 1 μ m as calculated earlier. To further test this resolution grids that cover these values are needed.

6.5.3. Magnification, FOV and vignetting test over Orion OPD

A relative magnification check was performed (as in Arrangement 3, however to get a useable FOV the photography lens was placed at 4 m as opposed to 9 m. A USAF grid resolution target was used for this section of testing, the target consists of a series of groups each of which contain 6 elements, each ascending element number in a group displays line pairs at progressively decreasing widths.

Group 3 Element 2 of a USAF grid 8.98 lp/mm which is 111.358 microns per line pair, so the grid placed at the intermediate image plane between tube lens 1 and tube lens 2 (in arrangement 3 with Tube lens 1 as 200f and tube lens 2 as 400f) will be 2x magnified and should (based on the information in table 6) have a line width of \sim 13 pixels and the observed image displayed \sim 16 pixels per line:

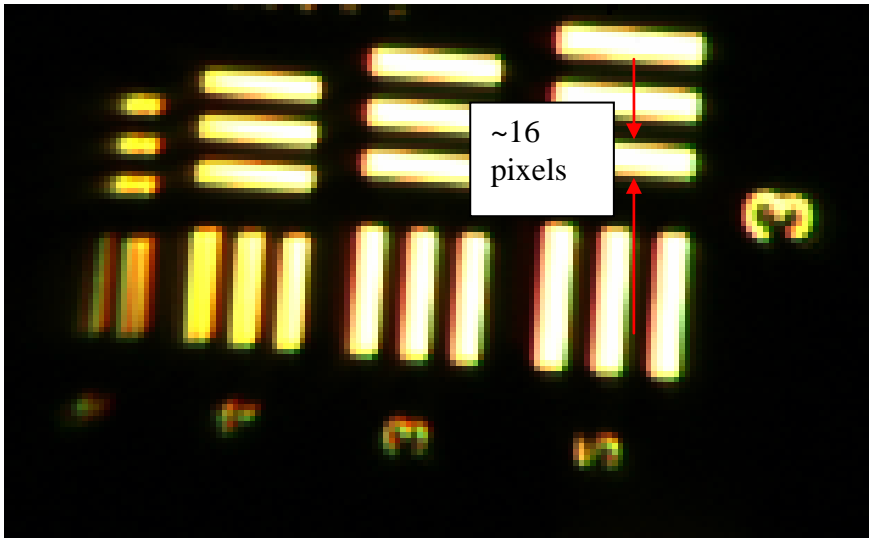


Figure 6.18 Magnification check at intermediate image plane

For the main grid Group 4 Element 3 was used which is 20.26 lp/mm at 12.5x magnification which should give an image with a line width of ~42 pixels, a line width of ~44 pixels was observed:

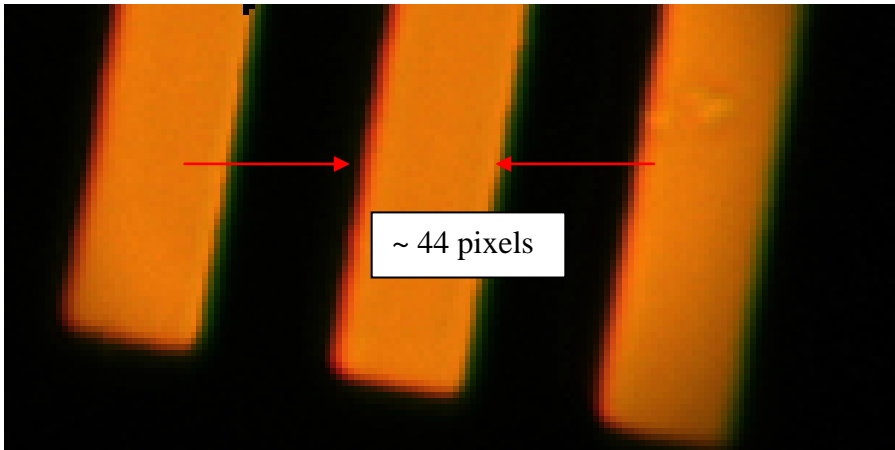


Figure 6.19 Magnification check after full pass of the system

PIKE f-210	Diagonal	Width	Height
Type 1 Chip	16.3 mm	14.2 mm	7.992 mm
Pixel	10.5 μm	7.4 μm	7.4 μm

Table 6.3 Firewire CCD parameters

In order to check the field of view is as predicted

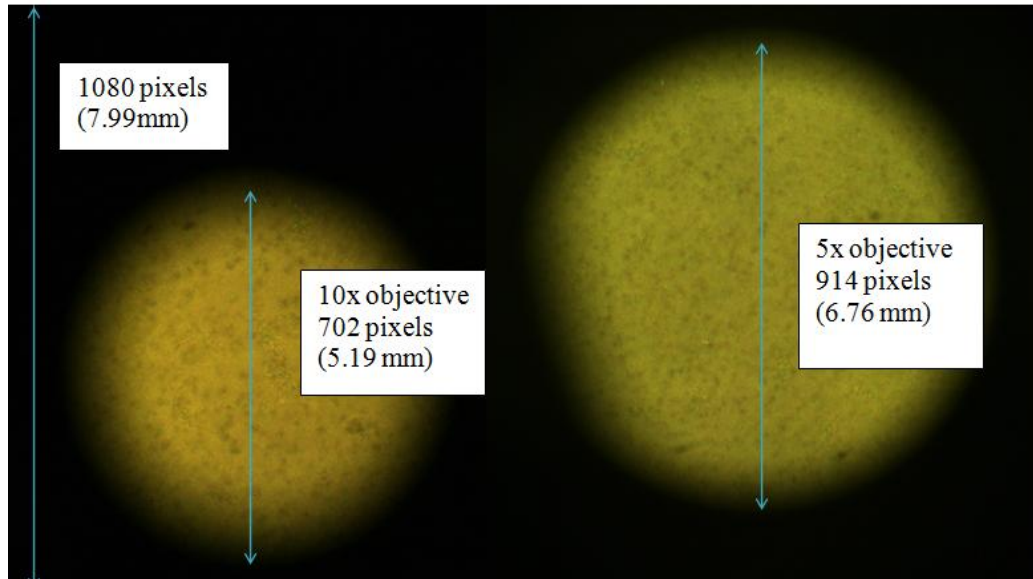


Figure 6.20 FOV of entire system for 10x and 5x magnifications

The 10x objective gives a system with an overall magnification of 12.5x, the 5x objective gives 6.25x magnification. The 10x objective system gives a FOV of 0.42 mm and the 5x objective a FOV of 1.08 mm.

Initial characterisation of the spectrum throughput for the entire system showed that it was most heavily dependent on the Red-UV splitter ('S' on Figure 6.15). This characterisation was performed by placing a linear band pass filter at the 'TCC' ('R' on Figure 6.15) and recording the reflected and transmitted spectrums. Further characterisation is planned to be carried out with a spectrometer at AWE. These results fit with the expected beam broadening and vignetting performance of the system.

6.5.4. Resolution of GOI

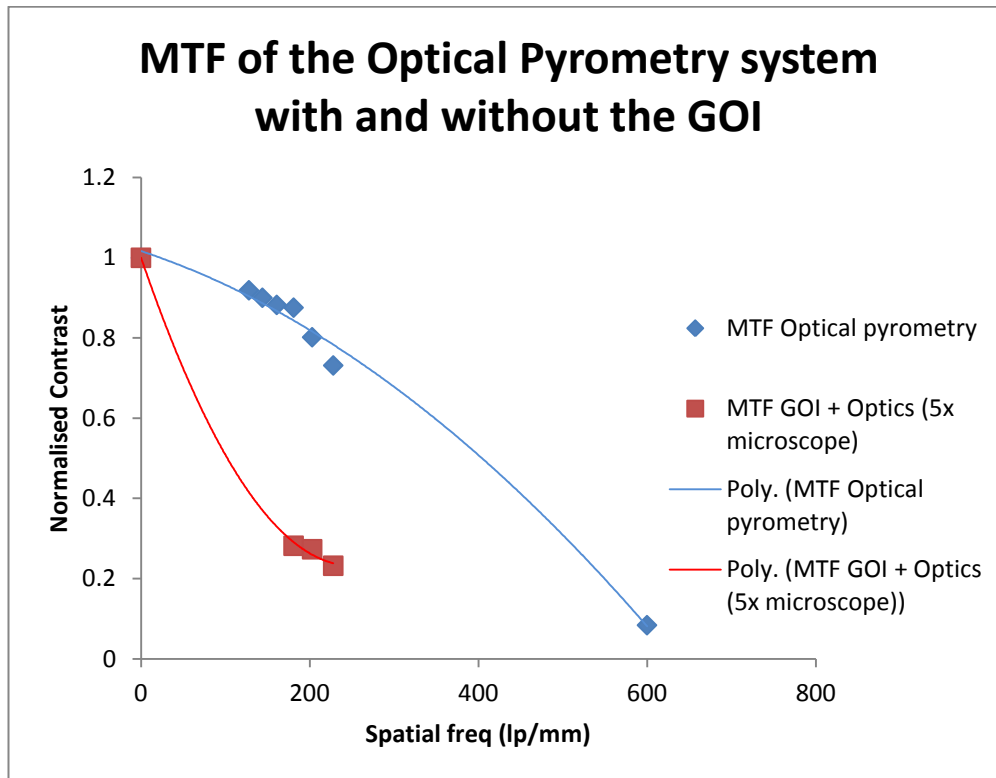


Figure 6.21 Resolution of system degraded by GOI

As shown in figure 6.21 there is an expected degradation in MTF from the fact that a less powerful objective is being used (5x as opposed to 10x). This is due to the large spatial resolutions of the photocathode and the MCP when compared to the diffraction limited resolution of the pyrometry microscope optics.

6.6. Discussion

The pyrometry system was fully characterised, the initial vignetting tests showed that the microscope objective and MT1 tube lens are functioning as quoted (once a Lambertian source was used) and that a very wide field of view can be transferred to the intermediate image plane. The resolution of the system is excellent and was able to resolve 1.6 μ m line pairs, although not at great contrast. The beam divergence was found to be as expected and gave a 0.43 mm unvignetted FOV in the full beam path mock up. The window at the back of the TIM was successfully simulated and found to have a very minimal effect which will not affect the overall resolution of the

pyrometry system. The beam splitter and compensator were successfully tested and the compensator was found to be a necessary component in order to avoid beam walk off. The broadband spectrum coming off the beam splitter was found to be as expected given the quoted curve. The resolution was degraded with the introduction of the GOI head, this was expected and is probably a result of the pore to pore distance in the MCP.

This particular application of the TIDI would be the application that requires the most space for front end optics. In particular, the limited space available within the TIM means that this application defines the amount of space the TIDI will take up. As previously analysed, this has a huge impact on the temporal resolution that can be available (due to the temporal resolutions heavy dependence on the drift length).

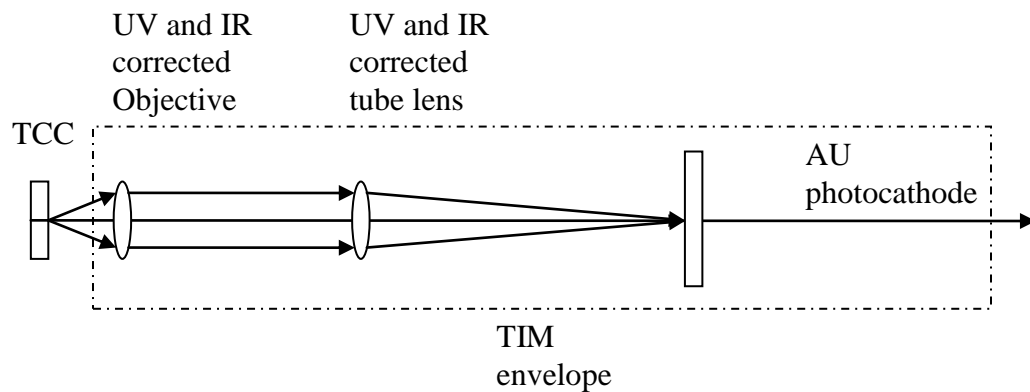


Figure 6.22 Example arrangement of TIDI used in conjunction with the pyrometry system

Figure 6.22 displays how the UV optics arrangement would differ from the tested optics, magnification would come only from the objective so the resolution would not be quite as good. The beam has no need to travel as long a path as tested for the optical pyrometry set up (due to the TIM based TIDI) and so there is no need for the relay lens arrangement. Also the reduction in spatial resolution caused by the MCP provides motivation for designing a TIDI which can function without that component; this is explored further in the design section.

Chapter 7

Conclusions and further work

Chapter 7 summarises the thesis. The aims of the work are restated. The results of the design study are collected and presented alongside the results from the characterisation of the optical pyrometry system.

The aims of this study were to:

- Establish the requirement for a diagnostic of very high temporal resolution
- Identify and outline the key experimental applications of such a device and how this would affect the design of the diagnostic
- Assess the feasibility of employing a pulse dilation device for HED experiments at the Orion Laser Facility
- Characterise an optical pyrometry system in an attempt to further understand the restrictions that would be placed on a potential time dilation imager in coupling it with front end optics specific to application
- Restore and test a Gated Optical Imager to further understand the current limitations of gated imaging
- Analysis potential geometries of the Orion TIDI to ascertain the most appropriate design to move forward with.

It has been well established that the need is present for a high temporally resolving device. The experimental programme at Orion has evolved to the point where key information is unreachable due to restrictions in the current diagnostic suite's temporal, spatial, and/or spectral capabilities. The primary applications have been established as: time resolved broadband x-ray diffraction of shock compressed materials, UV colour temperature measurements, and time resolved point projection spectroscopy. All three primary applications require temporal resolution in 2D which is currently unavailable. The current diagnostic that comes closest to fulfilling these applications is the Gated X-ray Detector (with a spatial resolution of 60 μm and a temporal resolution of >70 ps), this does not however satisfy the requirements laid out in table 2 of <10 ps temporal resolution and $<50\mu\text{m}$ spatial resolution

The compatibility of the three primary applications with a potential TIM based geometry is likely not going to cause issue. Estimations of comparable signal collection and sensitivity differences of tried and tested techniques against the proposed TIDI diagnostic has found that sufficient signal should be collected. A roughly to scale drawing of the BBXRD set up has shown that the geometry should not be a problem. The UV colour temperature will be the limiting case in terms of longitudinal space and this has been taken into account in the designs for the TIDI.

The individual components that would comprise a likely design for an Orion TIDI have been identified and assessed, the potential problems each component could cause have been predicted and any potential solutions highlighted. An attempt has been made to keep the design simple in order to minimise potential issues, unnecessary components have been recognized for potential removal (e.g. MCP), and other methods suggested for completing their task.

The design constraints have been explained and justified, including; the necessity of a modular design for UV and x-ray sensitivity, ensuring compatibility of the device with a Ten-Inch Manipulator (TIM), and the benefits and trade-offs of certain critical design parameters like the drift region magnetic field and the photocathode voltage sweep.

Experimental work has been done to characterise an optical arrangement similar to one which would be used for the UV colour temperature measurements. The initial vignetting tests showed that the microscope objective and MT1 tube lens are functioning as quoted (once a Lambertian source was used) and that a very wide field of view can be transferred to the intermediate image plane.

The resolution of the system was 1.6 μ m line pairs, although not at great contrast. The beam divergence was as expected and gave a 4.3 mm

unvignetted FOV in the full beam path mock up. The whole system was found to be well colour corrected and a simulation of the Orion optical path found a minimal effect from a window (with no overall affect on the resolution), and walk off from a beam splitter which was successfully corrected for using a compensator window.

Further experimental work has been performed into bringing a Gated Optical Imager online (the Kentech GOI). The GOI work was not successful, given more time it would be worth establishing where the problem with the gating mechanism lies, the GOI is ~20 years old and it would be useful to identify the issue not only for bringing the diagnostic online but also as it may potentially shine a light on how the TIDI will age and allow for future proofing. The GOI experiments were however instructive in consideration of the design of the TIDI, especially the individual component analysis.

Reviewing the potential designs (TIDI 1-3) has lead to the conclusion that TIDI 3 would be the optimum design to push forward with. The high level of flexibility of the photocathode means that the design can continually be developed for specific applications. All the designs have the potential to exchange the detection back end with a ns framing CCD when the technology is established, however TIDI 3 will provide the best spatial resolution in the mean time due to the removal of the MCP.

TIDI 3 is estimated to provide <10ps temporal resolution, 4 frames at a spacing of ~100ps, a spatial resolution of <50 μ m, and a dynamic range of 300 counts with an interchangeable photocathode with a flexible design structure allowing for a high level of adaptability for specific applications. This design is achievable with existing technology and would provide the diagnostic capability required for the Orion experimental programme that is currently unavailable.

References

- 1) J.Wark, *The AWE Introductory Course in Plasma Physics* (Department of Physics, University of Oxford, 2004),p.141
- 2) 'Frontiers in High Energy Density Physics: The X-Games of Contemporary Science' 2003, visited June 2013, <http://fsc.lln.rochester.edu/hedp.php>
- 3) Info Jupiter suite NIF, Visited September 2012, https://lasers.llnl.gov/programs/science_at_the_extremes/jlf.php
- 4) AWE Plasma Physics Department annual report 2006, visited December 2012
- 5) Short-pulse matter interaction figure, AWE Intranet ,Accessed September 2012
- 6) M. Siegbahn,*50 years of x-ray diffractions: Chapter 16 X-ray Spectroscopy*, (International Union of Crystallography, 1962, 1999)
- 7) J.Wark, *The AWE Introductory Course in Plasma Physics* (Department of Physics, University of Oxford, 2004),Ch. 11
- 8) Jerrold T. Bushberg, J. Anthony Seibert, Edwin M. Leidholdt, and John M. Boone (2002). *The essential physics of medical imaging*. Lippincott Williams & Wilkins. p. 38
- 9) A. Rubenchick, S.Witkowski, *Physics of laser plasmas* v3, pg193 (1991)
- 10) A.J. Comley, B.R. Maddox, R.E. Rudd, et al, Physical Review Letters**110**, 115501 (2013)
- 11) T.P. Hughes, *Plasmas and laser light*, Adam Hilger (London,1975)
- 12) Private communication with J. Hares and T. Dimoke-Bradshaw, Kentech
- 13) D.K. Bradley, P.M. Bell, J. Oertel, et al, Rev. Sci. Instrum. **66(1)**, (1995)
- 14) D. G. Stearns, J. D. Wiedwald, B. M. Cook, et al, Rev. Sci. Instrum. **60**, 363 (1989)

- 15) M. Koga, K. Shigemori, H. Shiraga, et al, Journal of Physics: Conf. Ser. **244** (2012)
- 16) K.S. Budil, J.D. Hares, P.L. Miller, et al, Rev. Sci. Instrum. **67**(2), 1996
- 17) M. Borghesi, G. Sarri, C.A. Cecchetti, Laser and Particle Beams (impact factor: 1.62) 2010
- 18) S. Glenzer, B. MacGowan, P. Michel, LLNL-JRNL-420984, 2009
- 19) T. Hilsabeck, J. Hares, J. Kilkenny, Rev. Sci. Instrum. **81**, 10E317 (2010)
- 20) S. Nagel et. al., Rev. Sci. Instrum., **83**, 10E116 (2012)
- 21) S. Nagel, et al, LLNL-CONF-566512, 2012
- 22) T. Hilsabeck, J. Hares, Presentation to 7th NIF diagnostic workshop, 2012
- 23) J. Hares, *A single line-of-Sight X-ray Framing Camera for the NIF*, unpublished white paper 2013
- 24) S. Qiu, H. Amano, A. Kasai, Radiation Protection Dosimetry, Vol. 22, **3**, pp. 197-200 (1988)
- 25) Private communication with M. Giesel, ICOPS 2012
- 26) M. Edwards, B. Rus, C. McKenna, et al, Central Laser Facility Annual Report (2005/2006)
- 27) J. Foster, S. Rose, T. Perry, et al., Phy. Rev. Let. Vol 67, **23**, 1991
- 28) P. Audebert, P. Renaudin, S. Bastiani-Ceccotti, Phys. Rev. Let. **94**, 025004 (2005)
- 29) J. E. Miller, T. R. Boehly, A. Melchior, et al, Rev. Sci. Instrum. **78**, 034903 (2007)
- 30) Private communication with E. Gumbrell, AWE
- 31) Operations Manual for Gated Optical Imager, Kentech Instruments Ltd, 1995
- 32) O'Shea, *Elements of Modern Optical Design*, pp.91-93, (1985)
- 33) Mitutoyo Catalogue, <http://www.mitutoyo.co.uk/>, visited multiple times throughout 2012/13

- 34) Sigma website, <http://www.sigma-foto.de/fileadmin/content/TS-Tabellen/Tiefenschaerfetabelle%2010-20mm%20F4-5.6%20EX%20DC.pdf>, visited March 2013
- 35) Knoll, *Radiation Detection and Measurement*, 2nd Ed pg 173, 252-253, and 270
- 36) Krolkowski, Spicer, Phys. Rev. **185** 882 (1969)
- 37) P. Townsend, Contemporary Physics, 44:1, 17-34 (2003)
- 38) C. Halvorson, T. Houck, Rev.Sci. Instrum. **81**, 10E309 (2010)
- 39) I. Frumkin, et al., Nuclear Instrum. Meth. Phys. Res., A329, 337, (1993)
- 40) Yuan Zheng, Liu Shen-Ye, Cao Zhu-Rong et al. Selective photoemission of Au photocathode. Acta Phys. Sin., 2010, 59(7): 4967-4971.
- 41) J.L. Wiza, Nuclear Instrum. And Methods, Vol. 162, 1979, pp. 597-601
- 42) D.K. Bradley, P.M. Bell, J. Oertel, et al, Rev. Sci. Instrum. **66(1)**, (1995)
- 43) CMOS fundamentals website, http://www.siliconimaging.com/cmos_fundamentals.htm, visited March 2013
- 44) Photonik, Image capturing, *Electronic shuttering for High Speed CMOS Machine Vision Applications*, www.photonik.de 5003, visited December 2012
- 45) D. Eder, R. Anderson, D. Baily, et al., 6th *International Conf. On Inertial Confinement Fusion Sci. and Applications*, IOP publishing Ltd, Bristol, 2008, Vol 224
- 46) C. Brown, A. Throop, D. Eder, et al., 5th *International Conf. On Inertial Confinement Fusion Sci. and Applications*, IOP publishing Ltd, Bristol, 2008, Vol 112
- 47) Private communication J.Hares and T. Dymoke -Bradshaw, November 2012

- 48) University of York, '*FINAL REPORT GR/T27280/01 'Opacity measurements at EUV wavelengths'*', 2007
- 49) J. Pan, 'Opacity effects in Inertial Confinement Fusion Implosions', http://www.lle.rochester.edu/media/publications/high_school_reports/documents/hs_reports/2012/Pan.pdf, visited August 2012

Appendix:

Table A.1 shows the capabilities of the current x-ray diagnostic suit at the Orion laser facility. The table is included in order to highlight the place for a Time Dilation Imager (TIDI).

Diagnostic features	Diagnostic					
	DANTE	HEX-ID	FFLEX	HXRS	TLD ARRAY	GXD
Spectral range	50eV – 2keV	1 – 10keV	20 – 100keV	100keV – 2MeV	100keV – 20MeV	6eV – 17.5keV
Purpose	Absolutely calibrated, time-resolved measurement of low-energy x-ray emission from laser-target interactions to measure target	Plasma opacity measurements, high-resolving power spectroscopy of x-ray backlighter materials. Simultaneous spectral and temporal	Time-integrated measurement of hard x-ray spectrum from laser-plasma experiments. Information on hot electron temperatures.	Time-integrated measurement of hard x-ray and bremsstrahlung spectrum from laser-plasma experiments. Information on hot electron temperatures.	Measure bremsstrahlung radiation dose levels and infer hot electron fractions in the electromagnetic pulse environment of a laser-plasma interaction.	X-ray detection system using microchannel plate (MCP) technology. Provide 2D spatially resolved, time gated images of x-ray emission. Record x-ray images and x-ray spectra from

	temperature.	measurements for a laser shot.				laser-irradiated targets.
Technique	Filters and x-ray diodes (XRDS).	Filters, convex reflection crystals & image plate, diamond PCDs or complementary metal oxide semiconductor (CMOS) sensors.	Filters, scintillators and photomultiplier tubes (PMTs).	Filters, scintillators and photomultiplier tubes (PMTs).	Filters, thermoluminescent (TL) phosphor.	MCP, HV pulsed phosphor screen and CCD
Dynamic range (orders of magnitude or	XRDS ≈ 5	PCDs $\approx 2 - 3$, image plate ≈ 5 , CMOS ≈ 4	PMTs ≈ 5	PMTs ≈ 5	TL phosphor $\approx 4 - 5$	300

value)						
Detector Sensitivity	$\approx 2 \times 10^{-4} - 0.2$ mA / W	≈ 0.5 mA / W (PCDs) $\approx 2 - 6$ mPSL / 5keV x-ray (image plate) $\approx 0.2 - 0.8$ mA / W (CMOS, at 555nm)	85mA / W (PMT, at 420nm)	85mA / W (PMT, at 420nm)	$10^{-2} - 400$ rad	Varies with MCP gain, typical MCP detection efficiency to soft x-rays of 5 - 15%
Signal-to-noise ratio	$\sim 50 - 500$	≈ 40 (PCDs) $\approx 20 - 40$ (CMOS) ≈ 17 (image plate)	~ 10	~ 10	~ 4	> 20
Spatial resolution	None	$\approx 50\mu\text{m}$ (CMOS) $\approx 75\mu\text{m}$ (image plate)	None	None	None	Up to $60\mu\text{m}$

		plate)				
Temporal resolution	< 200ps	< 300ps (PCDs)	~ 230ns	~ 17ns	None	70 – 500ps
Resolving power (E/dE)	1 – 10	> 500	~ 1 – 5	~ 1	None	~ 10 – 50
Fielded on TIM / port?	Port	TIM	Port	Port	TIM	TIM

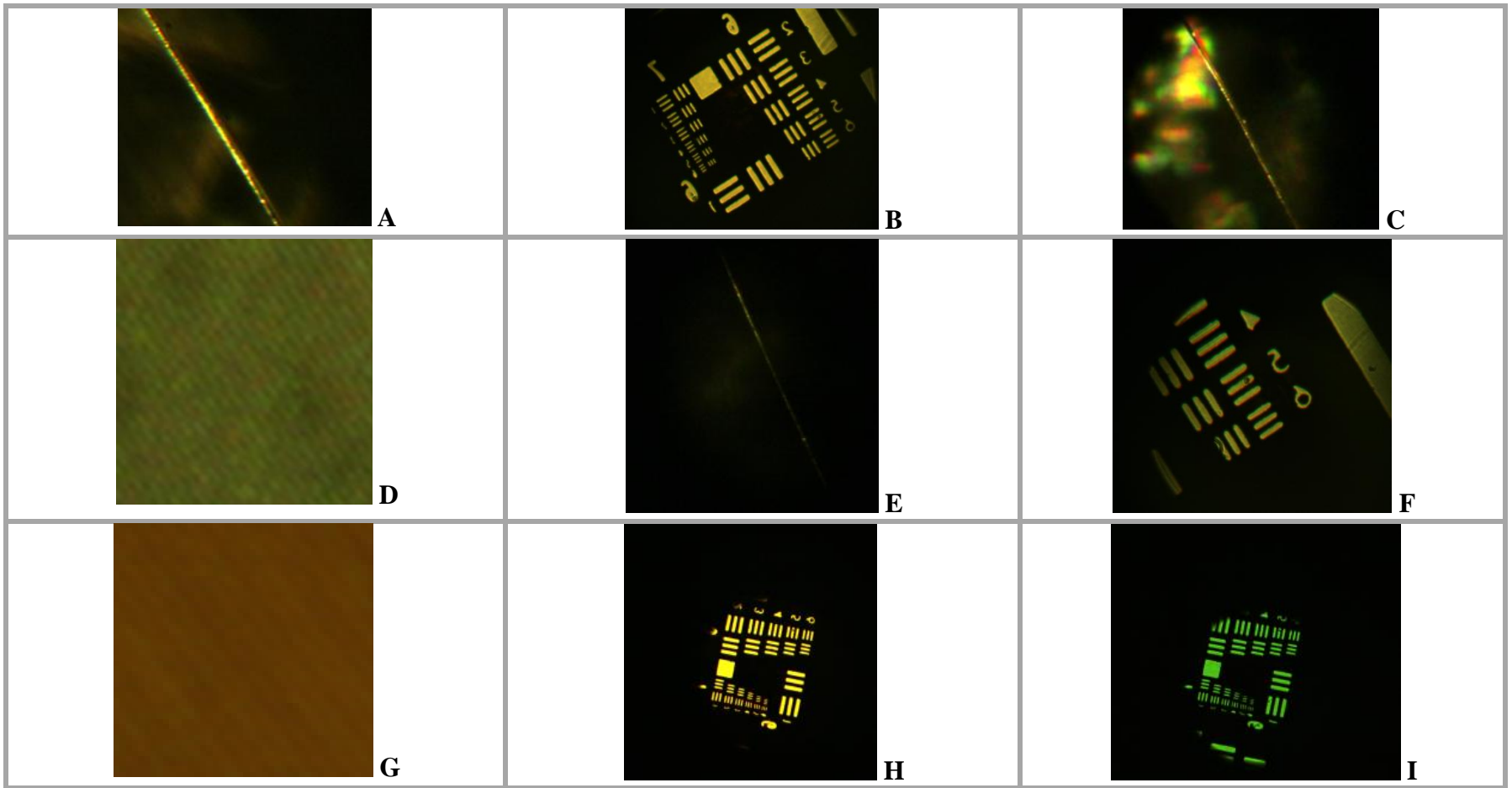
Table A.1 Orion diagnostic Suite

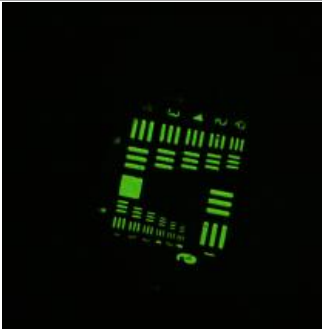
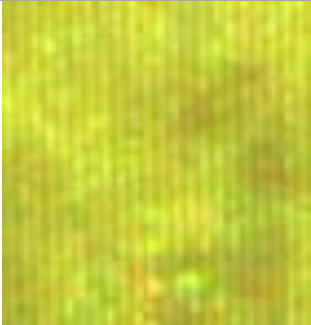
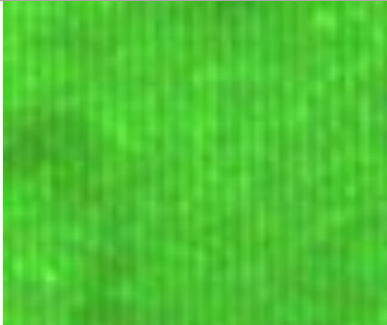
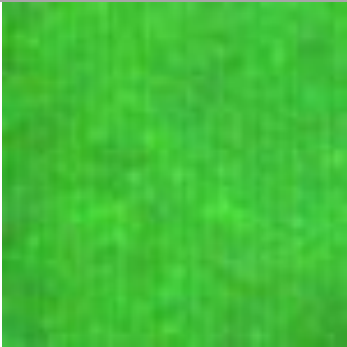
Tables A.2 and A.3 are the various experimental configurations and images recorded for the characterisation of the optical pyrometry system in Chapter 6.

Resolution (μm)	Fig table ref	Compensator	Splitter	Window	Objective	Tube lens 1	Tube lens 2	Optical Path Distance (m)	Resolution element
5	A	N	N	N	10x	200f	400f	1.5	Wire grid
4.3	B	N	N	N	10x	200f	400f	8	USAF

2	C	N	N	N	10x	200f	400f	8	Wire grid
1.7	D	N	N	N	10x	200f	400f	8	Ronchi fluorescent
1	E	N	N	N	10x	200f	400f	8	Wire grid
4.3	F	N	N	N	10x	400f	400f	8	USAF
1.7	G	N	N	N	10x	200f	400f	8	Ronchi Transmissive
4.3	H	N	N	Y	10x	200f	400f	8	USAF
4.3	I	Y	N	Y	10x	200f	400f	8	USAF
4.3	J	Y	Y	Y	10x	200f	400f	8	USAF
1.7	K	N	N	N	10x	200f	400f	4	Ronchi fluorescent
1.7	L	Y	Y	N	10x	200f	400f	4	Ronchi Fluorescent
1.7	M	N	N	Y	10x	200f	400f	4	Ronchi fluorescent
1.7	N	Y	Y	Y	10x	200f	400f	4	Ronchi fluorescent

Table A.2 Summary of Resolution Results



J

K

L

M

N

Table A.3 Pictures for table A.2

Table A.4 is a summary of the full experimental potential of the Orion TIDI, this is useful to include as it is the basis of the user requirements defined in Chapter 3.

Experiment	Required Spec	Currently Achievable?	Achievable with a Dilation Imager
Doped Capsule Implosion experiments	<10 ps temporal res ~10 μm	Streak cameras can provide the temporal resolution; an x-ray microscope would be able to give us the spatial resolution.	SLOS is predicted to have an increased spatial resolution when compared to DIXI (~20 μm) and can produce four frames from a single shot 100 ps apart. It can provide both the spatial and temporal resolution required in one diagnostic device.
Line modelling of radiation hydrodynamics	<10 ns	GXD has suitable temporal resolution but not the required spatial resolution	With a SLOS type imager we can reach the required temporal and spatial resolution
UV-soft x-ray imaging	spectral response in the range of 3 eV – 10 keV	GXD and DANTE can currently cover this range, but with limited (GXD) or null (DANTE) spatial resolution	SLOS or any dilation imager can be made to cover this range with the correct design considerations.
Spectroscopy of warm-dense-matter	Temperatures in the range of 1-100	Streak cameras are as close as we can	A dilation imager would still not db28

<p>for EoS studies. For Example: Thermal emissions from micro-wire targets which requires 1-10ps Temporal resolution and very good spatial resolution.</p>	<p>eV Densities in the range of 10^{-3}-10^1 g/cm³ Sub picosecond temporal response to accurately evaluate rapid changes in warm-dense matter</p>	<p>get in terms of temporal resolution. Currently we rely on sub pico second x-ray sources</p>	<p>this justice temporally but would be able to add a spatial resolution that the streak camera is missing.</p>
<p>Pre-plasma characterisation with short pulse probe beams gating-out coherent self emission</p>	<p>Spatial resolution <50 μm X-ray spectrum</p>	<p>An X-ray microscope can get down to the required spatial resolutions but would only provide one time integrated image</p>	<p>SLOS would be able to the required spatial resolution as well as providing 4 frames of the developing system.</p>
<p>2DTime resolved X-ray diffraction</p>	<p>5-10 ps temporal resolution and the ability to record x-ray diffraction patterns</p>	<p>Sub 10 ps resolution using a streak camera, however this does not allow for 2D imaging of complex diffraction patterns</p>	<p>DIXI has shown the ability to get down to 6 ps resolution, TIDI should have sufficient spatial resolution also</p>
<p>Point Projection Spectroscopy</p>	<p>Record the evolution of x-ray</p>	<p>See above</p>	<p>See above</p>

	spectra with <10 ps resolution		
--	--------------------------------	--	--

Table A.4 Overview of TIDI experimental applications derived from interests of the Radiation physics department at AWE

Table 5 is a summary of the benefits and drawbacks of adjusting the key components for optimisation of the Orion TIDI for various experimental applications.

Variable	Increase	Decrease
Photocathode Area	<p>More photons collected per m²</p> <p>Will be able to place PC further away from target</p> <p>Requires a de-magnifying geometry which sacrifices spatial resolution</p> <p>Would possibly not fit inside a TIM</p>	<p>Would reduce the collection of photons so would require being relatively close to the target</p> <p>Would not require as high a B-field which would increase the spatial resolution as the spatial resolution is inversely proportional to the B-field</p> <p>Can have something more akin to a 1 to 1 geometry</p> <p>Would fit inside a TIM</p> <p>A smaller area closer to the target to increase the yield would also have an increased photoelectron density which would lead to high space charge effects</p>
Magnetic field	Increase in spatial resolution	Decreasing the magnetic field

strength	<p>due to tighter electron orbits (spatial resolution limited to 4x the electron orbit radius, which is inversely proportional to B)</p> <p>This could lead to issues with solenoid stored energy and require a mechanical adjustment to the TIM</p>	<p>will restrict the spatial resolution</p> <p>Would decrease space charge effects by having a lower current density</p>
PC-MCP distance	<p>Longer drift length increases either number of frames or temporal magnification</p> <p>Longer drift time will lead to higher instance of space charge effects</p> <p>Mechanical constraints may make it incompatible with a TIM</p> <p>Potential to have knock on effects on the position and size of a photocathode</p>	<p>Less space charge effect</p> <p>Less time for magnification</p> <p>Requires a higher gradient of voltage sweep</p>
PC Voltage sweep gradient	<p>Higher temporal spread</p> <p>Low voltage limited by space charge effects</p>	<p>Lower temporal magnification</p>
MCP size	<p>Would require a larger number of pixels at the CCD</p>	<p>Will either require a small PC or a de-magnifying geometry, either way we will sacrifice</p>

	Would require a larger B-field, the energy in the B-field is set by the number of pixels, a doubling of MCP size would leap to a quadrupling of B-field making stored energy a problem.	spatial resolution this way However we will be able to gate across a strip more quickly
PC bias voltage	Higher gate times	
PC gating pulse width	Higher gate time	
Modular PC	Allows for a range of experiments Will potentially require adjustments to solenoid field, pin hole to PC distance, any other mechanisms we have in place that depend of PC size/energy spread	Limited experiments can be performed with diagnostic No need for adjustment (fewer moving parts)

Table A.5 Benefits and Drawbacks of key design decisions